Norwegian University
of Life Sciences

Master's Thesis 2022 60 ECTS
Faculty of Biosciences
Department of Animal and Aquacultural Sciences

Prime Editing in Zebrafish and Atlantic Salmon – Exploring a New CRISPR Technique in Non-mammalian Species

Jenny Heyerdahl Bryhni
Master of Science in Genome Science

Acknowledgements

I would first and foremost like to thank my main supervisor, Guro Katrine Sandvik, for all guidance, encouragement and feedback I have received throughout the work on this thesis. I greatly appreciate how you have found time to help me even when time has been scarce, and for all the unscheduled chats in your office you have made time for when I have dropped by with yet another question or problem.

Many thanks to my co-supervisor PhD fellow Darshan Young, who has patiently helped me in the lab and always have had an open door.

Many thanks to PhD fellow Noman Reza, both for providing me with cells, primers and plasmids as well as for all help with issues I've had in the lab. Your knowledge has helped me a lot.

Thanks to all PhD fellows, post docs, lab technicians and others at CIGENE who have all provided help, good discussions and creative solutions when I have needed it.

Thank you, Emil, for all your love and support throughout this year. It would not have been the same without you by my side.

Lastly, thanks to Edith, Guro's dog, for being a good girl who always succeeds in calming a stressed master student. Also, my ankles would never have been as clean as they were during the work on this thesis were it not for you.

Jenny Heyerdahl Bryhni

15.05.2022

Abstract

The CRISPR-Cas system has enabled precise genome editing in a multitude of organisms, and gene knockout experiments can now be done with relative ease due to the simplicity of the system. However, unintended genomic side-effects of such editing have surfaced in the last couple of years.

In this thesis, the CRISPR-based genome editing system prime editing was explored as an alternative gene knockout approach to avoid the unintended editing outcomes seen in the wake of regular CRISPR-Cas editing. Prime editing was applied to zebrafish (*Danio* rerio) by microinjection of RNP complexes and to Atlantic salmon (*Salmo salar)* cells by electroporation of plasmids and RNP complexes.

No successful prime editing outcomes was observed in zebrafish. Low survival rate of both microinjected and uninjected embryos remained an obstacle throughout the project, and should be addressed before continuing zebrafish prime editing experiments. Prime editing of Atlantic salmon cells using plasmids did not produce any positive results. Prime editing with RNP complexes in Atlantic salmon cells showed signs of successful editing, but results remains inconclusive as further analysis is needed to properly validate the editing outcomes from this experiment.

Abstrakt

CRISPR-Cas har muliggjort presis redigering av genomer i en rekke organsimer, og kan brukes til å relativt enkelt slå ut gener for ulike formål. Til tross for at det er en presis og effektiv metode for genomredigering, har utilsiktede konsekvenser av bruk av CRISPR-Cas9 kommet til overflaten de siste årene.

I denne oppgaven ble det CRISPR-baserte genomredigeringsverktøyet prime editing utforsket, for å se om det kan fungere som en alternativ metode for å slå ut gener og unngå de utilsiktede konsevensene som kan oppstå i kjølvannet av vanlig CRISPR-Cas-redigering. Prime editing ble brukt i zebrafisk (*Danio rerio*) ved mikroinjesering av RNP-komplekser og i lakseceller (*Salmo salar*), ved elektroporering av plasmider og RNP-komplekser.

Bruk av prime editing i zebrafisk ga ingen positive resultater. Lav overlevelsesrate for både mikroinjesert fisk og uinjeserte kontroller var et vedvarende problem under prosjektet, og bør adresseres før videre forsøk med prime editing fortsetter. Prime editing-redigering av lakseceller ved elektroporering av plasmider ga ingen positive resultater. Resultatene fra prime editing-redigering med RNP-komplekser i lakseceller virker lovende, men det er for tidlig å kunne konkludere da videre analyser trengs for å kunne bekrefte resultatene.

Table of Contents

List of abbreviations

BFP – Blue fluorescent protein

bp – Base pair

DSB – Double stranded break

EGFP – Enhanced green fluorescent protein

EGFP KO pegRNA – Prime editing guide encoding enhanced green fluorescent protein knock-out

EGFP-SHK-1 – Enhanced green fluorescent protein-expressing salmon head kidney-1

FBS – Fetal Bovine Serum

G->B pegRNA – Prime editing guide encoding conversion of green fluorescence to blue

G->B RNP – Ribonucleoprotein complex with a prime editing guide encoding conversion of green to blue

GCR – Genetic compensation response

GnRH – Gonadotropin-releasing hormone

HEK – Human embryonic kidney 293

INDEL – Insertion and deletion

KD- Knock-down

KO – Knock-out

mRFP – Monomeric red fluorescent protein

NEB – New England Biolabs

NMD – Nonsense-mediated decay

PAM – Protospacer adjacent motif

PBS – Primer binding site

PCR – Polymerase chain reaction

PE – Prime editing

pegRNA – Prime editing guide RNA

RNP – Ribonucleoprotein

PTC – Premature termination codon

pU6 – Mammalian U6 promoter

qPCR – Quantitative PCR

RT – Reverse transcriptase

sgRNA – Single guide RNA

SHK-1 – Salmon head kidney-1

ZFU6 – Zebrafish U6 promoter

1 INTRODUCTION AND LITTERATURE REVIEW

The fast-paced development of next generation sequencing technology has increased the availability of high-quality DNA sequences for an ever-increasing number of living systems. Combined with the parallel development of the precise genome editing tool CRISPR, this has paved the way for the investigation of gene function by inducing loss-of-function mutations in gene encoding sequences in a broad set of organisms (Boel et al., 2016). However, this approach is not without its problems, as adverse effects of the use of CRISPR has surfaced in the last few years (Mack & Russell, 2021). Also, recent discoveries in zebrafish (*Danio rerio*) and *C. elegans* show that compensatory mechanisms triggered by CRISPR-use can mask the phenotypic effects of gene knockouts, making it hard to assess the role and importance of a gene (El-Brolosy et al., 2019; Serobyan et al., 2020).

In this thesis, the CRISPR-based genome editing system prime editing (PE) was explored as an alternative loss-of-function method to avoid the unintended editing outcomes seen in the wake of regular CRISPR-Cas9 editing. PE was applied with the aim of establishing the technique in zebrafish in our lab, and to circumvent the compensatory response as a secondary aim. PE was also tested in salmon cells, as the system has not yet been applied successfully in salmon.

This introduction starts with a short overview of loss-of-function methods including a short section on the CRISPR system, followed by a detailed description of the PE system. The recently discovered compensatory response and its mechanism will be described, before different aspects of the models used in this thesis is discussed and the aims of the thesis are presented.

1.1 Loss-of-functions methods

Loss-of-function studies have been crucial to discover and elucidate gene function in a wide range of systems (Housden et al., 2017). DNA and RNA can be targeted and perturbed to reduce or fully ablate gene function, and gene function can then be inferred by observing the phenotypic consequences of the impaired or absent gene product. Methods for generating loss-of-function models include gene knockdown and gene knockout, targeting specific, predetermined RNA and DNA sequences, respectively (Zimmer et al., 2019).

1.1.1 Gene knockdown

Classical gene knockdown (KD) by antisense oligonucleotides is not a 'pure' genetic approach as it does not target and change genomic sequences, but rather the transcripts produced by the gene of interest in the form of mRNA or pre-mRNA (Stainier et al., 2015). Regardless, KD approaches such as the use of morpholinos (MOs) has been extensively used in genetic research (Kher et al., 2011). MOs are synthetic anti-sense oligonucleotides (Summerton & Weller, 1997) blocking either mRNA splicing or -translation, depending on the design (Summerton and Weller 1997; Draper, Morcos, and Kimmel 2001), which results in loss of gene product.

More recently however, a CRISPR-based KD approach (CRISPRi) have been developed (the CRISPR system is described in section 1.1.2), which targets DNA and sterically blocks transcription factors or polymerases from accessing specific sequences, thereby inhibiting transcription initiation or -elongation (Huang et al., 2016).

1.1.2 Gene knockout

Targeted gene knockout (KO) is performed by programmable endonucleases, which induces sequence specific DNA double stranded breaks (DSBs). Gene KO is achieved after DSB repair by the non-homologous end joining pathway, a template-free and error-prone mutagenic repair pathway that often result in the insertion or deletion (indel) of DNA bases at the break site upon repair (Lieber, 2010). The addition or loss of bases not in multiple of three in gene encoding sequences causes frameshift mutations and results in generation of premature termination codons (PTCs). PTC-bearing mRNA transcripts are degraded by the nonsense-mediated decay (NMD) pathway (Kurosaki et al., 2019), resulting in no translation. If escaping degradation, mutated mRNA is translated into a truncated protein, leading to hypomorphic or ablated gene function (Cox et al., 2015).

The CRISPR-Cas9 system confer multiple advantages over other programmable genome-editing nucleases with respect to cost, efficiency, ease of use and target design, which has contributed to its widespread use as a gene KO tool among other uses over the last ten years (Adli, 2018). The system consists of an RNA-guided endonuclease (Cas9) and a single guide RNA (sgRNA). The sgRNA contains a variable 5' spacer sequence of 20 base pairs (bps) which can easily be altered to target any genomic sequence (Doudna & Charpentier, 2014). Complexing with Cas9 through interactions between the protein and the invariable sgRNA 3' scaffold sequence, the sgRNA guides the endonuclease to its genomic target, where the latter induces a DSB (Jinek et al., 2012). The main limitation of the system is the need of a protospacer adjacent motif (PAM) just downstream of the target sequence, which is required for Cas9 binding (Jinek et al., 2012). Upon PAM recognition, Cas9 facilitates unwinding of upstream DNA allowing for RNA-DNA hybridization given sequence complementarity. Hybridization is followed by cleaving of both DNA strands by the Cas9 endonuclease domains RuvC and HNH some bases upstream of the PAM (Jinek et al., 2012). The 10 or so PAM-proximal nucleotides of the sgRNA comprises the 'seed sequence'. Mismatches between the target- and seed sequence is rarely tolerated and results in no DNA binding or -cleavage, while mismatches present in the PAM-distal part of the sgRNA can result in off-target binding and -cleaving (Jiang & Doudna, 2017).

Despite its many benefits, there are some challenges related to CRISPR-Cas9 editing. Off-target editing can cause phenotypic change not related to disruption of the target gene (Kimberland et al., 2018), and CRISPR-Cas9 mediated DSB formation can result in large-scale genomic damage (Mack & Russell, 2021) such as chromothripsis, where DNA breakage leads to a shattering of the genome and the following genomic reorganization upon chromosome reassembly can result in severe genetic diseases and cancer (Leibowitz et al., 2021).

1.2 Prime editing

Prime editing (PE) is a newly developed CRISPR tool able to mediate targeted base insertions, deletions and all possible base-to-base conversions without inducing DSBs (Anzalone et al, 2019), providing a high-precision alternative to regular CRISPR-Cas (Gao et al., 2021; Jang et al., 2021; Schene et al., 2020). Taking the genome-editing world by storm, there are now 366 papers on prime editing available on PubMed alone since the

original paper was published late in 2019, and the system has already been successfully applied in plants (Li et al., 2020; Lin et al., 2020), mammals and mammalian cells, including human embryonic kidney 293 (HEK) cells (Anzalone et al., 2019; Liu et al., 2020; Park et al., 2021), fish (Petri et al., 2021) and insects (Bosch et al., 2021).

The PE system comprises two components, a protein complex (PE2) and a prime editing guide RNA (pegRNA). The PE2 consists of a Cas9-H840A nickase (Cas9 mutant nicking the strand not hybridising with the sgRNA spacer sequence) fused to a reverse transcriptase (RT), which has been mutated to increase reverse transcription efficiency at 37 °C (Anzalone et al., 2019). The pegRNA is a sgRNA with an extended 3'-end. Embedded in the very end of the pegRNA 3'-extension is a primer binding site (PBS) sequence, followed by an RT template sequence encoding the desired edit. PE2 binds the pegRNA through interactions between the nickase and pegRNA scaffold sequence, and is guided by the pegRNA to the target DNA where induces a nick. The pegRNA PBS then anneals to the DNA sequence just upstream of the nick as it is designed to be complimentary to this, and the RT template sequence is reverse transcribed by the RT onto the 3' end of the nicked DNA (Anzalone et al., 2019). An intermediate product containing two redundant single stranded DNA 'flaps' with either an exposed 3'- or 5'-end is produced. The flap with an exposed 5'-end contains wild type sequence, the flap with an exposed 3'-end contains edited sequence. They anneal to the complimentary genomic sequence interchangeably (Anzalone et al., 2019), and hybridization of the 3' flap is favoured as exposed 5' ends are vulnerable to degradation (Y. Liu et al., 2004). Integration of the 3'-end flap generates a heteroduplex which upon DNA mismatch repair can result in either the incorporation of the edit or the original wild type-sequence in the genome.

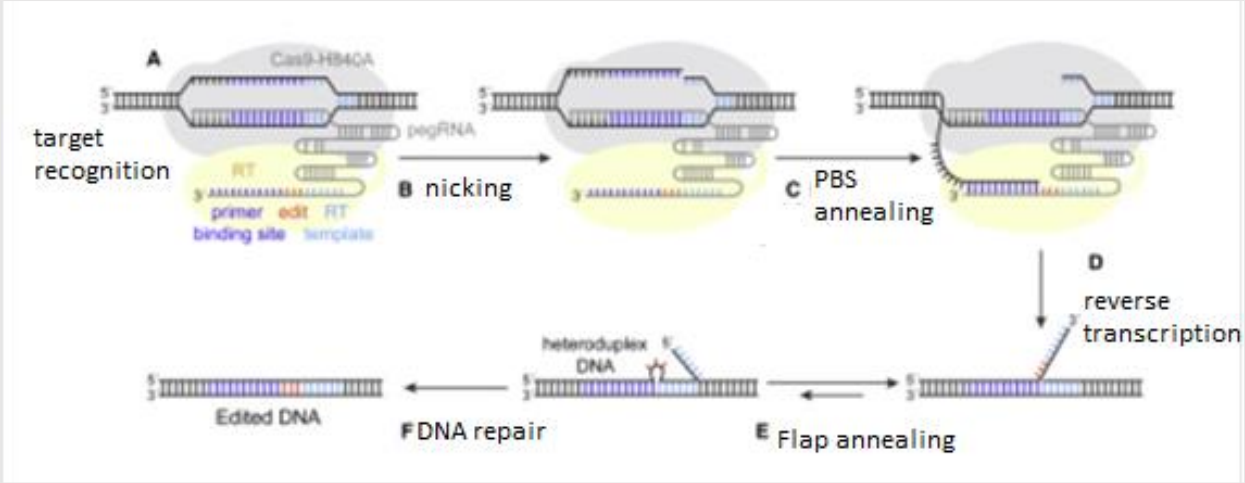

*Figure 1.1. Mechanisms of Prime Editing (PE): **A**: A Cas9 nickase (grey) fused to reverse transcriptase (RT, yellow) is brought to its genomic target by the 5' pegRNA spacer sequence (pegRNA shown as a grey line). The pegRNA 3' primer binding site is shown in dark blue, and the RT template in light blue. The intended edit encoded in the template is shown in red. **B** and **C**: The nickase induces a nick in the target sequence, and the PBS anneals to the 3' end of the nicked DNA. The exposed 3'-OH group on the DNA upstream of the nick functions as a primer for the RT, and the RT template sequence is reverse transcribed onto the 3' end of the nicked DNA strand (**D**). **E**: After reverse transcription occurs, the PE complex dissociates and the resulting 5' and 3' flaps anneal interchangeably, and upon 5' flap degradation by nucleases, the 3' flap containing the edit is integrated to the target site, creating an area of heteroduplex DNA. **F**: integration of the edit into the genomic sequence upon DNA repair where the edited strand has been used as template for mismatch correction. Figure adapted from Yan et al. (2020).*

An additional sgRNA targeting the edited strand can be delivered with the PE components to increase the chance of integrating the edited sequence. The additional sgRNA leads the PE2 to nick the unedited strand, which directs the cell's DNA repair machinery to use the edited strand as a template when resolving the heteroduplex. Two versions of this strategy exist: PE3, where the nsgRNA nicks >20 bps away from the edit, and PE3b, where the nsgRNA seed sequence is designed to match the edit, so that nicking and recruitment of the DNA repair machinery only will occur after PE has resulted in a heteroduplex DNA (Anzalone et al., 2019).

Compared to regular CRISPR-Cas9, PE reduces the occurrence of off-target effects as complementarity between the pegRNA PBS and target DNA is required in addition to that of the sgRNA and protospacer, and precision is further increased as RT-product and target DNA complementarity is required as well (Anzalone et al., 2019). While CRISPR-Cas9-mediated integration of specific sequences, targeted substitutions and deletions are possible (a method called 'CRISPR knock-in') (Uddin et al., 2020), the efficiency and precision of this approach is low (Yang et al., 2021) and usually restricted to specific

stages of the cell cycle of dividing cells (Matsumoto et al., 2020). PE has been found to more precisely and equally or more efficiently install insertions, deletions and substitutions compared to CRISPR-Cas9 (Anzalone et al., 2019; Jang et al., 2021; Park et al., 2021; Petri et al., 2021) and is not dependent on specific cell cycle stages for successful editing outcomes (Anzalone et al., 2019)

1.3 Delivery methods of genome editors in animal systems

Delivery methods of genome editors includes microinjection, where mRNA or ribonucleoprotein (RNP) complexes (complexes comprising protein and RNA, for example Cas9 and sgRNA) are injected into embryos in the one-cell stage for *in vivo* genome editing. Using a micropipette connected to a microinjector providing pressure, genome editing constructs are injected into the cell or yolk (Xin & Duan, 2018).

For delivery of constructs into cultured cells, electroporation has proven effective (reviewed for example by Lino et al., 2018). Cultured cells are added to a solution of RNP complexes, mRNA or plasmids, and a high-voltage shock is then applied to the cells causing transient increase in cell membrane permeability. This allows for highly increased cellular uptake of surrounding RNP, mRNA or plasmid and subsequent genome editing (Neumann et al., 1982).

1.4 Zebrafish

The zebrafish (*Danio rerio)*, a small freshwater teleost, is an important model organism for the study of vertebrate development and genetics (Ribas & Piferrer, 2014) due to its short generation time and its eggs being externally fertilized and transparent, allowing for phenotypic observations in all embryonic stages (Malicki et al., 2002). The zebrafish genome comprises 26.200 genes distributed over 25 chromosomes, and contains numerous ohnologues (duplicated genes retained after a whole genome duplication event) from a teleost-specific whole genome duplication event taking place early in the teleost lineage, in addition to whole genome duplication events in the early vertebrate lineage (Glasauer & Neuhauss, 2014). It also has a high degree of species-specific genes relative to most other vertebrates (Howe et al., 2013), stemming from additional gene duplications occurring within the zebrafish lineage (Lu et al., 2012).

1.4.1 Genome editing in zebrafish

The use of MOs is the main, widely used KD technique in zebrafish, as other approaches such as RNA interference has had limited success in the species (Kelly & Hurlstone, 2011; Pauli et al. 2015). Since first being used in zebrafish in 2000 (Nasevicius & Ekker, 2000), the use of MOs has expanded greatly, and well over 2000 papers on zebrafish MO treatments has been published (Housden et al., 2017). After CRISPR in 2013 proved to be an easy and efficient genome editing tool in zebrafish (Hwang et al., 2013, Jao et al., 2013) further use of CRISPR-Cas9 genome editing was triggered, and as of now there are over 1000 publications on zebrafish CRISPR genome editing listed in PubMed. In 2021, zebrafish embryos was successfully edited using PE, showing up to 30% editing efficiency (Petri et al., 2021). Comparison of targeted mutations induced by PE and CRISPR-Cas9 at several target sites showed PE inducing correct insertions, deletions and base substitutions as or more efficient than CRISPR-Cas9, and with higher precision (Petri et al., 2021).

1.5 Phenotypic discrepancies and genetic compensation in zebrafish

In the wake of the increased use of CRISPR-Cas9 in zebrafish, discrepancies between zebrafish phenotypes produced by KD and KO of the same genes have surfaced (Kok et al., 2015). Where observable change in phenotype of morphants (MO treated individuals) has been reported, the same phenotypes have not been recapitulated in mutants (genome edited individuals) in up to 70% of zebrafish genes, when phenotypic consequences of KO and KD on the same genes has been compared (Kok et al., 2015). As the nature of gene KO by genome editors allows for complete ablation of gene expression while gene KD only reduces expression, gene KO would generally be expected to cause a more pronounced phenotype (Bunton-Stasyshyn et al., 2019). An interpretation of the phenomenon has been that genes found in MO KD experiments to be important or essential for development are in fact not when KO experiments on the same genes have found the opposite, and that impaired or catastrophic phenotypes produced in the KD cases are not due to a lack of functional genes or gene expression, but rather MO toxicity (Kok et al. 2015).

For several of the genes where such discrepancies have been observed, MO toxicity and off-target effects has been ruled out as the cause of phenotypic difference by various means, such as CRISPRi, MO titration and injection of gene specific MOs into mutants

lacking the MO target genes (Rossi et al., 2015; Sztal et al., 2018; Zhu et al., 2017). Interestingly, only mutants carrying frameshift mutations was found to display no phenotype (i.e. phenotype similar to unedited wild-type), and genes homologous to the mutated ones showed significant upregulation in the frameshift mutants, leading to the hypothesis that some compensatory effect caused the phenotypic disjunctions (Rossi et al., 2015; Sztal et al., 2018; Zhu et al., 2017).

Exploring this potential compensatory effect further, El-Brolosy et al. (2019) knocked out six zebrafish genes and observed subsequent increase in expression levels of genes homologous to the mutated ones in mutants carrying frameshift mutations resulting in premature stop codons (PTCs). Protein loss-of-function proved not to be the trigger of the compensatory effect, as injection of wild-type mRNA into mutants did not decrease mRNA expression of the upregulated genes (El-Brolosy et al., 2019). Levels of mutated mRNA were found to be low compared to the pre-mRNA levels, indicating that mRNA decay is involved in the response, and that it is mutant mRNA rather than the DNA lesion itself that is triggering compensation in frameshift mutants (El-Brolosy et al., 2019). Probing the role of RNA degradation in this context, both El-Brolosy et al. (2019) and Ma et al. (2019) both found that the compensatory effect was impeded by inhibition of components in the NMD pathway. Both groups also found signs of increased methylation at the transcription start sites of the upregulated homologous genes, as well as the need for a certain degree of nucleotide identity between the aberrant transcript and the upregulated homologues (El-Brolosy et al., 2019; Ma et al., 2019).

The studies by El-Brolosy et al. (2019) and Ma et al. (2019) have been used to propose a model of the compensatory response. Termed the genetic compensation response (GCR) by Ma & Chen (2020), the model suggests that certain genetic mutations trigger the upregulation of expression of genes homologous to the mutated one, which in turn masks the mutant phenotype (illustrated in *Figure 2.1*). The model proposes that certain transcripts containing frameshift mutations resulting in PTCs are recognized by proteins involved in the NMD pathway. Either a 'regular' NMD factor, Upf1, leading to fragmentation (El-Brolosy et al., 2019) or a factor thought to preserve the transcript in its entirety, Upf3a (Ma et al., 2019), is recruited to the PTC-bearing transcript, on this the studies differ. The PTC-bearing transcript (or its fragments) is believed to associate with the COMPASS methylase complex. The complex is then guided to sequences homologous

to the mutated one by the PTC-bearing transcript (or its fragments) and the COMPASS complex is thought to methylate the transcription start sites of the homologous genes, resulting in upregulated expression of compensatory homologues which masks the mutant phenotype (El-Brolosy et al., 2019; Ma et al., 2019).

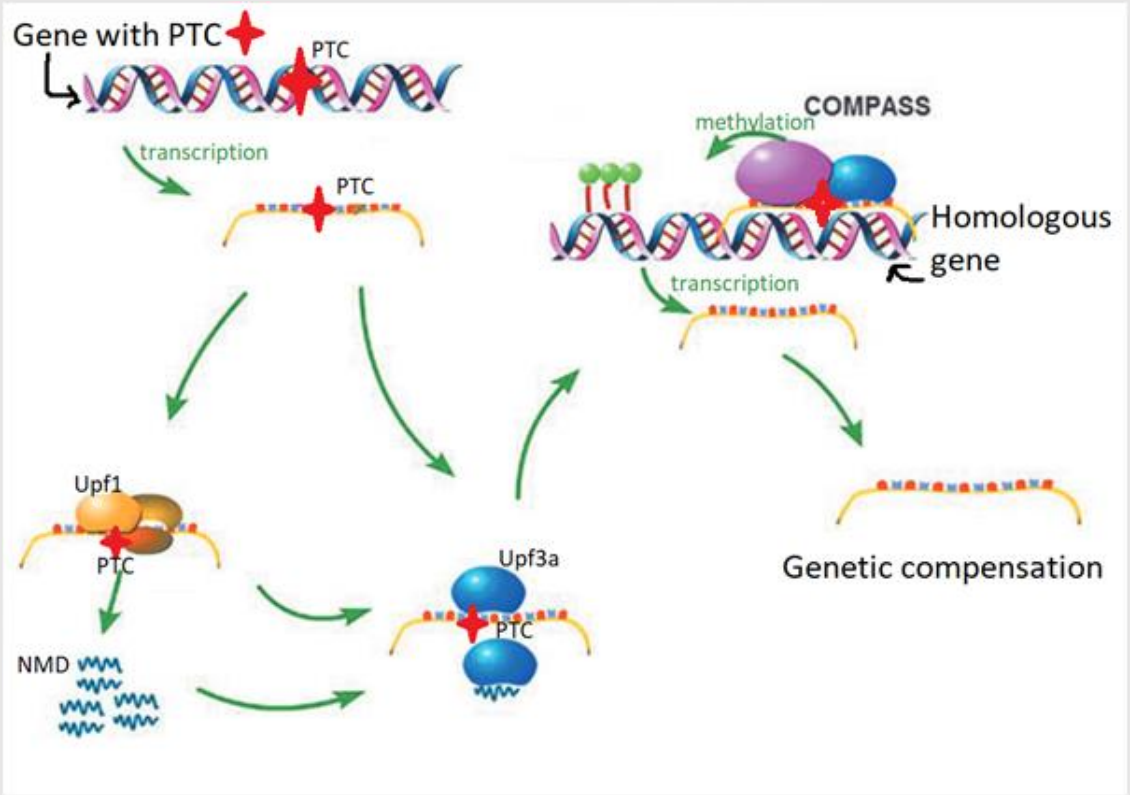

Figure 1.2. Figure showing the proposed pathway of the genetic compensation response. A gene containing a premature termination codon (PTC, illustrated as a red star) is transcribed, and Upf-proteins are recruited to the complex. Both Ma & Chen's (2020) and El-brolosy et al.'s (2019) findings of Upf recruitment and fragmentation or conservation of the transcript is included here. The PTC-bearing transcript or its fragments complexes with the COMPASS complex, and is relocated into the nucleus, where complementarity between the transcript (or fragments) and homologous gene sequences guides the transcript-bound COMPASS complex to these genes. The complex then methylates the nearby transcription start sites, which results in polymerase recruitment and upregulated gene expression. Figure adapted from Ma & Chen (2020).

1.5.1 Genetic compensation and phenotypic discrepancies in other organisms

After its discovery in zebrafish, the GCR has been identified in *C. elegans*, where genetic compensation is observed in response to knockout of the genes *act-5* and *unc-89* (Serobyan et al., 2020). Thus, the GCR is not a phenomenon limited to neither teleosts nor vertebrates. Although GCR has not been identified in other model organisms as of yet, knockout of certain genes in mutant mouse embryonic fibroblast and stem cells results in upregulation of similar genes, leading researches to suspect that the GCR is at play also

in these cells (El-Brolosy et al., 2019). Also, difference in KD and KO phenotypes has been observed in *Drosophila* and *Arabidopsis* (Tiebe et al., 2018, Y. Gao et al., 2015), although potential off-target effects of KD constructs has not been investigated as the potential cause for the phenotypic differences to the same degree in these instances.

1.5.2 Circumventing genetic compensation

In the case of gene KOs, genome editors are usually designed to target coding sequences close to the N-terminus, but downstream of any alternative start codon (Doench, 2018), as frameshift mutations early in the protein are more likely to introduce PTCs and disrupt protein function (Doench et al., 2014). The use of targeting nucleases is thus likely to cause a compensatory response when targeting genes able to elicit it. A proposed genome editing strategy for circumventing the GCR when performing gene KO is to target gene sequences encoding protein domains and amino acids critical for protein function and generate mutants carrying in-frame deletions (Sztal & Stainier, 2020), resulting in expression of inactive proteins. PE might be a suitable tool for such an operation, as it potentially can be used for installing precise, in-frame deletions in critical protein domains, and so disrupt gene function without creating frameshift mutations and PTCs in gene encoding sequences.

1.5.3 Zebrafish genes able or potentially able to elicit genetic compensation

Salanga and Salanga (2021) list a number of genes able to elicit genetic compensation in their review of GCR in zebrafish. One such gene is *nid1a,* where KD of *nid1a* interferes with embryonic development, resulting in zebrafish larvae with shortened body length (Zhu et al., 2017), while KO of *nid1a* results in larvae developing normal body length after a delay in growth 4-5 days post fertilization (Ma et al., 2019; Zhu et al., 2017). *nid1a* expresses the structural glycoprotein Nidogen1, involved in the assembly of the basement membrane (a type of extracellular matrix) by linking networks of glycoproteins (Khalilgharibi & Mao, 2021). Consisting of several protein domains, the highly conserved G2 domain is responsible for binding collagen IV and perlecan (Hopf et al., 2001).

Similarly, different treatments for KO of *gnrh3* produce different phenotypes, but the GCR has not yet been explored as the potential cause of the phenotypic discrepancies. *gnrh3* expresses gonadotropin-releasing hormone 3 (GnRH3), a neurodecapeptide central to the regulation of reproduction in vertebrates (Zohar et al., 2010). Similar to the role of the GnRH1 isoform found in mammals, GnRH3 stimulates the release of gonadotrophins

in zebrafish by receptor binding activities (Abraham et al., 2010; Steven et al., 2003). Ablation of GnRH3 producing neurons results in zebrafish infertility (Abraham et al., 2010), while *gnrh3* KO-individuals are still fertile (Spicer et al., 2016). KO of the only zebrafish gnrh isoform *gnrh2* in addition to *gnrh3* has ruled out a compensatory role for *gnrh2,* as both *gnrh3*$^{-/-}$ and *gnrh3*$^{-/-}$*/gnrh2*$^{-/-}$ individuals are fertile (Marvel et al., 2018).

In this project, the two genes described above were selected as targets for PE-mediated in-frame deletions in zebrafish.

1.6 Atlantic salmon

The genome of the family Salmonidae differs from most other teleosts as the salmonid ancestral species recently underwent an additional species specific whole genome duplication event (Allendorf & Thorgaard, 1984). For the Atlantic salmon (*Salmo salar*), this has resulted in a genome consisting of an estimated 37.200 genes on 29 chromosomes (Lien et al., 2016). Being an important production animal, genome editing in Atlantic salmon for uncovering the genetic basis of production-related traits and improving these is of much interest (Gratacap et al., 2019), and CRISPR-Cas has enabled efficient genome editing in the non-model species (Edvardsen et al., 2014). Biallelic mutations in Atlantic salmon have for example been successfully introduced with CRISPR-Cas9, leading to knockout of the pigmentation genes *tyr* and *slc45a2* (Edvardsen et al., 2014), and our lab has established CRISPR-mediated KO of *abcg2-b*, a gene putatively involved in Atlantic salmon flesh coloration (Wagnerberger, 2020). CRISPR-Cas9-mediated gene knock-in was recently successfully performed (Straume et al., 2020; Straume et al., 2021), but there are no reports on successful PE in Atlantic salmon as of yet. Not until 2020 was the first Atlantic salmon cell line successfully edited using CRISPR-Cas9, when Gratacap et al. (2020) edited Atlantic salmon head kidney cells (SHK-1) and Atlantic salmon kidney cells *in vitro* by electroporation of CRISPR-Cas9 RNP complexes.

1.7 EGFP

EGFP is an enhanced, constitutively green fluorescent protein. Three amino acids (at position 65, 66 and 67) forms the protein chromophore, which emits green fluorescence in the presence of UV light (Heim et al., 1994). A base substitution in EGFP (196T>C) results in a change in the codon and corresponding amino acid at position 66 (Y66H) within the chromophore of the protein, changing the fluorescence from green to blue (Heim et al., 1994). Green to blue color conversion has for example been used to measure

CRISPR-Cas9-mediated gene knock-in success (Glaser et al., 2016). In this thesis, EGFP in two different models (described below) was chosen as a target for PE-mediated color conversion for easy detection of successful editing outcomes, and EGFP KO by a targeted three-base pair PE-deletion of the central amino acid in the chromophore in one of the systems.

1.7.1 vas::EGFP transgenic zebrafish

A transgenic zebrafish line expressing EGPF has been established by Krøvel and Olsen (2002). In this line, EGFP is expressed under the *vasa* locus, which regulates the expression of VASA and subsequent germ cell development. EGFP-expression under this locus enables tracking of primordial germ cells during zebrafish embryonic development (Krøvel & Olsen, 2002).

1.7.2 EGFP-SHK-1 cells

The SHK-1 cell line was established by Dannevig and colleagues (Dannevig et al., 1995), and our lab has created EGPF-expressing SHK-1 ('EGFP-SHK-1') cells, where ~70 % of the cell population expresses EGFP and fluoresce green (Noman Reza, personal communications).

1.8 Aims of the thesis

This thesis has two main aims, both regarding the application of PE in fish:

1. To establish the protocol for PE by microinjection of RNP complexes in zebrafish in our lab, targeting EGFP and using conversion of green to blue fluorescence to measure success.

   As a secondary aim, PE will be explored as an alternative gene knockout approach to avoid or investigate the presence of the genetic compensation in zebrafish by introducing in-frame deletions in critical protein domains of *nid1a* and *gnrh3*, respectively.
2. Test PE for the first time in Atlantic salmon, targeting EGFP in green fluorescent salmon cells using PE both to make a targeted substitution for color conversion, and perform a targeted three-base deletion for EGFP KO.

2. MATERIALS AND METHODS

All PCR primers used in the experiments in this project were designed using Primer3 (Primer3web version 4.1.0, https://primer3.ut.ee/). Plasmid design and DNA alignment and sequence visualisation was done using Benchling (https://www.benchling.com).

2.1 Experimental outline

In this project, prime editing was tested in zebrafish embryos and Atlantic salmon cells. Targets were selected and pegRNAs designed for both systems. Synthetic pegRNAs and PE2 protein was ordered and microinjected as RNP complexes into zebrafish embryos. pegRNA-expressing plasmids were constructed and electroporated into cells together with PE2-expressing plasmids. Cells were also electroporated with an RNP complex targeting EGFP in zebrafish. Editing outcomes were detected in both systems by different means (visual assessment, sequencing and flow cytometry). The experimental outline is visualized in *Figure 2.1.*

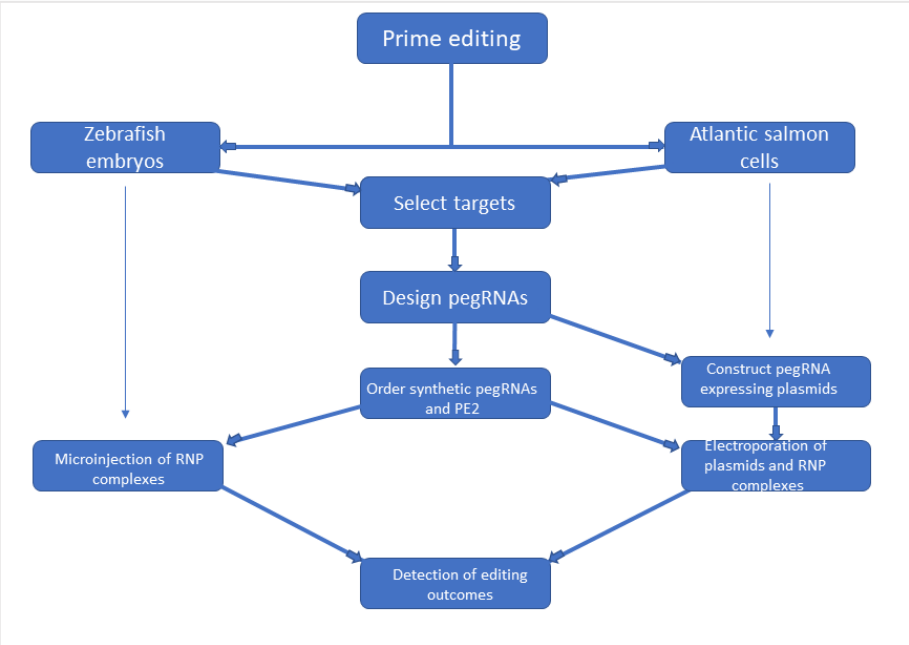

Figure 2.1. Flow chart describing the experimental outline of this project. Prime editing was applied to two systems (zebrafish embryos and Atlantic salmon cells). Target genes were chosen and pegRNAs designed for both systems. Synthetic pegRNAs were ordered together with the PE2 protein, complexed and microinjected into zebrafish embryos. PegRNA-expressing plasmids were constructed and electroporated into Atlantic salmon SHK-1 cells together with PE2-expressing plasmids. One of the RNP complexes generated for zebrafish microinjections targeting EGFP was also used in electroporation of cells. Editing outcomes in both systems were detected by various means (visual assessment, sequencing and flow cytometry).

2.2 pegRNA design

The design of each pegRNA used in this experiment is described in detail in this chapter, after a brief explanation of the design process in general.

EGFP and the zebrafish genes *nid1a* and *gnrh3* were chosen as PE targets, the former gene was chosen as it allows for easy, visual detection of PE outcomes, the two latter were chosen as they allow for testing PE as a knockout-tool able to circumvent or potentially detect the GCR. pegRNAs targeting the genes were designed using pegFinder (http://pegfinder.sidichenlab.org/), an online tool designing and ranking pegRNAs for genetic modifications at any genomic site. 500 base pair (bp) target wild-type sequence was provided as input, where approximately 250 bases flank the site to be edited, along with a second input: 500 bp of the same sequence, but containing the intended edit. A sgRNA guide sequence is given as output, chosen by the program based on the distance between the induced nick and the intended edit, along with RT template- and PBS sequences of varying lengths and the invariable scaffold sequence (Chow et al., 2021). RT-templates encoding changes that disrupts the PAM and/or target sequence after prime editing were chosen, as this inhibits rebinding of PE2 and increases the chance of successful editing (Anzalone et al., 2019; Chow et al., 2021). RT template- and PBS sequence lengths were chosen based on the recommendations of Petri *et al.* (2021) of 8-13 bps for RT template sequences and 12-17 bps for PBS sequences for *in vivo* editing of zebrafish when possible. The sequences suggested by pegFinder were chosen for pegRNA constructs used in *ex vivo* PE in Atlantic salmon EGFP-SHK-1 cells. pegRNA RT templates were designed so that the 5' most base was not a cytosine, as a cytosine in this position is believed to impair PE efficiency by interacting with other pegRNA-bases, forming secondary structures (Anzalone et. al 2019).

2.2.1 EGFP

The EGFP sequence information used to design EGFP-targeting pegRNAs was downloaded from Addgene (Addgene, #45561) to Benchling for visualization. The codons comprising the EGFP chromophore were identified and annotated in order to design two pegRNAs, one for converting the fluorescence from green to blue by a single base substitution, and one for knocking out the fluorescence by the removal of the three bases comprising the middle amino acid in the chromophore.

The pegRNA for color conversion ('G->B pegRNA') was designed to encode a single base substitution resulting in the change of amino acid 66 within the EGFP chromophore from tyrosine to histidine, by changing the first nucleotide of the tyrosinase-encoding codon from thymine to a cytosine, see *Figure 2.2*. The base substitution results in disruption of seed sequence binding.

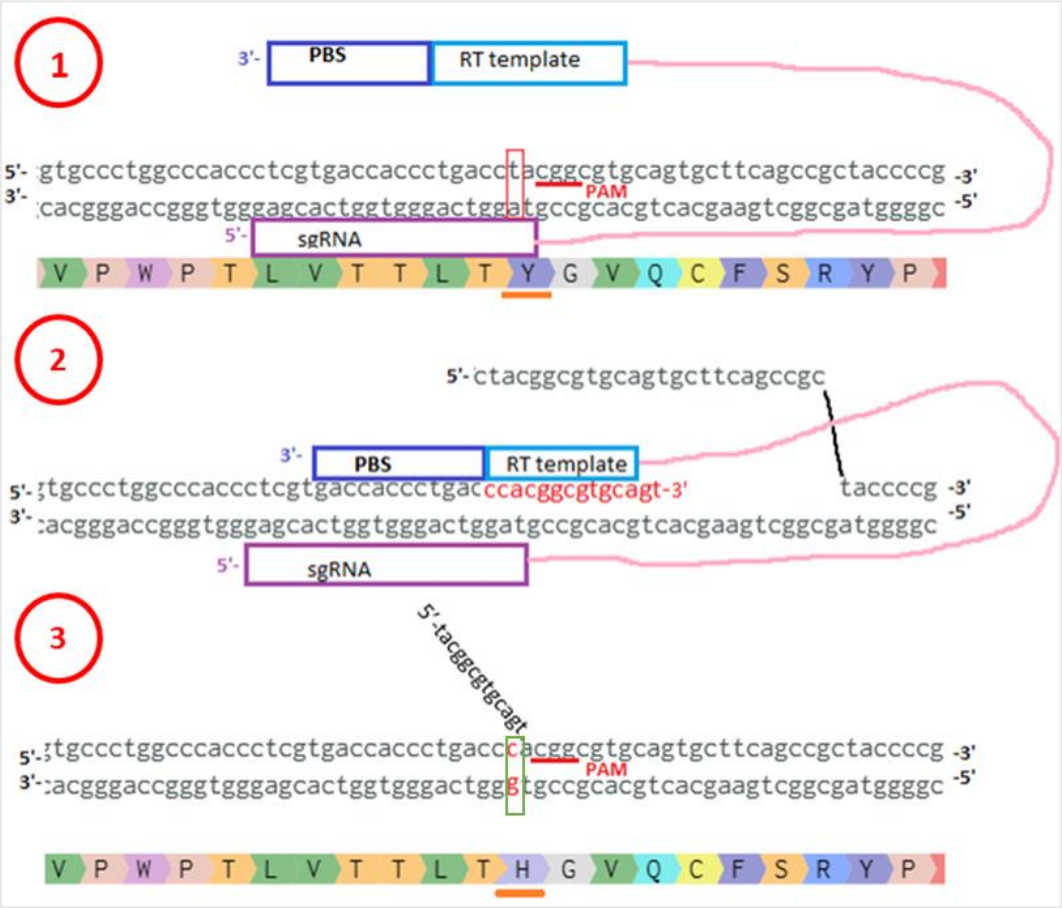

Figure 2.2: Mechanics of the EGFP-targeting pegRNA for conversion of color. 1): Positioning of the gRNA on the EGFP encoding sequence. Amino acids are aligned to their corresponding codons. The sequence within the red box contains the base pair to be changed, and underlined with orange is the amino acid to be changed. 2) Positioning of the pegRNA after PE2 nickase and RT activity. The sequence in red is the reverse transcribed pegRNA RT template sequence. 3) Resulting sequence after reverse transcription and successful integration of the edit, the new base pair is marked in red, and the substitution results in the codon encoding a new amino acid. The PAM sequence is intact after edit, but the seed sequence altered. The 5' sequence is the 5' flap containing wild type sequence, which is degraded by nucleases. The pink loop in the pegRNA is the nickase-interacting scaffold sequence.

The pegRNA for EGFP KO ('KO pegRNA') was designed the same way using the same PBS and gRNA sequence as the color converting pegRNA, but where the RT template encoded the deletion of the three bps comprising the tyrosine-encoding codon (TAC). Mechanisms

of pegRNAs encoding deletions are illustrated in *Figure 2.3* and *2.5* in the following sections, positioning of pegRNA PBS and sgRNA on the EGFP target sequence is illustrated in *Figure 2.2*. *Table 2.1* in chapter 2.2.4 summarizes the EGFP-targeting pegRNA sequences.

2.2.2 *gnrh3*

Sequence information for zebrafish *gnrh3* was found in the Ensembl database (ENSDARG00000056214) and imported to Benchling. The *gnrh3* mRNA sequence was found in NCBI Reference Sequence Database (NM_182887.2) and aligned to the gene sequence for annotation of exons. The gene is 4455 bp long and consists of four exons, and the GnRH3 decapeptide-encoding sequence is located on the second exon. The zebrafish GnRH3 decapeptide sequence was first identified by Torgersen et. al (2002), and the decapeptide encoding sequence was annotated in the *gnrh3* sequence. The N- and C-terminal parts of the peptide are especially important for GnRH1 receptor binding (Muñoz-Cueto et al., 2020), and Roch et al. (2014) shows that there is high degree of conservation of amino acids in the N-terminal between mammalian GnRH1 and zebrafish GnRH3. Reasoning that the degree of conservation reflects importance for the function of the domain or feature, codons encoding highly conserved amino acids in the N-terminal of the peptide were chosen as PE targets. A pegRNA encoding a 9 bp deletion, removing the 2nd, 3rd and 4th N-terminal amino acids H, W and S in the *gnrh3* decapeptide sequence was thus designed. *Table 2.1* in chapter 2.2.4 summarizes the *gnrh3*-targeting pegRNA sequence (see *Figure 2.3)*.

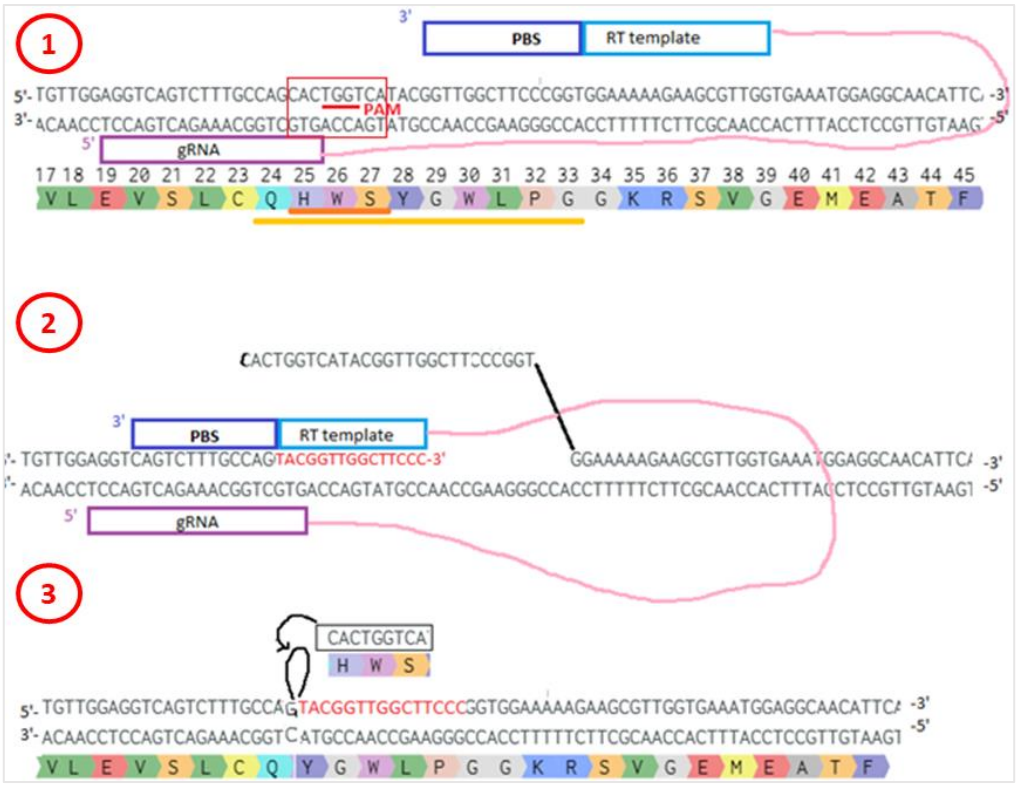

Figure 2.3. Mechanics of the gnrh3-targeting pegRNA. 1) shows pegRNA binding the gnrh3 target sequence. The sequence within the red box encodes the three codons (nine bps) to be removed, and below are their corresponding amino acids underlined with red. The whole amino acid sequence making up the decapeptide is underlined in orange 2) shows positioning of the pegRNA after PE2 nickase and RT activity. The sequence in red is the reverse transcribed pegRNA RT template sequence. 3) Resulting sequence after reverse transcription. Annealing of the newly transcribed sequence will displace the original wild-type sequence on the opposite strand (black hairpin loop). The sequence in red is the reverse transcribed pegRNA RT template sequence. Neither PAM nor the whole seed sequence is present in the resulting sequence if the edit is incorporated. The pink loop in the pegRNA is the nickase-interacting scaffold sequence.

2.2.3 *nid1a*

Sequence information for zebrafish *nid1a* was found in Ensembl (ENSDARG00000068710), and imported to Benchling. The *nid1a* mRNA sequence was found in NCBI Reference Sequence Database (XM_686064.8) and aligned to the gene sequence for annotation of exons. *nid1a* is 76662 bp long and consists of 20 exons. The PE target is located on the sixth exon which is 253 bp long, and the introns flanking it consists of highly repetitive sequences.

The NCBI Conserved Domain Database Search tool was used to identify conserved regions and amino acids of *nid1a* across distantly related species (NCBI Conserved Domain Search (nih.gov)). Conserved protein domains of interests were aligned to the *nid1a* gene sequence and annotated. Codons encoding highly conserved single amino acids were also annotated in the conserved protein domain regions, and used to select a suitable target for *nid1a* KO by PE. The conserved collagen- and perlecan interacting domain G2 found was chosen as a broad target for PE. *Figure 2.3* shows the amino acid sequence alignment of the N-terminal part of the G2 sequence between distantly related species, with amino acids highlighted in yellow being conserved. Reasoning that the degree of conservation reflects importance for the function of the domain, deletion of three of the highlighted amino acids (R, Y and A, see *Figure 2.4*) was chosen as the target for PE, hypothesizing that the loss of these features within the domain will interfere sufficiently with glycoprotein binding, thus disrupting the ability of Nidogen1 to form a stable basement membrane structure.

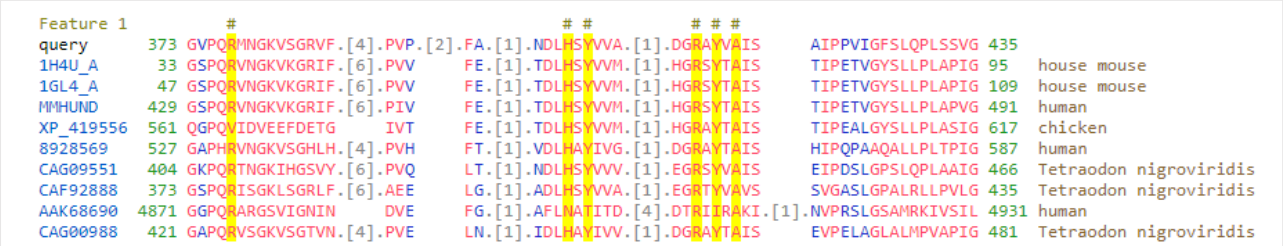

Figure 2.4. Alignment of the N-terminal part of nid1a in different vertebrates, 'G2 domain". The figure shows the 56 first amino acids of the N-terminal part of the G2 domain. Amino acids highlighted in yellow represents highly conserved features within the sequence. 'query' refers to the zebrafish nid1a sequence, to which the nid1a sequences for other species are aligned against. The three rightmost highlighted amino acids, along with the two non-conserved features in between were chosen as a target for PE.

Two amino acids among the three highly conserved ones were included in the deletion, resulting in the design of a pegRNA encoding a deletion of 15 bases, and disruption of the PAM (see *Figure 2.5)*.

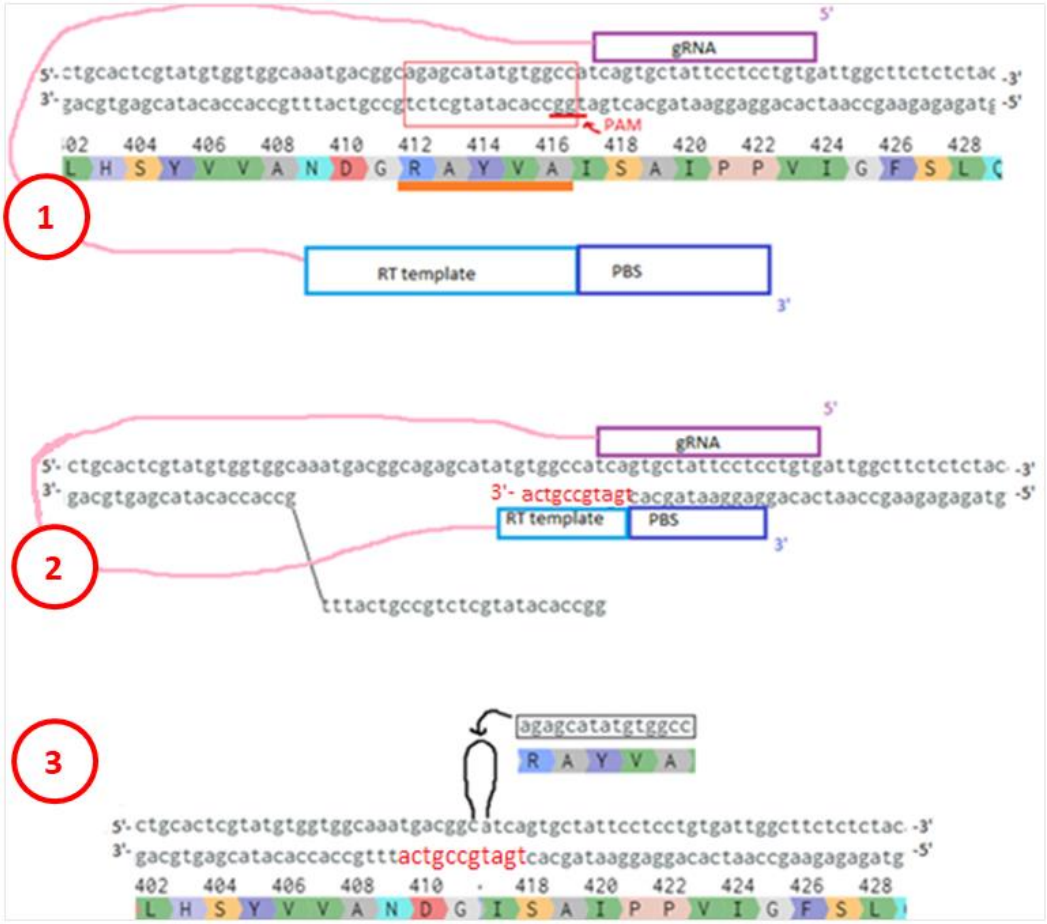

Fig 2.5. Mechanics of the nid1a-targeting pegRNA. 1): Positioning of the gRNA on the nid1a target sequence. Amino acids are aligned to their corresponding codons. The sequence within the red box is the five codons (15 bps) to be removed, and underlined with orange are their corresponding amino acids. 2) Positioning of the pegRNA after PE2 nickase and RT activity. The sequence in red is the reverse transcribed pegRNA RT template sequence. 3) Resulting sequence after reverse transcription. Annealing of the newly transcribed sequence will displace the original wild-type sequence on the opposite strand (black hairpin loop). The sequence in red is the reverse transcribed pegRNA RT template sequence. Neither PAM nor the whole seed sequence is present in the resulting sequence if the edit is incorporated. The pink loop in the pegRNA is the nickase-interacting scaffold sequence.

2.2.4 pegRNAs for *in vivo* editing

pegRNAs for *in vivo* editing of zebrafish embryos by microinjection of RNP complexes were ordered from Integrated DNA Technologies (IDT). Following the recommendations from Petri *et. al* (2021) and Gao et al. (2021) for modifications on synthetically manufactured pegRNAs, 3' phosphorothioate internucleotide linkages and 2'-O-methyl analogues were added to the three first (5'-most) and last (3'-most) RNA nucleotides to increase RNA nuclease resistance and decrease RNA degradation. Three uridines were added to the 3'-end of the pegRNAs.

Table 2.1. Table of synthetic pegRNAs, showing their target genes, guide-, scaffold- and 3' extension sequence. Also listed is the type of edit made, and whether the PAM sequence and/or the sequence complimentary to the pegRNA seed sequence is disrupted after installation of the edit.

Target gene	**Guide sequence (5' -> 3')**	**Scaffold (5' -> 3')**	**3'extension (5' -> 3')**		**PAM/seed disruption**	**Edit**
			RT template	**PBS**		
EGFP	CUCGUGACCAC CCUGACCUA	GUUUUAGAGCUAG AAAUAGCAAGUUA AAAUAAGGCUAGU CCGUUAUCAACUU GAAAAAGUGGCAC CGAGUCGGUGC	ACUGCACGC CGUGG	GUCAGGG UGGUCUU U	PAM	Single base substit-ution
gnrh3	AGGUCAGUCUU UGCCAGCAC	GUUUUAGAGCUAG AAAUAGCAAGUUA AAAUAAGGCUAGU CCGUUAUCAACUU GAAAAAGUGGCAC CGAGUCGGUGC	GGGAAGCC AACCGUA	CUGGCAA AGACUGU UU	BOTH	9 bp deletion
nid1a	CACAGGAGGAA UAGCACUGA	GUUUUAGAGCUAG AAAUAGCAAGUUA AAAUAAGGCUAGU CCGUUAUCAACUU GAAAAAGUGGCAC CGAGUCGGUGC	UGACGGCA UCA	GTGCUAU UCCUCUU U	BOTH	15 bp deletion

2.2.5 pegRNAs for *ex vivo* editing

pegRNAs for *in vitro* editing of EGFP in EGFP-SHK-1 cells by electroporation of plasmids were ordered as dsDNA oligos from IDT for ligation into a recipient vector (described in chapter 2.3). When designing the pegRNA-encoding DNA oligos, sequences flanking the pegRNA 5'- and 3'-ends were added, containing recognition- and cut sites for the restriction enzyme BsaI along with six nucleotides added outside of the BsaI recognition site (to the '5- and 3'-most ends of the dsDNA oligos) to enable BsaI cleavage activity close to the ends of the dsDNA oligos.

Table 2.2. Table of DNA oligos encoding EGFP-targeting pegRNAs, listing their guide-, scaffold- and 3' extension sequence. The flanking sequences, containing BsaI recognition- and restriction sites, added to both ends of the dsDNA oligos are also listed, and the BsaI recognition sites are highlighted in yellow. Also listed is the type of edit made, and whether the PAM sequence and/or the sequence complimentary to the pegRNA seed sequence is disrupted after installation of the edit.

		G -> B pegRNA	**EGFP KO pegRNA**
5' flanking sequence (5'->3')		TGCACAGGTCTCACACC	TGCACAGGTCTCACACC
Guide sequence (5' -> 3')		CTCGTGACCACCCTGACCTA	CTCGTGACCACCCTGACCTA
Scaffold sequence (5' -> 3')		GTTTTAGAGCTAGAAATAGCAAGTTAAA ATAAGGCTAGTCCGTTATCAACTTGAAAA AGTGGCACCGAGTCGGTGC	GTTTTAGAGCTAGAAATAGCAAGTTAAA ATAAGGCTAGTCCGTTATCAACTTGAAAA AGTGGCACCGAGTCGGTGC
3'extension sequence (5' -> 3')	**RT template**	ACTGCACGCCGTGG	AGCACTGCACGCCG
	PBS	GTCAGGGTGGTC	GTCAGGGTGGTC
3' flanking sequence (5'->3')		TTTTTGAGACCACGATC	TTTTTGAGACCACGATCT
PAM/seed disruption		SEED	BOTH
Edit		Single base substitution	3 bp deletion

The synthetic G->B pegRNA for EGFP editing in zebrafish was also used for *ex vivo* editing of EGFP-SHK-1 cells by electroporation of RNPs.

2.3 Plasmid construction

Plasmids carrying the pegRNA encoding sequences listed in *Table 2.2* were constructed using regular restriction cloning and Golden Gate cloning.

2.3.1 pU6 and PE2 plasmid DNA extraction

The pU6-pegRNA-GG-acceptor vector ('pU6 plasmid') (Addgene #132777) for expression of pegRNAs and the pCMV-PE2 plasmid carrying PE2 protein ('PE2 plasmid')(Addgene, #132775), both gifts from dr. David Liu, were ordered from Addgene. Both plasmids contain a gene conferring ampicillin resistance, enabling growth of bacteria carrying the plasmids on selective media. The pU6 plasmid contains a monomeric red fluorescent protein ('mRFP') expressed under a mammalian U6 promoter ('pU6').

The bacteria were grown up separately in 5 mL LB broth medium (Invitrogen, 12780052) containing 100 µg/mL ampicillin (Fischer Scientific, BP17605) and grown up overnight at 37 ˚C in a shaking incubator (220 rpm), before being plated and incubated at 37 ˚C for 24 hours. Colonies carrying the pU6 plasmid was identified with red or pink colour due to expression of mRFP. A subset of pink colonies and randomly chosen colonies of bacteria carrying the PE2 plasmid was picked for midiprep using ZymoPURE II Plasmid Midiprep Kit (Zymo Research, D4200) as per manufacturer's instructions, using 50 µl elution buffer instead of 200 µl as to increase plasmid concentration. Plasmid concentration was found using NanoDrop (Thermofisher Scientific, ND-8000-GL).

Verification of the PE2 plasmid was done by enzymatic digestion. 1 µg of PE2 plasmid was digested using 1 µl EcoRV (NEB, R0195S) resulting in two fragments, 3831 and 5922 bps long, and was run on a 1% agarose gel along with along with a 1 kb ladder (GeneRuler 1 kb, ThermoFischer, SM0311).

2.3.2 Exchanging U6 promoters

U6 promoters recruits RNA polymerase III, which expresses short RNA fragments (Nie et al., 2010). The mammalian U6 promoter ('pU6') in the recipient vector has been found not to be effective for RNA expression in fish (Escobar-Aguirre et al., 2019). However, the zebrafish U6 promoter ('ZFU6') has been shown to be functional in Chinook salmon cell lines (Escobar-Aguirre et al., 2019) and in SHK-1 cells by our lab (Noman Reza, personal communications). Thus, the pU6 sequence in the recipient vector was replaced with ZFU6 by means of regular restriction cloning, described in the following sections.

2.3.2.1 PCR amplification of zebrafish U6 promoter

The ZFU6 sequence was amplified by PCR from the plasmid LentiCRISPR-Cas9-2A-mCherryU6ZF (Escobar-Aguirre et al., 2019). The forward and reverse PCR primers were designed to contain tails in their 5' ends, with restriction sites for the restriction enzymes BamHI-HF and BbvCI on the forward and reverse primer, respectively. The primers are listed in *Table 2.3*, and *Figure 2.6* shows their positioning on the ZFU6 sequence.

Table 2.3. Forward and reverse primers for amplification of zebrafish U6 promoter, with tails. PCR primers are highlighted in yellow. Sequences highlighted in green and blue are PCR primer tails containing BamHI and BbvCI recognition- and restriction sites, respectively. The purple sequences are nucleotides added to facilitate later enzyme digestion. The highlighted grey sequence is a tonB terminator sequence, which is cut out during restriction digestion of the recipient vector, and which will be reintroduced upon subsequent ligation of the amplicon into the digested vector.

	Primer sequence	Tm (˚C)
Forward	5'-GGCATCGGATCCCACCTCAACAAAAGCTCCTC-3'	53.1
Reverse	5'- AGTCGTCCTCAGCCAAGTCAAAAGCCTCCGACCGGAGGCTTT TGACTACGGTCTCGGGTGTTTCTGGGAGTCTGGAGGACGG-3'	56.6

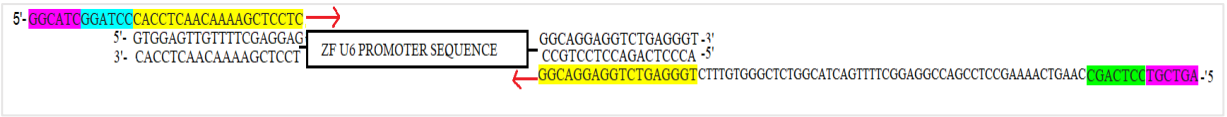

Figure 2.6: positioning of primers with tails. Tails are added to the ZFU6 sequence during PCR and are integrated into the resulting PCR product

PCR was performed using the Platinum II Taq HS DNA polymerase (Invitrogen, 14966001) in a 50 µl reaction following Invitrogen's protocol, before being subjected to the manufacturers recommended 2-step thermal cycling protocol for simple amplicons (<1 Kb), with annealing temperature set to 60˚C.

The resulting ZFU6 PCR product is 469 bp long. A small aliquot of the PCR reaction was run on a 1.7% agarose gel along with a 100 bp ladder (GeneRuler 100 bp DNA Ladder, ThermoFischer SM0241) to confirm successful amplification and the remaining PCR reaction was cleaned up using the column-based DNA Clean & Concentrator-25 kit from Zymo Research (D4005), before assessing the concentration using NanoDrop.

2.3.2.2 Restriction digestion and ligation

For the digestion reaction, 1 µg of pU6 plasmid and the cleaned ZFU6 PCR product was digested separately with 1 µl each of BbvCI and BamHI-HF (NEB; R0601S, R3136S). The BbvCI restriction site is positioned so that more than the pU6 sequence is cut out of the vector. The additional sequence removed (a tonB terminator sequence) will be reintroduced to the vector upon ligation of the amplified ZFU6 fragment into the vector.

The pU6 plasmid is 3004 bp (bp) long, and successful digestion produces two fragments which are 2683 and 321 bps in length. Digestion of the ZFU6 PCR product results in a 454 bp long fragment plus two short fragments of 10 and 11 bps.

The digested ZFU6 PCR product was cleaned as described in Section 2.3.2.1, removing the short fragments generated during the restriction reaction as these are too small to be retained in the DNA binding column.

The digestion reaction was run along with a 1 kb ladder on a 1% agarose gel, and the band with linearized plasmid devoid of pU6 sequence was cut out of the gel. DNA was extracted using QIAquick Gel Extraction Kit (QIAGEN, 28706) before concentration was measured using NanoDrop. The digested ZFU6 PCR product and the promoter-less linearized pU6 vector was run on a 1% gel along with the 1kb ladder to confirm the presence and correct length of both.

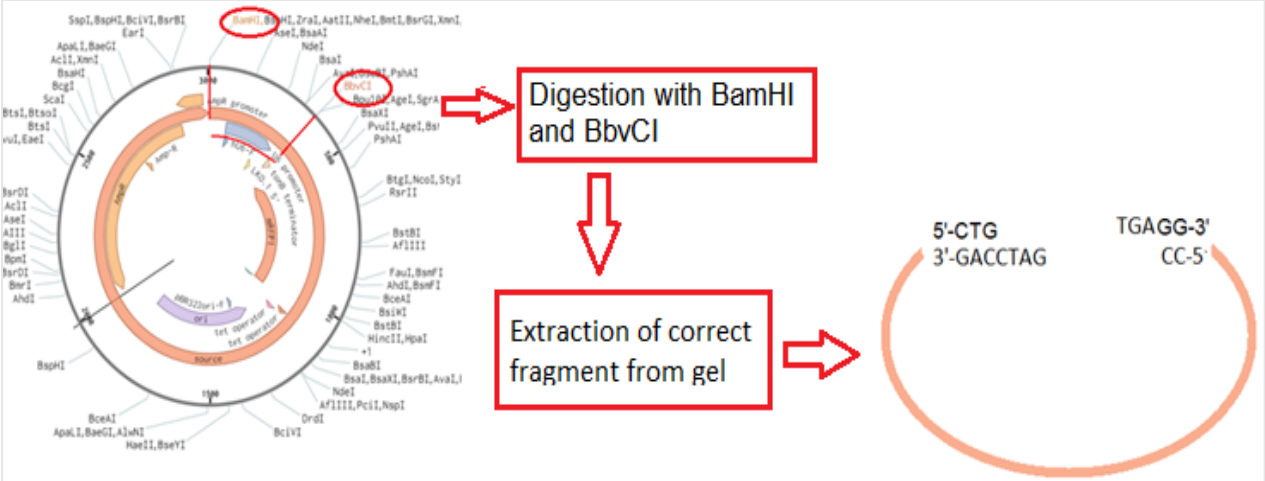

Figure 2.7: Digestion of the pU6-pegRNA-GG-acceptor plasmid by restriction enzymes BamHI and BbvCI (cut sites marked with red lines on the circularized plasmid to the left) generates two fragments: a longer fragment consisting of most of the plasmid sequence, and a shorter fragment containing the pU6 sequence (not shown in the figure). Running the digestion reaction on a gel, linearized plasmid backbone devoid of the pU6 promoter sequence can be extracted from the gel and purified, resulting in a linearized plasmid with non-palindromic 5' overhangs.

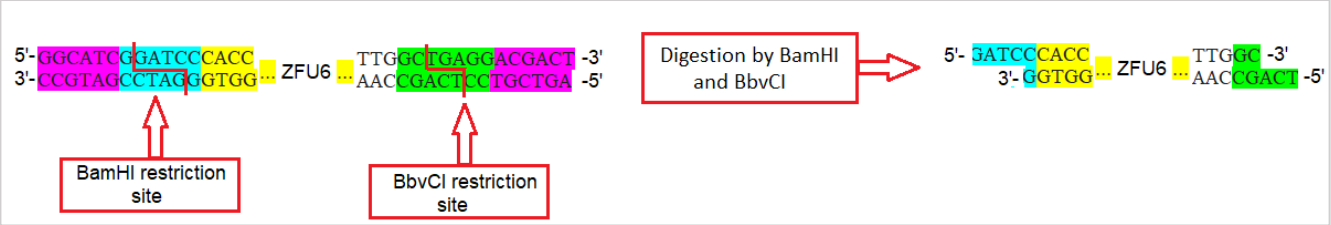

Figure 2.8: Digestion of the ZFU6 PCR product with BamHI and BbvCI creates a ZFU6 fragment with non-palindromic 5' overhangs.

A 3:1 insert-vector molar ratio with a total of 100 ng DNA was used for the ligation reaction recommended by NEB for T4 DNA ligase reactions. The calculations for getting the right amount in ng of insert and vector DNA were done using the NEB Ligation Calculator (https://nebiocalculator.neb.com/#!/ligation). Ligation of the ZFU6 fragment and the pU6-less linearized plasmid was performed using 1µl T4 DNA ligase (NEB, M0202S), 2 µl T4 10x ligase buffer (NEB, B0202S), 66 ng digested vector DNA and 26.7 ng insert fragment DNA, along with 14 µl nuclease-free water (Invitrogen, AM9938) to a total reaction volume of 20 µl. After incubating the reaction at room temperature for 10 minutes, temperature was increased to 65 ˚C for 10 minutes as to inactivate the ligase.

2.3.2.3 Transformation with, and verification of, recombinant plasmid

Competent Stbl3 E.coli cells were transformed with the ligation mix using the OneShot Stbl3 Chemically Competent E.coli kit (ThermoFischer, C737303) following the manufacturer's instructions. 100 µl of transformation mix was plated out on LB agar plates containing 100 µg/mL ampicillin and incubated for 16 hours.

The one colony that grew was further grown in liquid media containing ampicillin overnight at 37 ˚C and miniprepped using ZymoPURE Plasmid Miniprep Kit (Zymo Research, D4209) before the concentration was checked using NanoDrop. ZFU6 sequence specific primers (Forward: 5'-TTCCTTCGCATACGCTTACAG-3', Reverse: 5'-TATACCAGTGACTTCTGGGTATGTG-3') amplifying a 200 bp fragment of the ZFU6 promoter was used to verify the insertion of ZFU6 by PCR, following the same protocol as described in chapter 2.2.2.1. The PCR-reaction was then run on a 1.7% agarose gel along with a 100 bp ladder to confirm band of correct size.

2.3.3 Inserting pegRNA encoding sequences

The recipient vector, now containing a ZFU6 promotor ('ZFU6 plasmid'), contains two recognition- and cut sites for the restriction enzyme BsaI just downstream of the

promoter region. These flank the mRFP, and the overhangs generated from the BsaI cut sites flanking the pegRNA insert sequences were designed to match the overhangs generated by BsaI restriction cutting in the vector, allowing for the use of Golden Gate assembly to replace the mRFP with the pegRNA insert sequences in the recipient vector. See *Figure 2.9* for details.

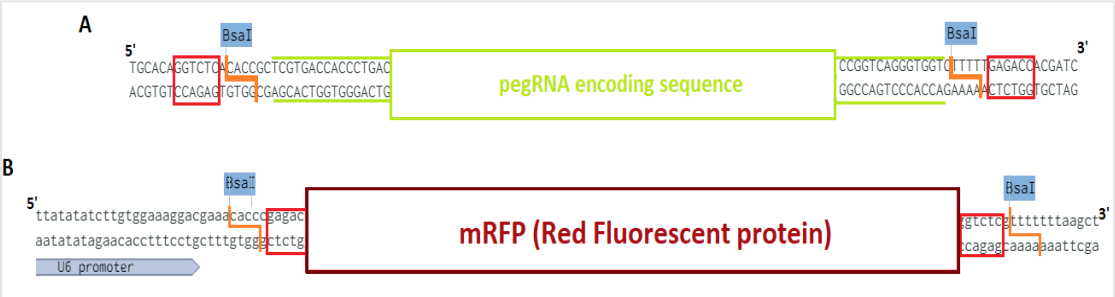

Figure 2.9 Top image (A) is the DNA oligo encoding the pegRNA for three bp deletion in EGFP, surrounded by BsaI cut sites (orange lines), BsaI recognition sites (bright red boxes) and extra bps on the distal ends of the oligo. The design is equal for the colour-converting pegRNA DNA oligo. The BsaI cut sites were designed to create overhangs complementary to the overhangs created upon BsaI digestion of the recipient vector. Bottom image (B) is part of the pU6-pegRNA-GG-acceptor plasmid, showing BsaI restriction sites (bright red boxes) flanking the sequence for mRFP (dark red box) and BsaI cut sites (orange lines).

2.3.3.1 Golden Gate Assembly

Golden Gate assembly facilitates restriction cutting of both vector and insert(s) and the ligation of insert(s) into the vector within the same reaction, taking advantage of the ability of type II restriction enzymes to cut outside their recognition sequence. Proper placement of restriction sites relative to the recognition sites and design of restriction sites to be non-palindromic and complimentary allows for directional assembly (Marillonnet & Grützner, 2020). See *Figure 2.10* for details.

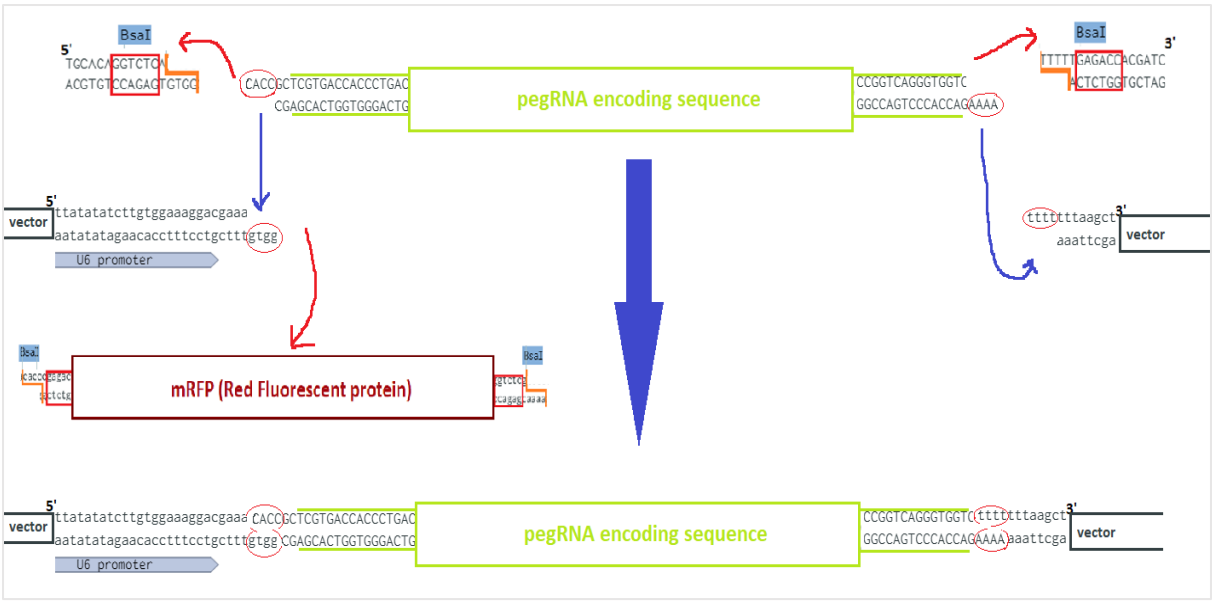

Figure 2.10. Restriction cutting and ligation of vector and one fragment in a single reaction. First, a type II restriction enzyme (here BsaI) cuts the distal parts of the insert and within the vector (BsaI recognition sites marked in red boxes, restriction sites marked by orange lines). Restriction enzyme activity is shown with red arrows, pointing to the digested fragments containing the restriction enzyme recognition site, which are not part of the finished recombinant product. Non-palindromic overhangs are created in the vector upon digestion, and compatible overhangs are likewise created in the insert. Ligation (blue arrows) of the correct elements results in a recombinant sequence devoid of restriction enzyme recognition sites. Re-ligation of digestion fragments containing restriction enzyme recognition sites will result in further digestion upon the next cycle of cutting and ligation, increasing the amount of recombinant product for each cycle.

Golden Gate cloning was performed by following a combination of the Golden Gate cloning protocol by Marillonett and Grützner (2020) and that of New England Biolabs (NEB) (https://international.neb.com/protocols/2018/10/02/golden-gate-assembly-protocol-for-using-neb-golden-gate-assembly-mix-e1601). Following the recommendations of NEB, 75 ng of the ZFU6 plasmid was used in each cloning reaction, and both a 2:1 and 1:1 molar insert:vector ratio was tested for both pegRNA constructs. Using NEBs Mass to Moles Converter (https://nebiocalculator.neb.com/#!/dsdnaamt), 75 ng ZFU6 plasmid was found to equal 39 fmoles.

For the Golden Gate Assembly reactions, 0.5 µL BsaI was used along with 1.5 µL T4 10x ligase buffer and 1 µL T4 DNA ligase. In the 1:1 insert:vector reactions, 39 fmol of pegRNA and ZFU6 plasmids was used, and 6.36 µL nuclease-free water was added to a final reaction volume of 15 µL. For the 2:1 insert:vector reactions, 78 fmol pegRNA was used and 2.46 µL nuclease-free water was added to a final reaction volume of 15 µL.

The Golden Gate incubation protocol for one to three inserts by Marillonett and Grützner (2020) was followed, first incubating the reaction at 37˚C for 4 hours, allowing BsaI and

ligase activity. Temperature was then increased to 50˚C for 5 minutes, which is the optimal digestion temperature for BsaI, making sure that only whole recombinant products remain in the reaction mix. Lastly, temperature was increased 80˚C for 10 minutes to inactivate the enzymes, before holding the reaction at 16˚C.

2.3.3.2 Transformation and sequencing of recombinant plasmid

Competent Stbl3 *E.coli* bacteria were transformed using the different Golden Gate reaction mixes following the transformation protocol described in section 2.2.2.3, plated out on four agar plates containing ampicillin and incubated at 37˚C. Five white colonies were miniprepped from each plate, as removal of mRFP results in colony color change. Concentration was checked using NanoDrop before 9 µl of each plasmid was combined with 1µl 25 µM sequencing primer (5'-AGGGTTATTGTCTCATGAGCGGA-3') covering both the ZFU6 and the pegRNA sequence, and was sent for Sanger sequencing.

Six different EGFP KO pegRNA plasmids and six different G->B pegRNA plasmids displaying correct ZFU6 and pegRNA encoding sequences were used to transform Stbl3 E.coli as described in section 2.2.2.3. Colonies of these transformants were midiprepped as described in section 2.2.1 and the plasmids were sent for sequencing using the same primer as listed in section 2.2.3.2. Plasmids displaying correct ZFU6 and pegRNA-encoding sequence were later used for electroporation (described in section 2.6)

2.4 PE2 protein

Purified PE2 were ordered from GenScript following the protocol described in Petri et al. (2021). 8 mL of protein was received in a 1.535 µM concentration.

2.5 Cell culture maintenance

Cell thawing and maintenance was performed similar to the guidelines for SHK-1 cell line maintenance at the European Collection of Authenticated Cell Cultures (EC ACC), but using 10% fetal bovine serum (FBS) in the cell culture media instead of 5%.

EGFP-SHK-1 cells were kindly provided by PhD fellow Noman Reza. Cells were cultured in Leibovitz' L-15 Glutamax (ThermoFischer, 31415029) combined with 10% FBS (SigmaAldrich, F5724-500mL) and 50 mg/mL antibiotics (penicillin-streptomycin. ThermoFischer, 15140122). 40 µM 2-mercaptoethanol (SigmaAldrich, M1348-100mL)

was added to the cell culture media to prevent toxic levels of oxygen radicals when filtered cell culture flasks were used.

Frozen EGFP-SHK-1 cells stored in liquid nitrogen were thawed in a 20 ˚C water bath. Thawed cells were added to 10 mL of SHK-1 cell medium and centrifuged at 100 g for three minutes. The supernatant was aspirated before the pellet was resuspended in 5 mL fresh cell medium and transferred to a T75 cell culture flask containing 10 mL cell medium, which was incubated at 20˚C.

Cells were washed with PBS every third day. The medium in the flasks were inspected, as cloudy media indicates bacterial contamination, and cells were examined under a microscope for further signs of contamination. When no contamination was detected, the medium was aspirated before adding 5-10 mL PBS (depending on cell culture flask size), gently tilting the flask as to cover the whole cell flask surface containing attached cells and then aspirating the PBS. This step was performed twice before providing the cells with fresh medium and further incubation. Cell subculturing was performed whenever the culture reached 80-90% confluency. 1:2-splitting was done by first washing cells with PBS as described above before trypsinizing with 2-3 mL 0.05% trypsin-EDTA, allowing cell detachment from the cell flask surface. When most cells were detached (after about eight minutes), the trypsination reaction was neutralised with ~4 mL fresh cell culture media. 10 µl was aliquoted for cell counting using the TC-20 Automated Cell Counter (BioRad, 1450102) and the rest of the cells were pelleted by centrifugation at 200 g for 5 minutes, the supernatant aspirated and the pellet resuspended in an appropriate amount of fresh medium. Cells were distributed in equal volumes into new cell culture flasks, each containing a suitable volume of fresh medium. As cell numbers increased, cells were transferred to T-175 cell culture flasks.

2.6 Prime editing of cells by electroporation

Electroporation of EGFP-SHK-1 cells was performed using the Neon Transfection System (Invitrogen, MPK5000) in combination with the Neon Transfection 10 µl Kit (Invitrogen, MPK1025). EGFP-SHK-1 cells were split two days prior to the day of electroporation. On the day of electroporation, 1 mL antibiotic-free EGFP-SHK-1 cell medium was plated pr well in a 24-well plate and incubated at 20˚C. Cells were collected following the same steps as for cell subculturing, diverging from the subculturing protocol as the pelleted

cells were washed with PBS and spun down again before being resuspended in 250 mL Opti-MEM Reduced Media (Gibco, 11058021). The suspended cells were added to a mix of plasmid DNA or RNP complex and 10 µl of the mixture was electroporated before being dispensed in a pre-filled well. The cells were kept on antibiotic-free medium for 24 hours after transfection, as newly electroporated cells are in a stressed condition and vulnerable to antibiotics. Cells were reintroduced to antibiotic-containing media after 24 hours. Plating volume and number of cells pr well has been experimentally optimized for EGFP-SHK1 cells by PhD fellow Noman Reza.

2.6.1 Electroporation of cells with plasmids

Testing of electroporation parameters were done for each plasmid combination (EGFP KO pegRNA- and PE2-expressing plasmid, and G->B- and PE2-expressing plasmid). The Neon Transfection System comes with a pre-programmed 24-well protocol, consisting of 24 programs with different settings for pulse, voltage and width (duration). Each program was tested in one of the 24 wells. The first program applies no voltage, thus the cells electroporated with the first program functions as negative controls.

A total of 2 µg plasmid DNA in a volume not exceeding a volume of 1 µL was used to electroporate $2x10^5$ cells pr well. The Neon Transfection optimization protocol was first done with the G->B pegRNA-plasmid and PE2-plasmid, in both 1:1 and 2:1 ratio of pegRNA- to PE2-plasmid (either 24 µg of each, or 36 µg and 12 µg of the pegRNA and PE2, given the respective ratios).

2.6.2 Incubation

Cells were incubated for seven days. Different incubation temperatures were tested for the cells electroporated with the PE2 and G->B pegRNA plasmids to see if temperature affected editing efficiencies or cell survival; cells were incubated for seven days, either at 20 ˚C for the whole incubation period, at 26 ˚C for 24 hours before changing the temperature to 20 ˚C, or at 26 ˚C for 4 hours before changing the temperature to 20 ˚C for the rest of the incubation period. Based on the results from temperature experiments, cells edited with EGFP KO PE and PE2 plasmids and RNP complexes were incubated at 26 ˚C for 24 hours before continuing incubation at 20 ˚C for six days.

2.6.3 Electroporation of cells with RNP complex

Electroporation was done following protocols from Gratacap et al (2020). However, due to the low starting concentration of PE2 protein, the RNP concentration was ten times lower than recommended by Gratacap et al. (2020). RNP complexes comprising PE2 and the synthetic G -> B pegRNA was made by combining 0.1 µl 200 µM pegRNA with 0.9 µl PE2 pr sample. Six samples were electroporated with G->B RNP complexes, along with two negative controls only being electroporated with PE2 and no guide and two negative controls receiving neither PE2 nor RNP complexes, electroporating $2x10^5$ cells pr well. Three samples/replicates and one of each negative control were incubated at 26 ˚C degrees for 24 hours before moved to 20 ˚C for six days while the three remaining samples/replicates and controls were incubated at 20 ˚C for seven days.

2.6.4 Editing of HEK-cells

To have some blue cells to use as a positive control for flow cytometry, EGFP-expressing HEK cells were edited following the protocol by Glaser et al. (2016), converting green fluorescence to blue by CRISPR-Cas9-mediated knock-in, using lipofectamine as method of transfection.

To test the prime editing complex in mammalian cells, HEK cells were electroporated with the G->B RNP complexes, using the electroporation settings recommended by the manufacturer for HEK cell transformation (1500 V, 30 ms, 1 pulse). The transformed HEK cells were incubated at 37 °C in Dulbecco's Modified Eagles Medium (SigmaAldrich, D6429-500ML), 10% FBS and 1% L-Glutamine (Gibco, 25030-024). 1% penicillin-streptomycin was added to the cell culture media after 24 hours.

2.6.5 Detection of editing outcomes in cells

EGFP-SHK-1 cells edited with the G->B pegRNA plasmid were examined under a fluorescence microscope (Zeizz Axio Vert.1A) for visual assessment of fluorescence seven days post editing. HEK-cells edited with CRISPR-Cas9 mediated knock-in by means of lipofection were assessed visually under a different fluorescence microscope (EVOS M5000, AMF5000, Invitrogen).

SHK-1 cells electroporated with the G->B RNP complex were harvested after seven days and subjected to flow cytometry to detect blue fluorescent cells, using the CellStream™ flow cytometer (Merck, CS-400104). Flow cytometry is a technique for sorting single cells

into different populations by hitting individual cells with lasers from different angles and detect the scattering of light and the fluorescent signals that results. This way, traits such as size and fluorescence can be measured (McKinnon, 2018). Laser intensity for forward and side scatter, measuring cell size, was set to 16% and 12%, respectively. The laser for excitation of blue fluorescence (wavelength 405 nm) was set to 1% and the laser for excitation of green fluorescence (wavelength 488 nm) was set to 5%. The minimum laser intensities able to detect fluorescence and resolve fluorescent and non-fluorescent cells was chosen as to avoid background noise. The wavelengths of the detectors detecting green and blue fluorescence was 507 and 455 nm, respectively. The lipofected HEK-cells edited to convert fluorescence from green to blue was harvested five days post transfection and was used to calibrate the cytometer. Flow cytometer data was analysed using the CellStream Analysis 1.2.1 software (Merck).

Due to difference in scattered light of cells, cell debris and dead cells, different clusters of signals can be detected in the analysis. The cluster having the largest proportion of fluorescent cells were defined as the cluster of live cells, and selected for further analysis. Individual cells from the cluster are represented on a graph, where the y-axis represents increasing intensity of green fluorescence, and the x-axis increasing intensity of blue fluorescence. The green and blue fluorescent control HEK-cells were divided into four different populations ('green fluorescence', 'blue fluorescence', 'no fluorescence' and 'other') based on their positioning on the graph. Division of the cells are done manually, and the spaces defining the fluorescent properties of the control HEK cells were used for subsequent analysis of the electroporated EGFP-SHK-1 cells, sorting these cells into the predefined spaces upon analysis.

DNA from cells edited with EGFP KO pegRNA plasmid in a 2:1 pegRNA:PE2 plasmid ratio was sent for sequencing. Sample preparations (DNA extraction, amplification and sequencing preparations) were performed by lab technicians. DNA extraction was done using the DNeasy Blood & Tissue Kit (Qiagen, 69504). PCR- and sequencing primers that have already been used for successful amplification and sequencing of the SHK-1 EGFP was kindly provided by PhD fellow Noman Reza at NMBU (forward PCR primer 5'-GATAGCGGTTTGACTCACGG -3', reverse 5'- CGCTTCTCGTTGGGGTCTTT -3', sequencing primer 5'- TGGCACCAAAATCAACGGG -3') along with an optimized Platinum II Taq PCR protocol, preparing samples according to manufacturers' instruction and using 15-50 ng

DNA and adding 2 µl GC enhancer pr sample. The following 3-step cycling protocol was used: 94 °C for two minutes; three cycles of 94 °C for 30 seconds, 59 °C for 15 seconds and 68 °C for 20 seconds; 30 cycles of 94 °C for 15 seconds, 57 °C for 15 seconds and 68 °C for 20 seconds; 68 °C for seven minutes before holding at 4 °C. Primers were removed from the post-PCR reaction mix using ExoSAP-IT (ThermoFischer, 78201.1.ML) following manufacturers' instructions, but using 1 µL post-PCR reaction product and 4 µL of the ExoSAP-IT reagent. The EXOSAP-IT-treated post-PCR reaction was sent for sequencing, and the resulting sequences were analysed using Synthegos ICE Crispr Analysis Tool (Synthego Performance Analysis, ICE Analysis. 2019. v3.0. Synthego; [09/05/2022]).

2.7 Prime editing of zebrafish embryos by microinjection

2.7.1 Micropipette pulling and grinding

Nashiringe G-1 glass capillaries were pulled using a mechanical micropipette puller (Sutter Instruments, P-1000). The ramp value, the lowest temperature needed to melt the capillary, was first set by doing a ramp test. After setting the ramp value, other parameters were found experimentally, adjusting each parameter until micropipettes with suitable tapered, sharp ends were pulled.

Values for the needle puller parameters that produced long sharp needles able to penetrate the chorion and cell membrane of zebrafish embryos in the one-cell stage easily are listed in *Table 2.5*.

Table 2.5: Settings used on the P-1000 micropipette puller (Sutter Instruments) to generate rightly sized micropipette tips.

Heat	Pull	Velocity	Delay	Pressure	Ramp
465	60	80	90	385	485

Micropipette pulling produces pipettes with sealed tips. A small opening in the tip was made by grinding the needle using the BV-10 Micropipette Beveler from Sutter Instruments. The capillary tip is grinded on a rotating rough surface coated with water and as an opening is created, water travels upwards in the needle due to capillary forces. Capillaries with differently sized openings were made and tested to see which were most suitable for microinjections. When a properly sized opening was made, the travel-length of the water inside the capillary was used as an indicator for when to stop grinding.

2.7.2 RNP injection solution

Following advice from Petri et al. (2021), 30 µl RNP injection solution with a pegRNA:PE2 2:1 ratio was made by combining 29.55 µl 1.535 µM PE2 solution and 0.5 µl 200 µM G->B pegRNA creating an injection mix consisting of 1.5 µM PE2 and 3 µM pegRNA. However, due to the low concentration of the received PE2 protein, the actual RNP concentration was much lower to that of Petri et al. (2021).

2.7.3 Calibrating and testing injection volume

Calibration of microinjection volume was done by placing a glass microscopy slide with a ruler with 0.01 mm intervals engraved under a microscope, covering the ruler with a drop of mineral oil (Sigma-Aldrich, M5904). Microinjection solution was loaded into a micropipette with a microloader pipette tip (Eppendorf, 5242956003), before being mounted to a micromanipulator (Narishige, MN-153) connected to a FemtoJet Microinjector (Eppendorf, 5252000021). One drop of solution was injected into the mineral oil and the diameter of the drop was measured. A drop of 0.15 mm corresponds to a volume of approximately 1.67 nL (Yuan and Sun, 2009). Adjusting the duration and pressure parameters on the microinjector can then be done to calibrate injection volume.

Different microinjection volumes were tested on embryos to see if volume affected embryonic lethality. Testing was done by dividing newly fertilized eggs into two groups, each comprising a total of 180 embryos. Over a period of six days, 30 eggs were injected with low volume of RNP injection solution and 30 with high volume pr day. The microinjection set-up was equal to that described in the paragraph above, and embryos were injected in the cell in the first cell stage, as this is the recommended injection site for RNP complexes in zebrafish embryos (Xin & Duan, 2018; Zhao et al., 2021). The same micropipette was used on both groups injected on the same day to make sure that difference in embryo survival rate was not due to difference in the micropipette, changing the pressure and duration to create different volumes from the same pipette. One group was injected with a small injection volume (drop diameter 0.05-0.1 mm, corresponding to a volume of ~0.56-1 nL) of PE RNP solution, while the other was injected with a larger injection volume (drop diameter >0.15 and <0.2 mm, corresponding to a volume of >1.67 and <2.23 nL) of PE RNP solution. An additional group of uninjected controls was also kept each day of testing. Embryos were incubated at 28˚C and rate of survival was registered two days after injections.

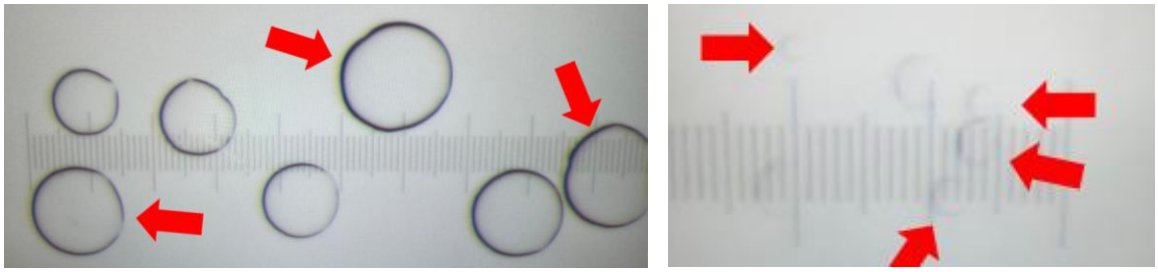

Figure 2.11. The left picture shows drops of microinjection solution with a diameter of 0.15 – 0.2 mm (1.67 – 2.23 nL) (marked by pointing arrows) injected into mineral oiled covering a ruler with 0.01 mm increments. The right picture shows drops with a diameter <0.05 mm (0.56 nL) (marked by pointing arrows). The differently sized drops were made by the same micropipette by adjusting the pressure and injection time when pipetting.

Analysis of the results was done using R, performing a one-way ANOVA and a subsequent Tukey's test to detect any significant difference between the injected groups, and between injected groups and the control group. The percentage of survival of each of the six injected batches of embryos comprising one group comprised the data used to calculate the mean and standard deviations of each group for the ANOVA analysis. Differences in survival rate between groups were considered significant when $P < 0.05$.

2.7.4 Microinjections and incubation

The single cell of newly fertilized eggs was injected with *nid1a* and *EGFP* RNP complexes (separately) and embryos were incubated at 28˚C for five days. The incubation solution provided by the zebrafish lab was changed twice a day by lab technicians, and dead cells and debris was cleaned regularly.

2.7.5 Detection of editing outcomes in embryos

Zebrafish larvae edited with the *nid1a* PE construct was examined under a microscope (Zeizz Axio Vert.1A) three days post editing, when the expected shortened body length of edited larvae can be observed (Zhu et al., 2017). Larvae edited with the G->B RNP complex was examined two and five days post editing under a fluorescence microscope (Nikon, SMZ25) to observe any change in fluorescence, and pictures were captured using the Nikon NIS Elements BR software. DNA from *nid1a*-edited larvae displaying short body length and larvae with change in fluorescence as well as from unedited controls from both groups was extracted by dissolving each larva in 50 µL alkaline lysis buffer (25 mM NaOH and 0.2 mM EDTA), incubating them at 95˚C for 5 minutes and vortexing frequently. The reaction was neutralized by adding 50 µL 40 mM Tris-HCL (pH 8), and the DNA concentration was measured using Nanodrop.

nid1a sequence was amplified using the forward and reverse PCR-primers 5'-AATTCACCTATACCTCATGCAA -3' and 5'- ATTGGTCAGTGAGACTAGTCTA -3' respectively. Using Phusion polymerase (ThermoFischer , F530S) and finding the optimal primer annealing temperature of 52 ˚C experimentally, amplification was performed according to manufacturers' suggested cycling protocol. The PCR products from control and putatively *nid1a*-edited larvae were sent for sequencing (sequencing primer 5'-AATTCACCTATACCTCATGCAA -3').

As the forward PCR primer for amplification of EGFP in SHK-1 cells binds to sequence upstream of the EGFP encoding sequence, separate primer pairs were created for amplification of zebrafish EGFP. Two primer pairs (forward 5'-GAGCAAGGGCGAGGAGCTGTTC -3' and reverse 5'- TTGTACAGCTCGTCCATGCCGA -3' and forward 5'- GCAAGCTGACCCTGAAGTTC -3' and reverse 5'- GACGACGGCAACTACAAGAC-3') were tested for PCR amplification of the zebrafish EGFP using both Platinum II Taq HS DNA polymerase (Invitrogen, 14966001) and Phusion™High-Fidelity DNA Polymerase (Thermo Scientific, F530S), using 50 ng DNA. The 3-step cycling protocol reccomended by the manfucaturer for each polymerase was tested, and optimization was done for each primer pair/polymerase combination, creating primer annealing temperature gradients (seven temperatures tested in each gradient, three samples tested with temperatures lower than the primer meling temperature and three samples tested with higher as well as testing the suggested melting temperature as the annealing temperature. Each gradient increased by two degrees).

3 RESULTS

3.1 Plasmid construction

Recombinant plasmids containing a zebrafish U6 promoter (ZFU6) and G->B or EGFP KO pegRNA encoding sequences were successfully constructed from the original pegRNA-acceptor plasmid containing a mammalian U6 promoter.

3.1.1 Changing of U6 promoters

The original mammalian U6 promoter was replaced by the ZFU6 promoter by means of restriction cloning. PCR of the plasmid DNA using ZFU6 specific primers amplifying a part of the ZFU6 promoter resulted in a PCR product of the expected length of 200 bps, shown in *Figure 3.1* (marked as 'ZF U6 partial sequence').

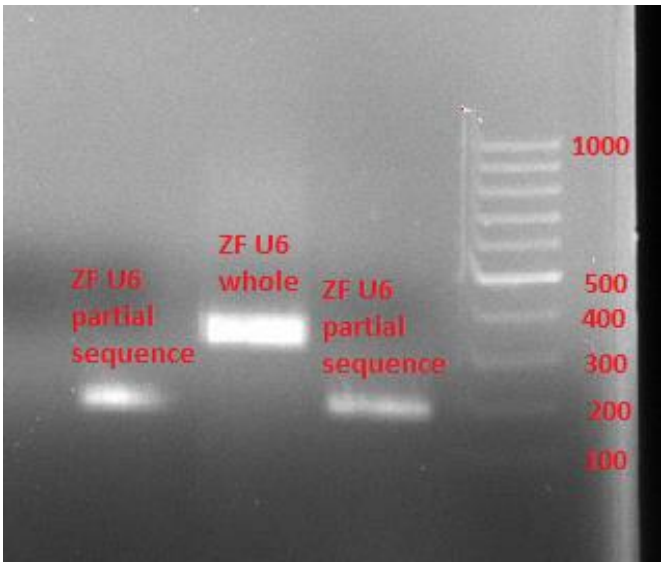

Figure 3.1: The PCR product after amplification of a 200-bp region of the ZFU6 sequence from the recombinant ZFU6 plasmid using specific ZFU6 primers. The numbers on the right indicate weight of the bands in the 100 bp ladder. The bands to the left and right marked 'ZFU6 partial sequence' corresponds to the 200-bp PCR product, while the band in the middle ('ZF U6 whole') is the PCR product from the amplification of the whole ZFU6 sequence, included as a positive control.

3.1.2 Insertion of pegRNA encoding sequences

Transformation of bacteria with plasmids from the Golden Gate Assembly reaction mixes resulted in good growth of bacterial colonies. All colonies displayed white color, indicating that the red fluorescent protein in the original plasmid was removed.

16 out of 20 randomly picked plasmids displayed correct sequences of both the promoter- and pegRNA sequence. The four remaining plasmids showed correct sequence for the ZFU6 promoter, but had errors in the form of indels or base substitutions in the pegRNA encoding sequences (see the Appendix for ZFU6- and pegRNA encoding reference sequences).

Competent E.coli was transformed with six different G->B pegRNA plasmids and six different EGFP KO pegRNA plasmids displaying correct ZFU6 and pegRNA sequences and sequenced. All plasmids displayed correct sequences and were used for electroporation. However, all plasmids had a single base insertion (a cytosine) just upstream of the ZFU6 – this was also seen in the sequences of the 20 miniprepped plasmids in the previous step.

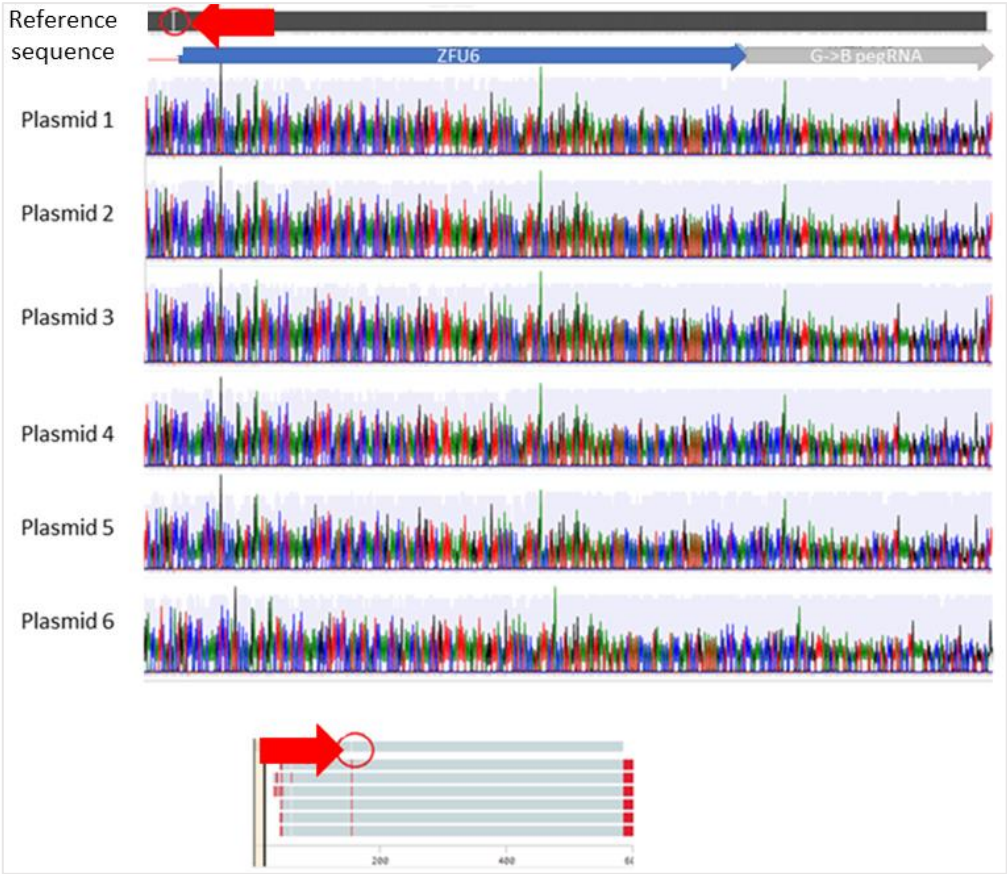

Figure 3.2. Alignment of plasmids (Plasmid 1-6) containing inserted ZFU6 promoter and G->B pegRNA encoding sequences to the correct reference sequence. The red arrow in the top left of the figure points to a single base missing in the reference sequence, caused by an insertion which is present at the same position in all plasmid sequences. This is also illustrated in the simpler alignment at the bottom of the figure, showing the base insertion in red in all plasmid sequences aligned to the reference sequence at the top. The sequences have been aligned using Benchling. The reference sequence can be found in the appendix (Appendix, sequence 1).

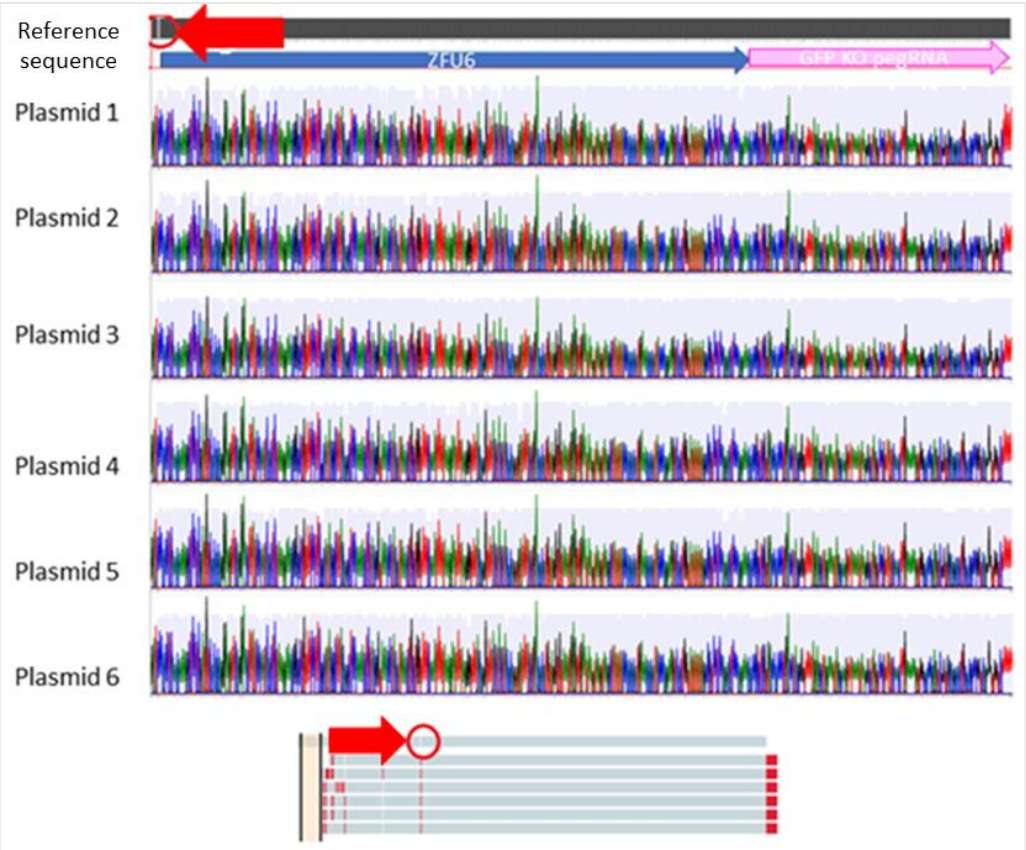

Figure 3.3. Alignment of plasmids (Plasmid 1-6) containing inserted ZFU6 promoter and EGFP KO pegRNA encoding sequences to the correct reference sequence. The red arrow in the top left of the figure points to a single base missing in the reference sequence, caused by an insertion which is present at the same position in all plasmid sequences. This is also illustrated in the simpler alignment at the bottom of the figure, showing the base insertion in red in all plasmid sequences aligned to the reference sequence at the top. The sequences have been aligned using Benchling. The reference sequence can be found in the appendix (Appendix, sequence 2).

3.2 Electroporation

3.2.1 Electroporation of plasmids

EGFP-SHK-1 cells were prime edited by electroporation with G->B pegRNA- and PE2 expressing plasmids in either a 1:1 or 2:1 pegRNA:PE2 plasmid ratio. Electroporated cells were then subjected to different incubation schemes.

No blue fluorescent EGFP-SHK-1 cells were observed after electroporation of the G->B pegRNA plasmids, regardless of ratio between pegRNA- and PE2 plasmid, time incubated at 26 ˚C, or electroporation settings.

A temperature of 26 ˚C did not seem to affect cells in terms of viability, based on visual assessment of the cells, as there were no obvious differences in confluency or cell death between cells subjected to the different incubation schemes.

Sanger sequencing of PCR products from EGFP-SHK-1 cells electroporated with the EGFP KO and PE2 plasmids in a 2:1 ratio and subsequent analysis with the program ICE was inconclusive. Out of 24 samples, one sample (2:1 EGFP KO PE:PE2 ratio electroporated with program 11 in the electroporation optimization protocol (1100V, 40 ms, 2 pulses)) showed signs of editing. However, the analysis indicated that two different edits was made in 3% of the sequences in the sample, both showing a three bp deletion just upstream of the PAM and the codon targeted for deletion. See *Figure 3.4* for details.

Figure 3.4. Sequences from the cell sample electroporated with a 2:1 GFP KO PE:PE2 plasmid ratio at 1100V, 40 ms, 2 pulses analysed using Sythego's ICE Analysis tool. The PAM sequence (CGG) is underlined for all aligned sequences, and the vertical line indicates the PE2 nick site. The targeted codon is marked in the red box, and the deletions in the two bottom sequences are indicated with a '-' per base deleted.

3.2.2 Electroporation of RNP complexes and flow cytometry analysis

SHK-1 cells were electroporated with the G->B RNP complex. Cells were first visually inspected to detect any change in fluorescence. No blue fluorescence was detected this way. Cells were then subjected to flow cytometry. A fraction of the EGFP-expressing HEK cells was successfully edited by CRISPR-Cas9-mediated knock-in to convert fluorescence from green to blue following the protocol from Glaser et al. (2016), as shown in *Figure 3.5*

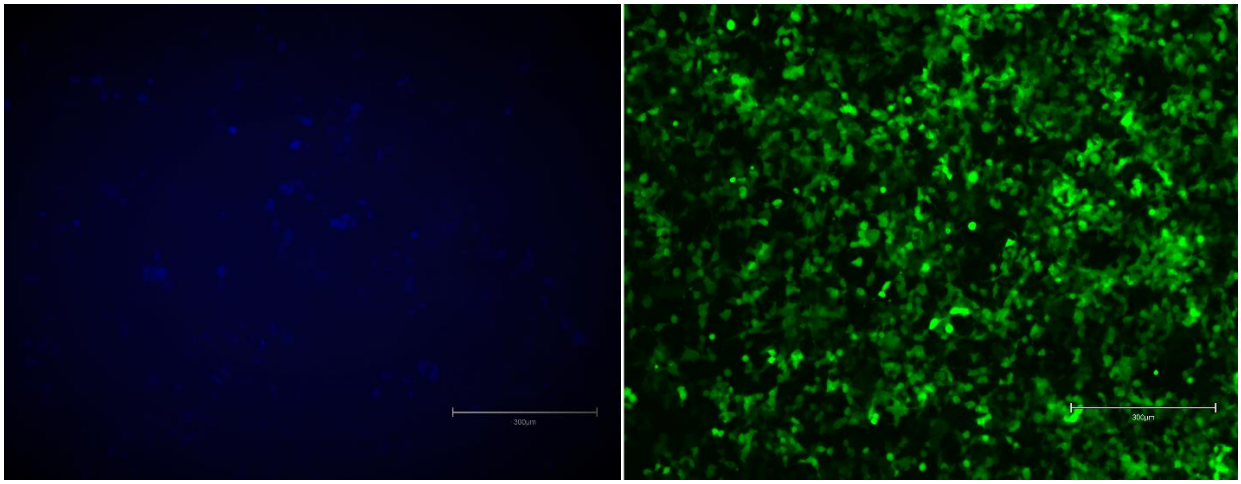

Figure 3.5. To the left are HEK-cells successfully edited following the protocol of Glaser et al. (2016), showing expression of BFP in a fluorescent microscope (EVOS M5000, Invitrogen). To the right are a picture of the same sample of cells, using a different filter, showing cells that have not been edited, still expressing EGFP. The pictures are captured with the EVOS M5000 imaging system from Invitrogen.

The mix of BFP and EGFP expressing HEK cells was used to calibrate the flow cytometer and differentiate cells into different populations based on fluorescence before analysing the EGFP-SHK-1 cells. Cells sorted as green fluorescent are marked in green, non-fluorescent cells in black, blue fluorescent cells are marked blue. The 'other' category is marked in red (see *Figure 3.6*).

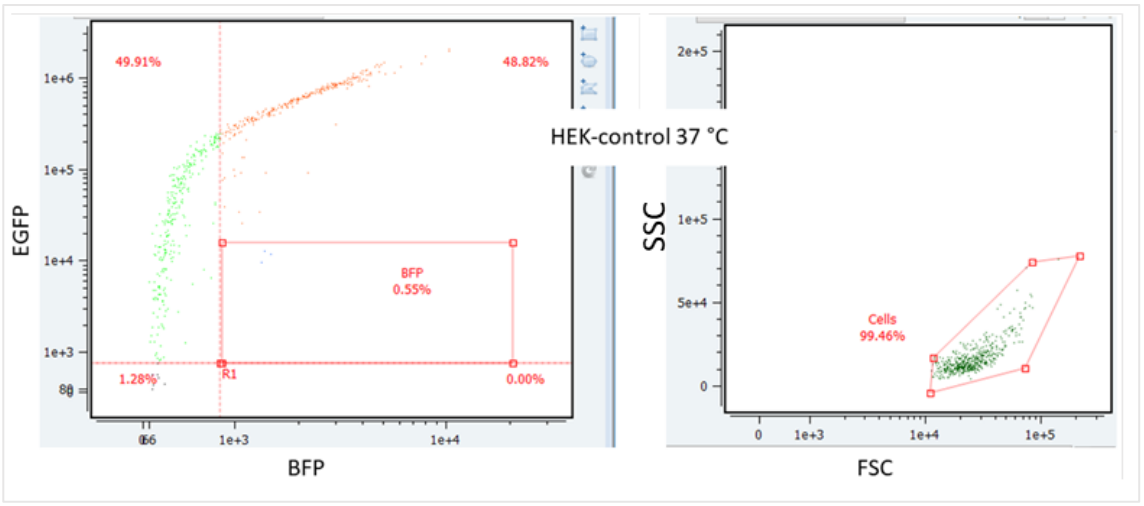

Figure 3.6: Flow cytometry analysis of EGFP and BFP expressing HEK cells using the CellStream Analysis 1.2.1 software. The figure to the right shows a single cluster of cells, grouped together based on the scatter of light they produce after being hit by the forward and side laser. Intensity of forward scatter (FSC) is given on the x-axis and intensity of side scatter (SSC) on the y-axis. In the figure to the left, each dot represents a single cell. Cells are sorted by fluorescence. The y-axis represents increasing intensity of green fluorescence (EGFP), and the x-axis increasing intensity of blue fluorescence (BFP). The HEK cells were divided into four groups based on their positioning on the graph (i.e. their fluorescent properties) The bottom right square captures the non-fluorescent cells and shows percentage of non-fluorescent cells. Green fluorescent cells are coloured green, and BFP expressing cells are coloured blue and captured in the square marked 'BFP'. The cells marked in red are grouped as 'others'.

Negative control cells (EGFP-SHK-1 cells electroporated without any RNP complex or PE2) were used to identify live cells in the samples as seen in the right panel of *Figure 3.7*. Some blue fluorescence was detected, in 0.02% of the cells in the sample (see *Figure 3.7)*.

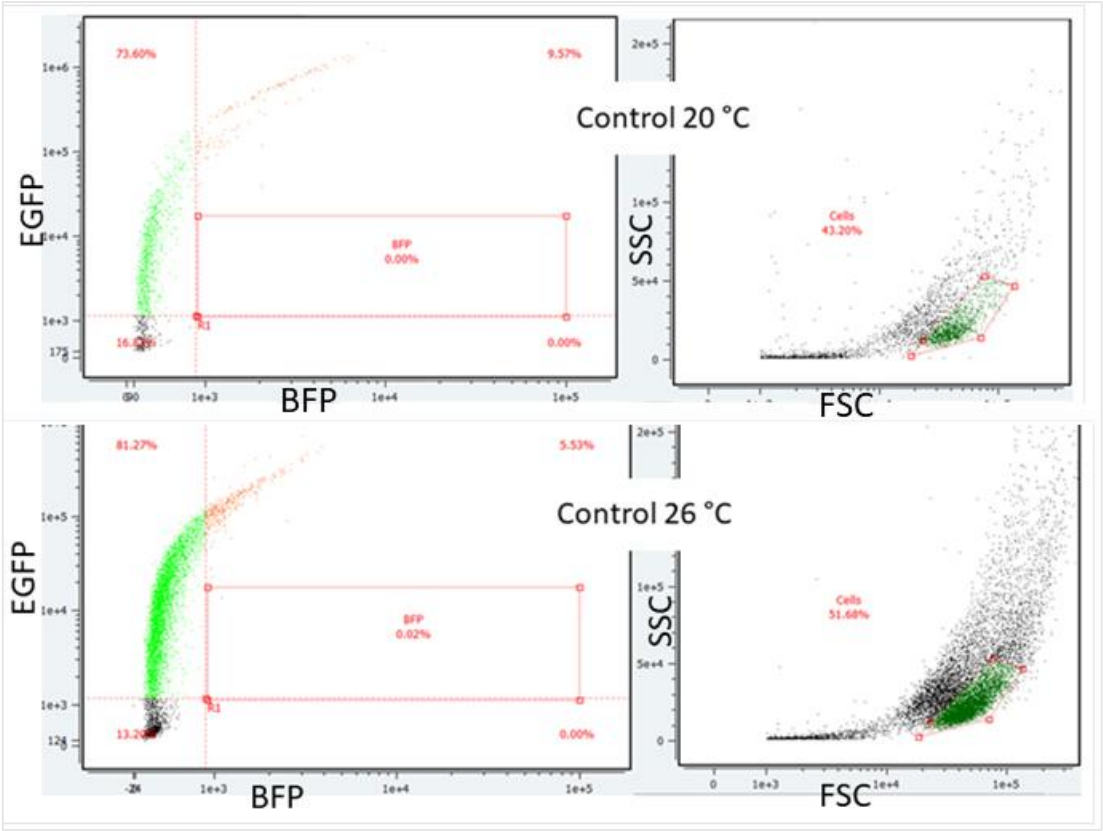

Figure 3.7. Flow cytometry analysis of two samples of negative control EGFP-SHK-1 cells incubated at 20 ˚C (top graphs), and 26 ˚C (bottom graphs) using the CellStream Analysis 1.2.1 software. The graphs to the right show three clusters of detected signals based on forward- and side scatter (FSC and SSC) of light. The graphs to the right show three clusters of detected signals based on light front- and side scatter (FSC and SSC). One of these clusters (marked in green) was selected as the live cell population. Intensity of forward scatter (FSC) is given on the x-axis and intensity of side scatter (SSC) on the y-axis. The graphs to the left show the division of cells in the population from each sample based on fluorescence. 0.02% of cells in the control sample incubated at 26 ˚C were sorted into the space defining blue fluorescence. Intensity of green fluorescence (EGFP) is shown in the y-axis and intensity of blue fluorescence (BFP) on the x-axis.

No blue fluorescence was detected in control samples (EGFP-SHK-1 cells electroporated with only PE2), as seen in *Figure 3.8.*

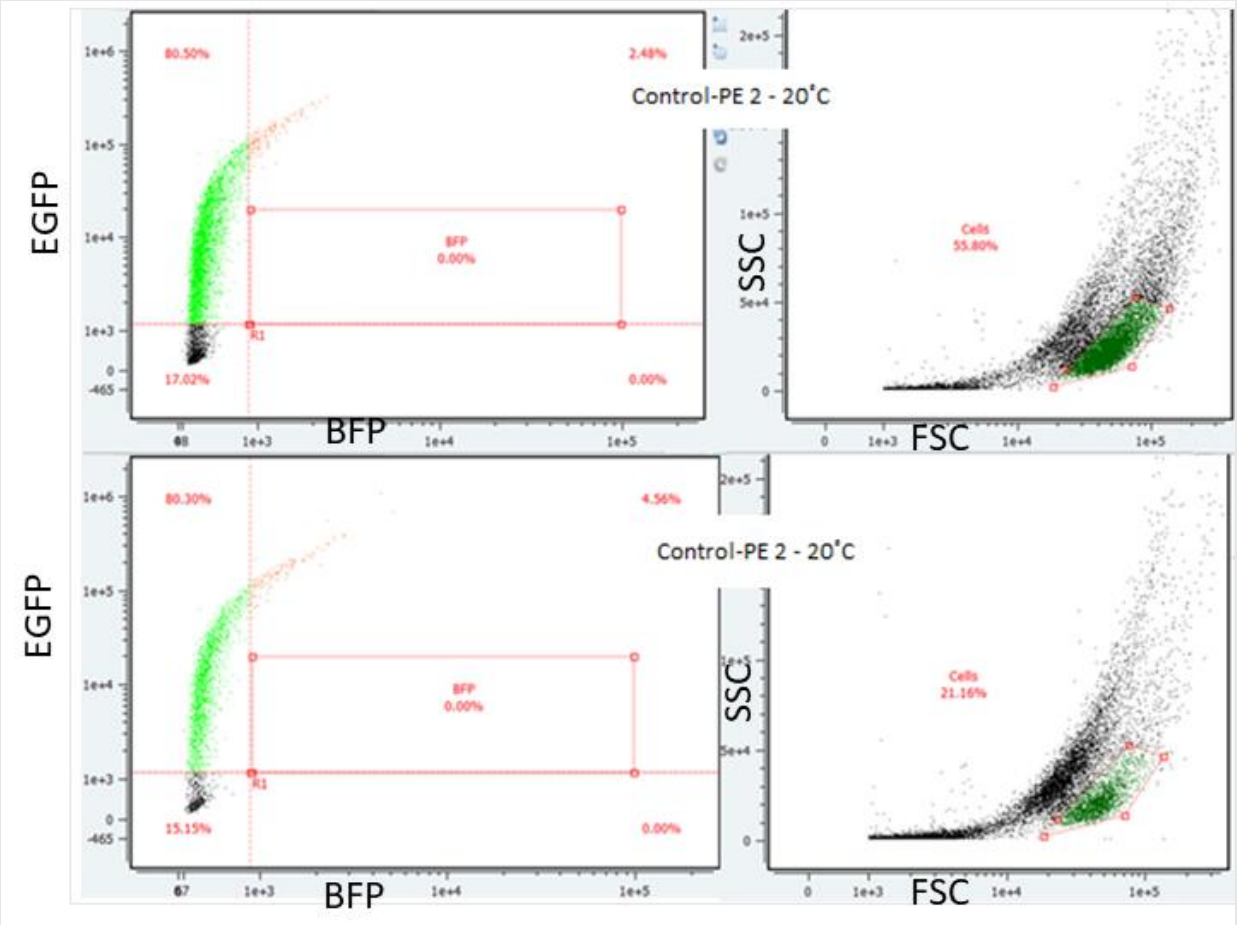

Figure 3.8. Flow cytometry analysis of two samples of negative control EGFP-SHK-1 cells electroporated with only PE2 incubated at 20 ˚C (pictures to the left), and 26 ˚C (pictures to the right) for seven days, using the CellStream Analysis 1.2.1 software. The graphs to the right show three clusters of detected signals based on front- and side scatter (FSC and SSC) of light. The cluster marked in green represents the live cell population. Intensity of forward scatter (FSC) is given on the x-axis and intensity of side scatter (SSC) on the y-axis. The graphs to the left show the division of cells in the population from each sample based on fluorescence. Intensity of green fluorescence (EGFP) is shown in the y-axis and intensity of blue fluorescence (BFP) on the x-axis. No blue fluorescence was detected in the negative control samples.

The cell population defined by the controls was used for analysing editing outcomes in the experimental cells incubated at either 20 or 26 ˚C. While cells incubated at 20 ˚C showed no or nearly no detectable blue fluorescence (0.00 - 0.01%, see *Figure 3.9*), two of the three replicates incubated at 26˚C had around 0.1% BFP expressing cells (0.09-0.12%, see *Figure 3.10)*.

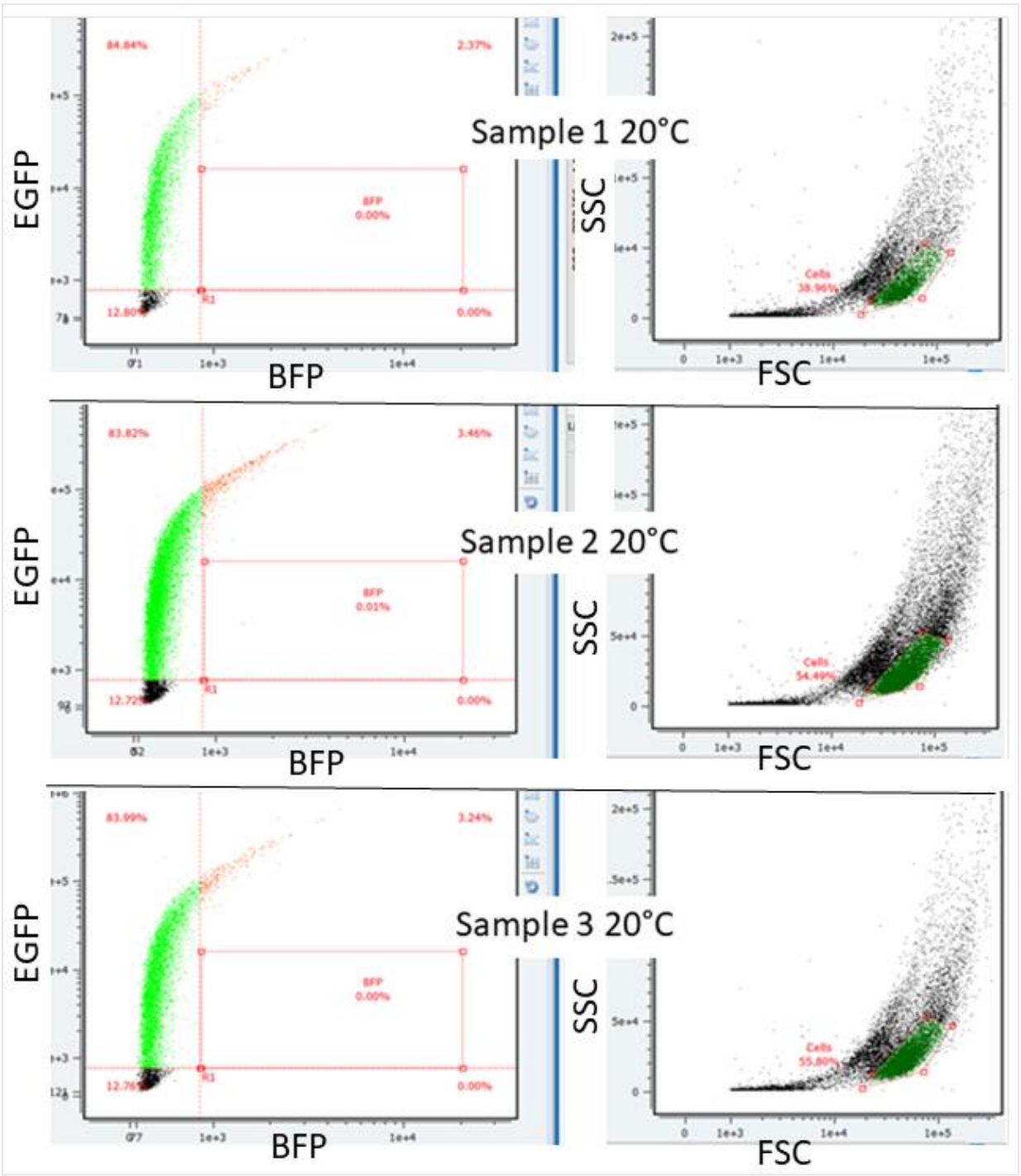

Figure 3.9. Flow cytometry analysis of the three replicates electroporated with the G->B RNP complex and incubated at 20 ˚C for seven days using the CellStream Analysis 1.2.1 software. The graphs to the right show three clusters of detected signals based on front- and side scatter (FSC and SSC) of light. The cluster marked in green represents the live cell population. Intensity of forward scatter (FSC) is given on the x-axis and intensity of side scatter (SSC) on the y-axis. The graphs to the left show the division of cells in the population from each sample based on fluorescence. Intensity of green fluorescence (EGFP) is shown in the y-axis and intensity of blue fluorescence (BFP) on the x-axis. 0.01% of cells in sample 2 were detected as blue fluorescent cells.

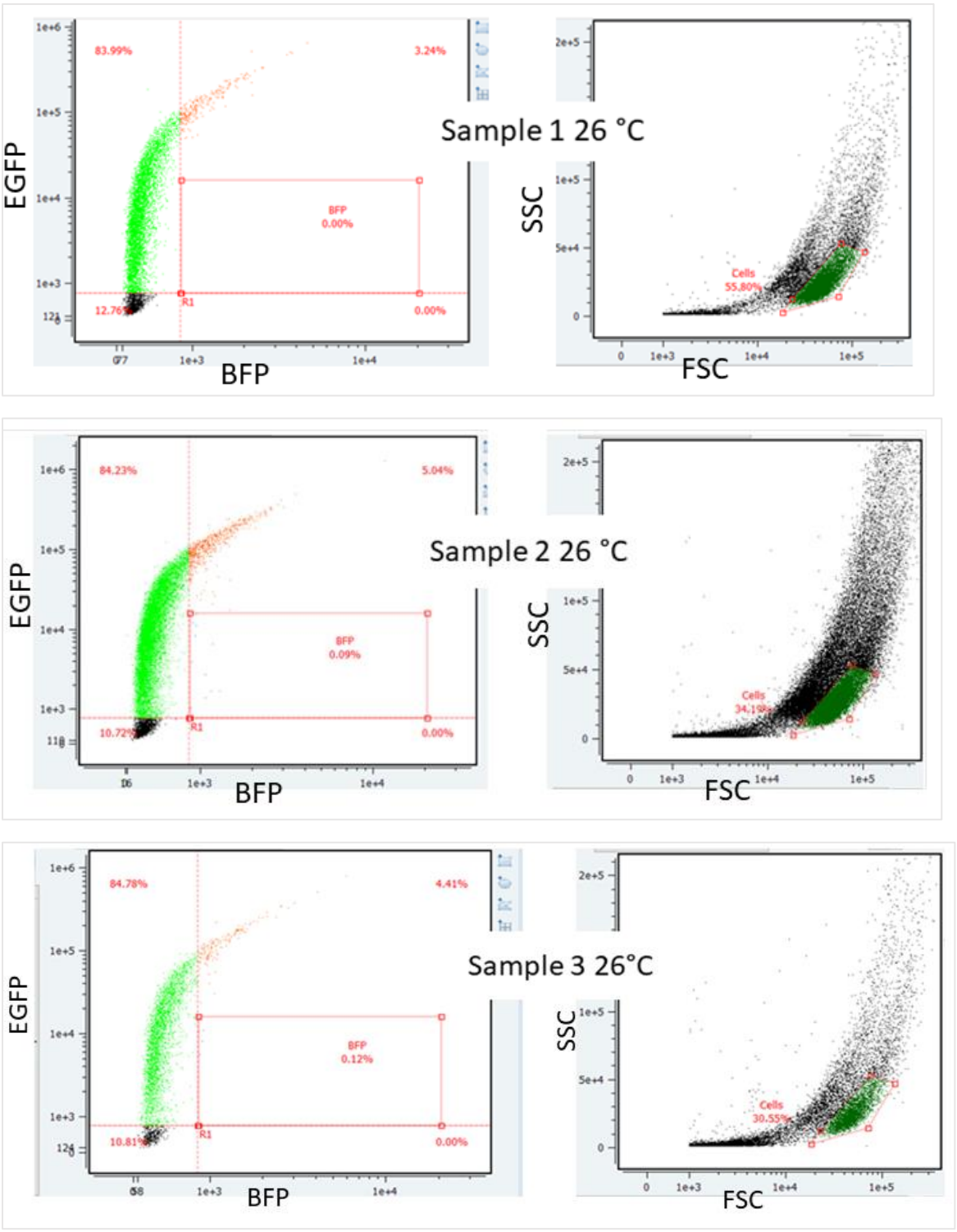

Figure 3.10. Flow cytometry analysis of the three replicates electroporated with the G->B RNP complex, and incubated at 26˚C for 24 hours before continuing incubation at 20 ˚C for six days, using the CellStream Analysis 1.2.1 software. The graphs to the right show three clusters of detected signals based on front- and side scatter (FSC and SSC) of light. The cluster marked in green represents the live cell population. Intensity of forward scatter (FSC) is given on the x-axis and intensity of side scatter (SSC) on the y-axis. The graphs to the left show the division of cells in the population from each sample based on fluorescence. Intensity of green fluorescence (EGFP) is shown in the y-axis and intensity of blue fluorescence (BFP) on the x-axis. Sample 2 and 3 shows 0.09% and 0.12% of cells from the live population being sorted into the space defining blue fluorescence, respectively.

The control sample incubated at 26˚C and sample 2 incubated at 20˚C, each had one cell sorted into the area defining blue fluorescence (top and bottom left pictures in *Figure 3.11*). Sample 2 and 3 incubated at 26˚C had 10 and four cells within the same area, respectively (top and bottom right pictures in *Figure 3.11*).

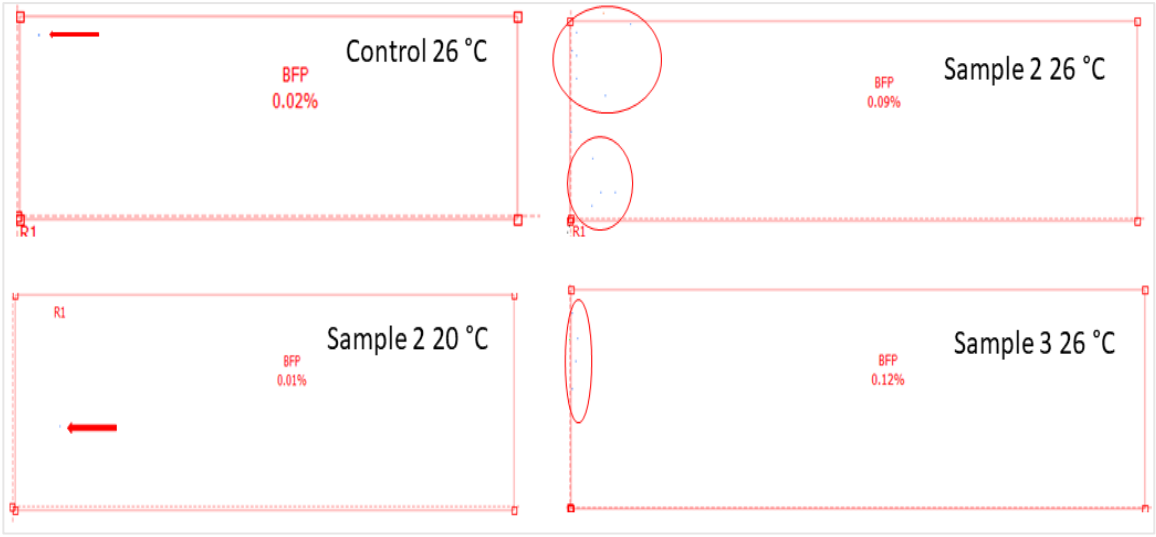

Figure 3.11. Magnification of space defining blue fluorescence from Figure 3.6, 3.8 and 3.9. Control 26 ˚C and Sample 2 20˚C each had one cell sorted into the area defining blue fluorescence when doing (each marked with a red arrow). Sample 2 26 ˚C had 10 cells sorted into the same area, while sample 3 26˚C had four (circled in).

Electroporation of HEK cells with the G->B RNP complex failed, as the cells did not seem to survive the electroporation.

3.3 Microinjections

As high mortality of injected embryos was observed, some time was spent optimizing survival rate by testing injection volumes before continuing with editing experiments. Testing of microinjection volume was done before zebrafish embryos were subjected to microinjections of RNP complexes in the first cell-stage.

3.3.1 Testing of injection volume

Survival rate for the total number of embryos injected with high volume (>1.67 and <2.23 nL) was 9.4 % and 38.3% for embryos injected with low volume (<0.56 nL), while 61.6% of uninjected control embryos survived. Embryos were injected with PE RNP mix, but only embryo survival rate and not editing outcomes was monitored when testing different volumes. The number of survivors from each group and subgroup is listed in

Table 3.1. The survival of control embryos fluctuated greatly, from 38% to 94%. Survival rate of embryos receiving high injection volumes was consistently low, ranging from 6.5% to 17%. Embryos receiving low-volume injections also displayed great variation in survival rate, ranging from 0% - 77%. The in- and between-group variation is visualized as boxplots in *Figure 3.12.*

Table 3.1. Table showing the total number of embryos and surving embryos in the three groups receiving high or low volume of PE RNP injection solution or no injections (control), as well as survival in percentage. Each group consists of six subgroups. One subgroup from each group was injected pr day over a six day period.

Group	Day	Survived embryos	Total embryos	Survival in percentage (%)
Control	1	19	50	38
Control	2	47	50	94
Control	3	52	62	84
Control	4	23	50	46
Control	5	31	50	62
Control	6	23	50	46
Total		**195**	**312**	**65 (mean)**
High Volume	1	3	46	6.5
High Volume	2	4	43	9.3
High Volume	3	8	47	17
High Volume	4	5	31	17
High Volume	5	0	25	0
High Volume	6	2	31	6.5
Total		**22**	**223**	**9.4 (mean)**
Low Volume	1	7	36	19
Low Volume	2	33	43	77
Low Volume	3	25	37	68
Low Volume	4	11	41	27
Low Volume	5	15	38	39
Low Volume	6	0	31	0
Total		**91**	**226**	**38.3 (mean)**

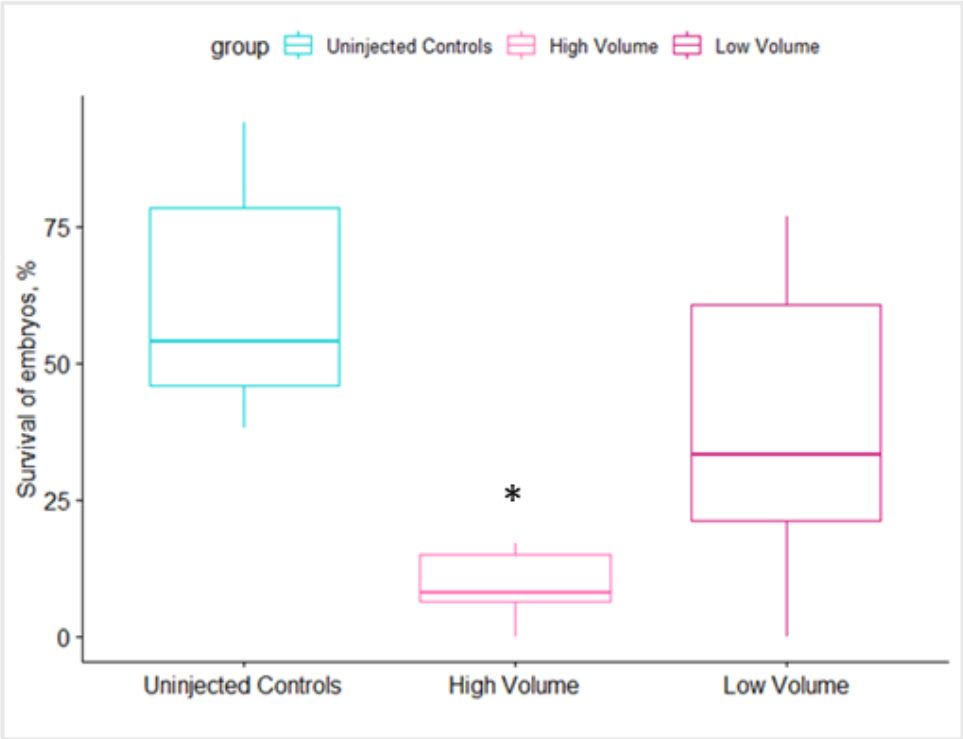

Figure 3.12: Boxplot visualizing the average survival rate and variation around the median for the three groups (uninjected controls, embryos receiving high volume of PE RNP injection solution and embryos receiving low volume of PE RNP injection solution). n = 6 (survival in percentage pr group pr day). There was a significant difference in embryo survival rate between the group receiving no injections and the group receiving high injection volume (P =0.0013).

Performing an ANOVA analysis and a subsequent Tukey's test on the dataset, the only significant difference in survival rate between the groups was between the control group and the group injected with a high injection volume ($P = 0.0013$). No significant difference between mean survival rate was detected between the control- and low injection volume group, or between the groups receiving high and low injection volumes ($P = 0.1221$ and $P = 0.0787$, respectively).

3.3.2 Prime Editing of Zebrafish Embryos

3.3.2.1 Prime Editing of EGFP

Newly fertilized eggs from the *vas::EGFP* zebrafish line was screened to confirm expression of EGFP.

Figure 3.13: Fertilized vas::EGFP zebrafish cell in the first cell stage showing maternal expression of EGFP.

Of the 301 embryos injected with the G->B RNP solution, 43 survived (11.1 %), while 138 of 239 uninjected control embryos survived (53.8 %). There is large variation in survival rate for control embryos also in this case, with survival rate ranging from 6% to 87%, and rate of survival of injected embryos is consistently low (4%-17%).

No blue fluorescence could be detected in any of the surviving embryos edited with the G->B RNP complex two and five days post editing. Three of the 43 surviving embryos injected with EGFP RNP complex displayed no fluorescence.

PCR amplification of the EGFP sequence was unsuccessful regardless of primer pair, polymerase or PCR cycling parameters used. No bands appeared when running the PCR reactions on gels and no EGFP sequence information was obtained, unfortunately.

Looking at two day old larvae in the control group, most larvae expressed EGFP which was visually detectable under a fluorescence microscope. However, a few larvae did not express any detectable fluorescence. *Figure 3.14* shows two days-old larvea expressing EGFP in primordial germ cell clusters, while *Figure 3.15* shows a larvae from the same unedited control group showing no fluorescence.

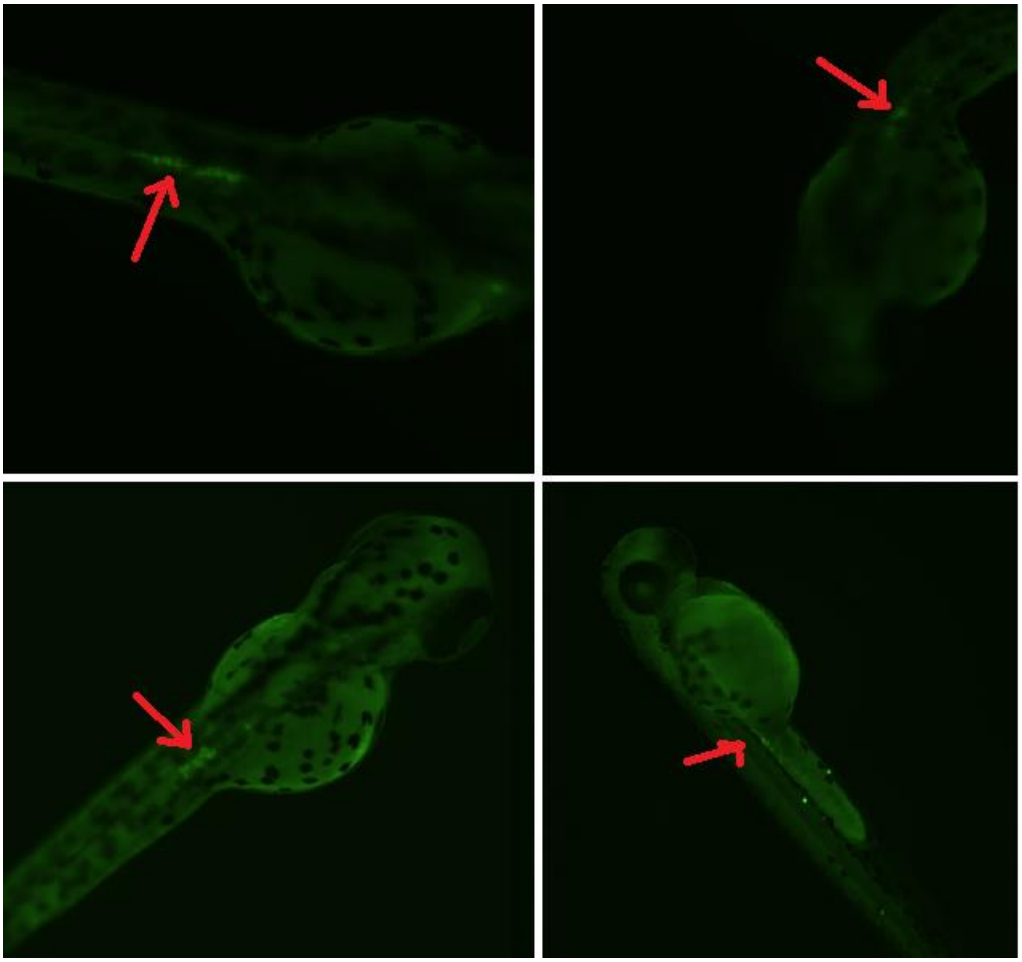

Figure 3.14. Two days old, unedited zebrafish larvae showing green fluorescence from clusters of EGFP-expressing primordial germ cells under a fluorescence microscope (Nikon, SMZ25). Pictures were captured using the Nikon NIS Elements BR software.

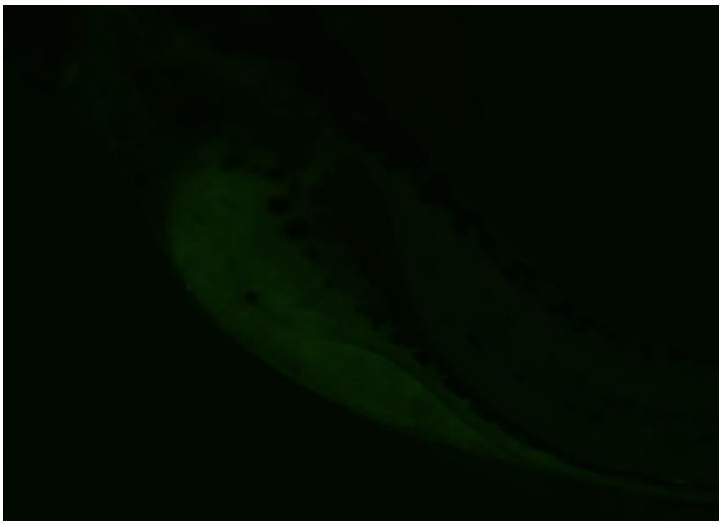

Figure 3.15. Two days old, unedited zebrafish larvae showing no green fluorescence under a fluorescence microscope (Nikon, SMZ25). The picture was captured using the Nikon NIS Elements BR software.

Five zebrafish larvae which survived injections displayed very unusual phenotypes, but showed signs of life such as heartbeat and circulation two days post editing nonetheless (see *Figure 3.16*).

Figure 3.6.. Zebrafish larvae injected with EGFP RNP constructs showing abberant non-wildtype morphology two days post injection.

3.3.2.2 Prime Editing of nid1a

Of the 226 embryos injected with the *nid1a* RNP complex, 46 embryos (19.5%) survived three days post editing. Survival rate of uninjected controls was 56.3% (163 surviving embryos out of 291). Large variation in survival rate was observed for both groups, ranging from 39-78% for uninjected controls and 6-31% for injected embryos.

Most edited fish were indistinguishable from wild-type. Some of the 46 injected survivors displayed somewhat shortened body length in the larval stage compared to unedited controls, but inexperience of zebrafish morphological assessment made it difficult to distinguish whether the differences stemmed from successful editing or were just due to natural within-species variation. Three larvae from the injected group displaying

somewhat shorter body lengths were sent for sequencing together with one uninjected control.

Sequencing of these three as well as the control revealed no successful edits in the target area when analysed using ICE. The sequence quality was consistently low in the target area for all sequences, as shown when aligned using Benchling (indicated by the peaks representing each base, where higher peaks indicate higher quality, and the grey areas indicating that sequence quality is too bad to give any valid sequence information, see *Figure 3.17*). Due to limited time, no new primer pairs or sequencing primers were designed and tested.

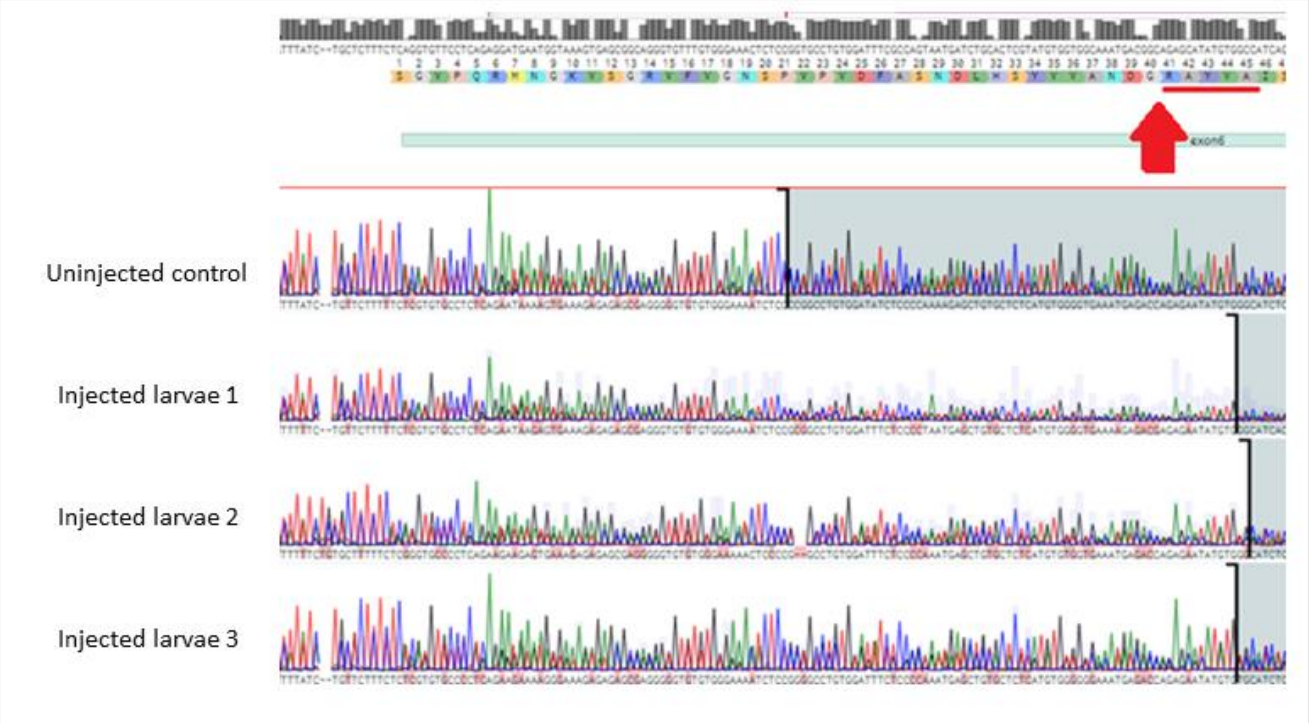

Figure 3.17. Sequence alignment of one uninjected control zebrafish larvae and three injected with nid1a RNP solution to the nid1a reference sequence. Sequence quality is represented by the individual peaks in the sequence traces, higher peaks represent better quality, i.e. higher certainty of the correct base being called. The sequence marked in grey has to low quality to be properly aligned to the reference sequence. The nid1a PE target is underlined in red. The sequences have been aligned using Benchling.

Three of the surviving injected larvae displayed similar, unusual phenotypes to those in the EGFP-group, but still showing signs of life such as heartbeat and circulation. These were not sequenced due to the bad sequencing results from earlier.

3.3.2.5 Prime Editing of *gnrh3*

Due to the combination of time constraints and high embryo mortality, attempts of prime editing of zebrafish *gnrh3* was not done.

4. DISCUSSION

The primary goals of this project were 1) to establish PE in zebrafish, and 2) to test the system in Atlantic salmon cells. As PE attempts in zebrafish were not successful, the secondary aim of testing PE as a gene KO tool able to circumvent the genetic compensation response (GCR) in zebrafish could not be explored. Whereas PE of Atlantic salmon cells by means of electroporation of plasmids did not produce any positive results, PE of cells using RNP complexes at elevated incubation temperatures showed signs of successful editing and might be a promising strategy to pursue for further PE in Atlantic salmon cells. However, the results from the RNP-mediated Atlantic salmon cell editing should be interpreted with caution, as further analysis is needed to properly validate the editing outcomes from this experiment.

4.1 *Ex vivo* prime editing in EGFP-SHK1-cells

Blue fluorescent cells were detected by flow cytometry in several of the samples, ranging from 0.02 - 0.12%. Before going into details on this, some aspects of the calibration of the flow cytometer and the sorting of cells into fluorescent categories based the positioning of the control HEK cells in the graph will be addressed.

The sample of EGFP expressing HEK cells subjected to GFP->BFP CRISPR knock-in was not an optimal control for calibrating the flow cytometer settings, as the cells are of a different cell line than the SHK-1 cells, has been transfected and edited by a different method and incubated at a different temperature, and where the ratio of EGFP- and BFP expressing cells is not known. Proper calibration of the flow cytometer should be performed prior to analysis of fluorescence (Herzenberg et al., 2006), and samples of pure green and blue cells (preferably SHK-1 cells) should have been used for calibration, allowing for more correct partitioning of cells based on their fluorescent properties.

The cells grouped into the 'other' cluster (containing the cells marked in red, seen in *Figures 3.6-3.10*) seems to trail off from the cluster of green fluorescent cells as they increase in both green and blue fluorescence intensity. The immediate thought was that this was due to the EGFP emission spectra overlapping with the blue detector wavelength (455 nm) causing detection of blue fluorescence in EGFP-expressing cells and were grouped together based on this, but as the EGFP emission spectra ranges from 468 – 625

nm (Heim et al., 1994; Lambert, 2019), the green fluorescence emitted from EGFP-expressing cells should not be detected by the blue fluorescence-detector.

In the HEK-control cells, where blue fluorescence was observed in the microscope prior to the flow cytometry analysis, some cells are positioned outside the EGFP-defining space, but underneath the main trail of cells in the 'other' cluster (that is, lower on the y-axis representing intensity of green fluorescence compared to the cells clustered in the 'trail', and more to the right on the x-axis representing blue fluorescence compared to the EGFP-expressing cells), and some of these are captured in the space that was chosen to define BFP expression ('BFP space') (see *Figure 3.6*). The hard-to-explain 'other'-cluster of cells as well as the pattern described above made it difficult properly sort BFP-expressing HEK cells. Thus, the space defining BFP-expressing cells sorting blue fluorescent HEK cells that was used for subsequent analysis of the EGFP-SHK-1 cells might capture non-BFP-expressing cells, or not capture all BFP-expressing cells in a sample. With this in mind, an attempt to interpret the flow cytometry results from the EGFP-SHK-1 cell samples is given in the following sections.

One of the negative controls showed 0.02% of cells expressing BFP due to a single cell being sorted into the BFP space. As the negative control received no PE constructs, no BFP-expressing cells are expected to occur in this sample. The cell is located to the far-left corner (see *Figure 3.11*), close to the cut-off between green and blue fluorescence, and the position high up on the y-axis within the BFP defining space indicates some green fluorescence. The BFP space might have been defined as too large of an area when identifying fluorescent populations in the control HEK cell population, leading to cells such as this one to be sorted wrongly. The same positioning of cells sorted within the BFP space is seen in sample 3 and for some of the cells in sample 2, both incubated at 26 ˚C, in *Figure 3.11*. Due to this, sample 3 should probably not be regarded as a success. However, sample 2 26 ˚C seems to have two clusters of putatively BFP-expressing cells. While one of these are located to the far-left corner, the other cluster is positioned towards the lower left corner and somewhat more towards the middle of the BFP-space (indicating lower intensity of green fluorescence and higher intensity of blue fluorescence). This *might* indicate some actual BFP-expression in this sample. The single cell sorted into the BFP space in sample 2 20 ˚C is also positioned relatively low on the y-axis and more towards the middle of the BFP space.

Given that the results from the flow cytometer analysis can be trusted despite the sub-optimal calibration and that there actually are BFP-expressing cells present in sample 2 26 ˚C and 2 20 ˚C, the intensity of the detected blue fluorescence from successfully edited cells is weak, as the cells are positioned to the left on the x-axis, and intensity of blue fluorescence increase towards the right of the same axis. BFP created from a single mutation in the EGFP emits weak fluorescence (Joly, 2007), so the positioning towards the left on the x-axis is not surprising. Their positioning on the y-axis, indicating detection of green fluorescence, could have been explained by monoallelic PE (shown to occur frequently by Schene et al. (2020)) creating heterozygous cells expressing both EGFP and BFP, as these will cluster in the middle between pure green and blue fluorescent populations (Loll-Krippleber et al., 2015). However, as the EGFP-SHK-1 cells used in this experiment are heterozygous and carries only a single EGFP gene copy, this cannot explain the observed pattern. EGFP has a half-life of approximately 26 hours in mammalian cells incubated at 37 ˚C (Corish & Tyler-Smith, 1999), and lower temperatures can decrease the rate of protein decay (Hough & Rechsteiner, 1984). There could be a possibility that some EGFP still present in edited SHK-1 cells was being detected. If this is the case, the incubation period needs to be extended in order to make sure all EGFP is degraded before analysis.

PE efficiency appears to increase with increased incubation temperatures, from 0.01% in cells incubated at 20 ˚C to 0.09% in cells incubated at 26 ˚C (assuming that all cells in the latter sample actually fluoresce blue). While low PE efficiency has been observed by other groups before PE optimization, such as Petri et al. (2021) initially editing zebrafish embryos with RNP complexes at 0.25% efficiency, and Bosch et al. (2021) experiencing editing efficiencies as low as 0.006% when transfecting S2R+ *Drosophila* cells with plasmids expressing PE components, the same groups also experienced an increase in PE efficiency when increasing temperature, from 25 and 28.5 °C to 29 and 32.5 °C, respectively. Given this, and the fact that the PE system is engineered to work optimally at 37 ˚C, the putative increase in BFP expression seen in this experiment as a result of increase in incubation temperature seems plausible. The low editing efficiency in the EGFP-SHK-1 cells could be explained at least partially by an incubation temperature of 26 ˚C, which might be too low for efficient RT activity. In addition, RNA can form secondary structures due to self-complementarity which can affect function, and

formation of such structures is at least partly due to temperature, where lower temperature increases chance of secondary structure formation.

Fellow master students Thea Marie Låstad and Sara Stenmark Andreassen have found in experiments on Atlantic salmon kidney cells that the cells can survive incubation at 28 ˚C when temperature is increased gradually over several days (Låstad and Andreassen, personal communications). Continuing experiments with PE of EGFP-SHK-1 cells by electroporation of RNP complexes in the future, the highest temperature SHK-1 cells can endure over time should be investigated. As the cells in this experiment was only exposed to 26 ˚C for 24 hours before continuing incubation at 20 ˚C, incubating them at 28 ˚C over a longer period of time might increase PE efficiency and overall editing success in the cells, similar to what was found by Bosch et al. (2021) in *Drosophila* cells.

As mentioned above, PE efficiency has been shown to improve with optimization, and optimization of pegRNA PBS- and RT template lengths for each new loci targeted is required (Anzalone et al., 2019; Lin et al., 2020; Liu et al., 2020; Petri et al., 2021). The G->B pegRNA designed and used in this project has not been used or validated in any system before, and optimization is likely required. The attempt to validate the G->B pegRNA by electroporation of HEK cells failed, but even if that had worked it would not be given that it would work in the EGFP- SHK-1 cells, due to species differences and difference in incubation temperature acting on the RNA and protein structures.

In regular CRISPR-Cas9 KO experiments, it is a common strategy to design multiple sgRNAs with different spacer sequences targeting the same gene and then assess the efficiency and precision of each before moving onwards with the best performing sgRNA (Graham & Root, 2015). Gao et al. (2021) and Jang et al. (2021) describes in their pegRNA design processes the use of programs such as CRISPOR and DeepSpCas for assessing sgRNA activity, and eliminates pegRNAs with poor-performing spacer sequences before testing different constructs. Assessing pegRNA spacer efficiency before designing full pegRNAs could be a step to include in the pegRNA design process when optimizing constructs, both for efficient color conversion in EGFP expressing SHK-1 cells and for other targets both in cells and other systems.

After systematically testing different G->B pegRNA constructs and finding the one providing maximal editing efficiency, different PE strategies could be explored to see if

successful editing outcomes can be increased further. While several PE experiments on mammal cells and animals have found the PE3 and PE3b strategies to increase PE efficiencies (Aida et al., 2020; Anzalone et al., 2019; Liu et al., 2020; Park et al., 2021), Petri et al. (2021) found no increase in editing efficiencies in zebrafish when employing either strategy compared to regular PE, and have attributed this to differences in cell division rate and DNA repair machinery between zebrafish and mammalian cells. If this is the case, it remains to be seen if the PE3 or PE3b strategy can increase editing efficiency in Atlantic salmon cells, but this should be explored.

Protein concentration is another thing that could be optimized. A drawback in this experiment was the low concentration of the PE2 protein and RNP complexes used, as the starting concentration of the PE2 protein was low. Gratacap et al. (2020) edited SHK-1 cells using Cas9-sgRNA RNP complexes where the final concentration of Cas9 in the RNP mixture was 10 μM, nearly tenfold the concentration of the PE2 protein used in this experiment, which could contribute to the low editing efficiencies observed.

Cells electroporated with the G->B RNP complex should of course have been sequenced to confirm any potential successful edits. Both 'pure' and 'impure' PE edits (correct edits and edits containing additional indels or integration of some pegRNA scaffold, respectively) occurs (Petri et al., 2021), and impure edits could lead to EGFP KO which would not be detected by microscopy or flow cytometry (at least not when the cell population is not 100% fluorescent from before). Due to low cell numbers, all cells in this experiment were used for flow cytometry analysis and no cells were left to be sequenced, but any potential successful edits should be verified by sequencing and any impure edits needs to be detected by the same method in future experiments.

EGFP-SHK-1 cells electroporated with the G->B pegRNA plasmid was only visually inspected for signs of blue fluorescence, but no color change was observed. Low intensity of blue fluorescence combined with low prime editing efficiency could make detection difficult and the conclusion of no blue fluorescence unreliable. If the PE with RNP complexes actually was successful, it shows that visual assessment might not be sufficient to detect successful editing outcomes in EGFP-SHK-1 cells, and that for example flow cytometry should be used for detection. Since there is already a percentage of the cells not expressing EGFP in the population, any impure edits potentially leading to EGFP KO

would also be hard to detect visually. Sequencing of the cells electroporated with the G->B pegRNA plasmids were planned, but was unfortunately not done in this project.

Sequencing of EGFP expressing cells electroporated with the EGFP KO PE plasmid showed that PE in these cells failed. One sample showed editing in 3% of the sequences (see *Figure 3.4*), but these sequences contained deletions upstream of the target in the sequence annealing to the pegRNA PBS rather than the expected edit. It is hard to explain this editing outcome in any good way related to PE, as the pattern of deleted bases on the sequence where the PBS should anneal is unexpected. Since ICE is just predicting the original sequences from the Sanger sequencing trace, the result could be caused by a poor prediction by the program. To be able to see the actual sequences, DNA strands from the PCR reaction could be inserted into a cloning vector and transformed into bacteria, and subsequent single colony sequencing can then be done in order to properly analyse sequences from the sample in question.

As for the rest of the sequences showing no signs of editing, there might be several reasons for this, including the points on pegRNA design and optimization and cell incubation temperatures discussed earlier, which might limit PE efficiency. What would be interesting to find out is if plasmids were actually delivered into the cells and expressed. No positive control was used in the experiment as no prime editing constructs has been successfully used in the SHK-1 cells before, and therefore no control confirming successful electroporation was used. Plasmids encoding regular Cas9 and sgRNA for EGFP KO might have been used as positive control. However, the size of a Cas9 encoding plasmid such as the pCS2+hSpCas9 plasmid (Addgene #51815), used for CRISPR-Cas9 editing in our lab, and the pCMV-PE2 plasmid encoding the PE2 protein differs with about 7500 bases. Differences in plasmid size can affect transfection, where larger plasmid size correspond to lower transfection efficiency (Kreiss et al., 1999; Ohse et al., 1995; Yin et al., 2005), making this at least not an optimal control. Although, it should not be a problem to generate a Cas9-encoding plasmid with filler sequence which could have the same size as the PE2-expressing plasmid, which might function better as a control.

Quantitative PCR (qPCR) could have been performed on the electroporated cells to detect whether the PE2 and pegRNA encoded in the plasmids actually were transcribed. This has been done previously by our lab with the purpose of detecting Cas9 and sgRNA transcripts in cells (Axmee Regmi, personal communications). Negative qPCR results

would indicate either insufficient cellular plasmid uptake during transfection or problems with expression, which might stem from plasmid design and construction, while positive qPCR results despite no editing success would indicate the need pegRNA optimization or inefficient RT activity in salmon cells (although the latter is ruled out as a cause of lack of editing success if the RNP-mediated editing discussed earlier is verified), giving an idea of what to improve or optimize in order to increase editing efficiencies.

Worth noting is the insertion of a cytosine in all pegRNA-expressing plasmids just upstream of the inserted ZFU6 promoter (see *Figure 3.2* and *Figure 3.3*). The cytosine-guanine bp which is included in the final plasmid is part of the BamHI recognition site is located between the BamHI restriction site and the ZFU6 promoter sequence, and was integrated in the plasmid upon ligation. As this is a small change in sequence upstream of the promoter it should not have any effect on transcription factor binding and directly affect transcription, but if this experiment is to be repeated, new plasmids designed to not have the base in question inserted could be constructed, and difference in success between the plasmids could be assessed.

4.2 *In vivo* prime editing of zebrafish embryos

The effect of no injections, low-volume and high-volume injections on zebrafish embryo survival rate was systematically tested. There was a clear significant difference in survival rate between uninjected embryos and those injected with a high injection volume, but no such difference was found between the low-volume group and the two other groups. The significant difference in survival between the high-volume and control group ruled out continued injections with high volumes for the rest of the experiments. The negative effect of the large volume is probably due to the injected solution taking up too much space in the cell, increasing pressure and potentially damaging cellular structures. Lower injection volumes are generally recommended for microinjection of zebrafish (Rosen et al., 2009; Schubert et al., 2014), and as a high volume clearly affected embryonic lethality negatively, a low volume (~0.56 – 1 nL) was used for further microinjection experiments in this thesis. An additional group of controls being injected with for example phenol red or salt water should also have been included, to test if the difference in survival was affected also by the injected RNP solutions.

The high spread in survival rate for the low-volume group ranging from 0-77% survival rate, and a 38.3% average rate of survival is not seen in the groups injected with low

volume of either *nid1a* or EGFP RNP solution, where survival rate rarely makes it over 20% (average survival rate of 19.5% and 11.1%, respectively). The difference between the survival rate in the former and the two latter groups might be due to microinjection practice and experience, as there is a possibility that several of the embryos in the low-volume testing group was actually not injected due to poor microinjection technique, and that I with practice was able to inject more embryos over time in the two other groups.

The survival rate of uninjected embryos was relatively low, and averages around 50-65%. Given the low survival rate of uninjected embryos, the even lower survival rate of injected ones is not surprising, as physical penetration of the embryo and injection into the cell probably causes stress that do not promote survival in already non-optimal conditions. Factors such as temperature, pH- and oxygen levels and exposure to ultraviolet light can all affect embryo survival rate (Andrade et al., 2017; Zhang et al., 2018) and in addition, the developing zebrafish was handled by different lab technicians, and might have been treated in different ways which might interfere with survival. The issue of low survival rate of control zebrafish embryos should be addressed before continuing with microinjection experiments in the future to ensure good survival overall and a higher number of surviving injected fish, which increases the possibility of detection of potential positive editing outcomes. When performing microinjections, the time spent injection should be as short as possible, to ensure that the embryos are kept in the incubator at 28 ˚C as much as possible to avoid embryos being subjected to fluctuations in temperature.

For the EGFP-expressing embryos injected with G->B RNP solution, no blue fluorescence was observed. Three injected larvae displayed no fluorescence, but it is hard to tell if this was caused by EGFP KO due to integration of impure prime edits, as some larvae in the control groups also did not display fluorescence. The lack of fluorescence observed in both groups can be due to the *vas::*EGFP zebrafish line not being properly maintained. As newly fertilized eggs were screened to confirm green fluorescence, it is likely to think that either the screening process did not capture the non-fluorescent eggs potentially present, or that maternal transcripts from heterozygous parents created fluorescence in the eggs (as these are present up to at least 50 hours after fertilization (Krøvel and Olsen, 2002)) while non-fluorescent individuals received no (functional) EGFP copies from the heterozygous parents and therefore lost fluorescence after degradation of the maternal transcripts. Unfortunately, PCR amplification of the zebrafish EGFP sequence was not

successful, so neither hypothesis could be confirmed. New forward PCR and sequencing primers should be designed to target the upstream *vasa* promoter sequence in order to generate in order to produce PCR products (like that of the design of EGFP PCR and sequencing primers for SHK-1 EGFP, as mentioned in the last paragraph of section 2.8.1).

Using regular CRISPR-Cas9, knockout of pigmentation genes such as *tyr* and *slc45a2* can serve as useful markers when co-injecting with sgRNAs targeting other genes for KO which will not display an obvious phenotype, as fish lacking pigmentation will indicate successful editing (Edvardsen et al., 2014). It would be advantageous to have such a marker for PE as well and change of fluorescence by PE would serve this purpose. If conversion of green fluorescence to blue proves difficult to achieve in further experiments, EGFP KO can also be tested. Petri et al. (2021) successfully introduced disruptive base substitutions in zebrafish *tyr* using PE, creating albino mutants. If the *vas::*EGFP line turns out not to be pure or the EGFP sequence prove difficult to edit, targeting *tyr* could be an option.

No successful editing outcomes were observed in zebrafish injected with the *nid1a* RNP complexes. Natural variation in zebrafish body length and differences in rate of development occurs (Parichy et al., 2009; Singleman & Holtzman, 2014), making it hard to distinguish what might be mutant phenotypes for one that is inexperienced in assessing zebrafish morphology at different developmental stages, and thus potentially edited individuals might not have been identified. Sequencing failed for some reason, producing low-quality sequence which gave little information on whether editing was successful or not (see *Figure 3.17*). As the PE target for *nid1a* is located in a short exon flanked by introns containing repetitive sequence, few PCR primer pairs were suggested by the Primer3 design program, probably as there is little sequence present between the repetitive intronic sequences to which suitable PCR or sequencing primers could be designed. Relaxing the settings in the Primer3 program could generate more primers that can be tested, as well as optimizing the PCR protocol further and testing other polymerases.

Hopefully, further work on PE of *nid1a* can be done, with a PCR protocol is optimized as to ensure high quality sequencing, if that is the cause of the low sequencing quality. If PE of the *nid1a* target succeeds, it would be interesting to see if the removal of the specific, conserved amino acids targeted for deletion is sufficient to create a *nid1a* KO phenotype.

As this might not be the case, proper sequencing must be ensured in order to make sure editing outcomes are detected. In addition, no PE of zebrafish *gnrh3* was done as there was not enough time to include this experiment in this thesis, so the role of PE as a tool for circumventing the genetic compensation response (GCR) remains inconclusive. It would be very interesting to see how an in-frame deletion in the *gnrh3*-encoding sequence affects zebrafish fertility. If it results in infertile fish, it could indicate that the GCR is at play. RNAseq of regular *gnrh3* knockout fish and fish with targeted PE-mediated in-frame deletion would be a natural next step to see if there are any differential expression of genes between the two, which could uncover homologs upregulated by the GCR.

pegRNA optimization discussed in the previous section on PE in cells is likely also required in order to achieve successful PE of zebrafish EGFP and *nid1a*, as well as better microinjection skills. As needle tips with smaller diameters is required for low-volume injections, the risk of needle clogging increases and the volume injected can vary greatly between injections (Schubert et al., 2014). This can cause issues with reproducibility of results (Schubert et al., 2014), and injection solution not being delivered to the cell at all (Shanmugam & Santra, 2016), leading to poor editing outcomes. Adding phenol red to the injection solution might be an option to make sure constructs are actually delivered to the cell, and give an indication of the injected volume (Rosen et al., 2009, Yuan & Sun, 2009).

As previously mentioned, Petri et al. (2021) experienced increased editing efficiencies at elevated incubation temperatures. However, whatever issues causing high zebrafish embryo mortality should be addressed before increasing incubation temperature, in order to ensure good survival also at higher incubation temperatures which might cause additional stress and increased mortality. The concentration of the PE2 protein in the RNP mixture used for microinjections is lower than what Petri et al. (2020) used (0.5 M PE2), which might contribute to lowered PE efficiency and should be increased in future experiments.

Some zebrafish embryos injected with EGFP and *nid1a* RNP complexes showed abnormal phenotypes during development, which were not expected if the editing had been successful (see *Figure 3.16*). As this was observed in both groups injected with different

constructs targeting different genes, I suspect that the observed phenotypes are caused by poor microinjection technique somehow damaging the developing embryos.

4.3 Concluding remarks

Having so far been identified in zebrafish and *C. elegans*, and with evidence pointing towards the response occurring in other organisms, the GCR is a potentially widespread phenomenon within the animal kingdom (Kontarakis & Stainier, 2020). With its many genome duplication events and retained gene duplicates similar to that of its fellow teleost zebrafish, the GCR could be occurring also in Atlantic salmon. CRISPR-Cas9 has shown to be a valuable tool for salmon gene knockout, and as the salmon is an important production animal, the use of CRISPR-Cas9 for investigation of genes involved in production traits such as disease resistance, filet coloration and quality is likely to increase over the coming years (Gratacap et al., 2019). When investigating the function of a gene in an organism where multiple paralogs occur, generation of PTCs should be avoided as to not elicit the GCR, so that a phenotype can be produced (Kontarakis & Stainier, 2020). Therefore, it might be highly relevant to explore alternative knockout strategies in salmon which do not result in PTC-formation in targeted genes. While other strategies for gene knockout without PTC-formation such as CRISPR-Cas9-mediated promoter knockout are possible, testing of prime editing in both salmon and zebrafish should continue in order to make it a reliable knockout technique, as this technique also confers the advantage of having low off-target editing effects and avoids the generation of genomic DSBs.

5. SOURCES

Abraham, E., Palevitch, O., Gothilf, Y., & Zohar, Y. (2010). Targeted Gonadotropin-Releasing Hormone-3 Neuron Ablation in Zebrafish: Effects on Neurogenesis, Neuronal Migration, and Reproduction. *Endocrinology, 151*(1), 332–340. https://doi.org/10.1210/en.2009-0548

Adli, M. (2018). The CRISPR tool kit for genome editing and beyond. *Nature Communications, 9*(1), 1911. https://doi.org/10.1038/s41467-018-04252-2

Aida, T., Wilde, J. J., Yang, L., Hou, Y., Li, M., Xu, D., Lin, J., Qi, P., Lu, Z., & Feng, G. (2020). *Prime editing primarily induces undesired outcomes in mice*. BioRxiv. https://doi.org/10.1101/2020.08.06.239723

Allendorf, F. W., & Thorgaard, G. H. (1984). Tetraploidy and the Evolution of Salmonid Fishes. In B. J. Turner (Ed.), *Evolutionary Genetics of Fishes* (pp. 1–53). Springer, Boston, MA. https://doi.org/10.1007/978-1-4684-4652-4_1

Andrade, T. S., Henriques, J. F., Almeida, A. R., Soares, A. M. V. M., Scholz, S., & Domingues, I. (2017). Zebrafish embryo tolerance to environmental stress factors-Concentration-dose response analysis of oxygen limitation, pH, and UV-light irradiation. *Environmental Toxicology and Chemistry, 36*(3), 682–690. https://doi.org/10.1002/etc.3579

Anzalone, A. V., Randolph, P. B., Davis, J. R., Sousa, A. A., Koblan, L. W., Levy, J. M., Chen, P. J., Wilson, C., Newby, G. A., Raguram, A., & Liu, D. R. (2019). Search-and-replace genome editing without double-strand breaks or donor DNA. *Nature, 576*(7785), 149–157. https://doi.org/10.1038/s41586-019-1711-4

Boel, A., Steyaert, W., De Rocker, N., Menten, B., Callewaert, B., De Paepe, A., Coucke, P., & Willaert, A. (2016). BATCH-GE: Batch analysis of Next-Generation Sequencing data for genome editing assessment. *Scientific Reports, 6*(1), 30330. https://doi.org/10.1038/srep30330

Bosch, J. A., Birchak, G., & Perrimon, N. (2021). Precise genome engineering in Drosophila using prime editing. *Proceedings of the National Academy of Sciences of the United States of America, 118*(1). https://doi.org/10.1073/pnas.2021996118

Bunton-Stasyshyn, R., Wells, S., & Teboul, L. (2019). When all is not lost: considering genetic compensation in laboratory animals. *Lab animal*, *48*(10), 282–284. https://doi.org/10.1038/s41684-019-0397-4

Chow, R. D., Chen, J. S., Shen, J., & Chen, S. (2021). A web tool for the design of prime-editing guide RNAs. *Nature Biomedical Engineering, 5*(2), 190–194. https://doi.org/10.1038/s41551-020-00622-8

Corish, P., & Tyler-Smith, C. (1999). Attenuation of green fluorescent protein half-life in mammalian cells. *Protein engineering*, *12*(12), 1035–1040. https://doi.org/10.1093/protein/12.12.1035

Cox, D. B. T., Platt, R. J., & Zhang, F. (2015). Therapeutic Genome Editing: Prospects and Challenges. *Nature Medicine, 21*(2), 121–131. https://doi.org/10.1038/nm.3793

Dannevig, B. H., Falk, K., & Namork, E. (1995). Isolation of the causal virus of infectious salmon anaemia (ISA) in a long-term cell line from Atlantic salmon head kidney. *The Journal of General Virology, 76*(6), 1353–1359. https://doi.org/10.1099/0022-1317-76-6-1353

Doench, J. G. (2018). Am I ready for CRISPR? A user's guide to genetic screens. *Nature Reviews Genetics, 19*(2), 67–80. https://doi.org/10.1038/nrg.2017.97

Doench, J. G., Hartenian, E., Graham, D. B., Tothova, Z., Hegde, M., Smith, I., Sullender, M., Ebert, B. L., Xavier, R. J., & Root, D. E. (2014). Rational design of highly active sgRNAs for CRISPR-Cas9-mediated gene inactivation. *Nature Biotechnology, 32*(12), 1262–1267. https://doi.org/10.1038/nbt.3026

Doudna, J. A., & Charpentier, E. (2014). Genome editing. The new frontier of genome engineering with CRISPR-Cas9. *Science (New York, N.Y.), 346*(6213), 1258096. https://doi.org/10.1126/science.1258096

Draper, B. W., Morcos, P. A., & Kimmel, C. B. (2001). Inhibition of zebrafish fgf8 pre-mRNA splicing with morpholino oligos: a quantifiable method for gene knockdown. *Genesis (New York, N.Y. : 2000)*, *30*(3), 154–156. https://doi.org/10.1002/gene.1053

Edvardsen, R. B., Leininger, S., Kleppe, L., Skaftnesmo, K. O., & Wargelius, A. (2014). Targeted Mutagenesis in Atlantic Salmon (Salmo salar L.) Using the CRISPR/Cas9 System Induces Complete Knockout Individuals in the F0 Generation. *PLOS ONE, 9*(9), Article e108622. https://doi.org/10.1371/journal.pone.0108622

El-Brolosy, M. A., Kontarakis, Z., Rossi, A., Kuenne, C., Günther, S., Fukuda, N., Kikhi, K., Boezio, G. L. M., Takacs, C. M., Lai, S.-L., Fukuda, R., Gerri, C., Giraldez, A. J., & Stainier, D. Y. R. (2019). Genetic compensation triggered by mutant mRNA degradation. *Nature, 568*(7751), 193–197. https://doi.org/10.1038/s41586-019-1064-z

Escobar-Aguirre, S., Arancibia, D., Escorza, A., Bravo, C., Andrés, M. E., Zamorano, P., & Martínez, V. (2019). Development of a Bicistronic Vector for the Expression of a CRISPR/Cas9-mCherry System in Fish Cell Lines. *Cells, 8*(1), 75. https://doi.org/10.3390/cells8010075

Gao, P., Lyu, Q., Ghanam, A. R., Lazzarotto, C. R., Newby, G. A., Zhang, W., Choi, M., Slivano, O. J., Holden, K., Walker, J. A., Kadina, A. P., Munroe, R. J., Abratte, C. M., Schimenti, J. C., Liu, D. R., Tsai, S. Q., Long, X., & Miano, J. M. (2021). Prime editing in mice reveals the essentiality of a single base in driving tissue-specific gene expression. *Genome Biology, 22*(1), 83. https://doi.org/10.1186/s13059-021-02304-3

Gao, Y., Zhang, Y., Zhang, D., Dai, X., Estelle, M., & Zhao, Y. (2015). Auxin binding protein 1 (ABP1) is not required for either auxin signaling or Arabidopsis development. *Proceedings of the National Academy of Sciences of the United States of America*, *112*(7), 2275–2280. https://doi.org/10.1073/pnas.1500365112

Glasauer, S. M. K., & Neuhauss, S. C. F. (2014). Whole-genome duplication in teleost fishes and its evolutionary consequences. *Molecular Genetics and Genomics, 289*(6), 1045–1060. https://doi.org/10.1007/s00438-014-0889-2

Glaser, A., McColl, B., & Vadolas, J. (2016). GFP to BFP Conversion: A Versatile Assay for the Quantification of CRISPR/Cas9-mediated Genome Editing. *Molecular Therapy - Nucleic Acids, 5*, Article e334. https://doi.org/10.1038/mtna.2016.48

Graham, D. B., & Root, D. E. (2015). Resources for the design of CRISPR gene editing experiments. *Genome Biology, 16*(1), 260. https://doi.org/10.1186/s13059-015-0823-x

Gratacap, R. L., Wargelius, A., Edvardsen, R. B., & Houston, R. D. (2019). Potential of Genome Editing to Improve Aquaculture Breeding and Production. *Trends in genetics : TIG*, *35*(9), 672–684. https://doi.org/10.1016/j.tig.2019.06.006

Gratacap, R. L., Jin, Y. H., Mantsopoulou, M., & Houston, R. D. (2020). Efficient Genome Editing in Multiple Salmonid Cell Lines Using Ribonucleoprotein Complexes. *Marine Biotechnology, 22*(5), 717–724. https://doi.org/10.1007/s10126-020-09995-y

Heim, R., Prasher, D.C, & Tsien, R.Y. (1994). Wavelength mutations and posttranslational autoxidation of green fluorescent protein. *Proceedings of the National Academy of Sciences of the United States of America,* 91(26), 12501-12504. https://doi.org/10.1073/pnas.91.26.12501

Herzenberg, L. A., Tung, J., Moore, W. A., Herzenberg, L. A., & Parks, D. R. (2006). Interpreting flow cytometry data: A guide for the perplexed. *Nature Immunology, 7*(7), 681–685. https://doi.org/10.1038/ni0706-681

Hopf, M., Göhring, W., Ries, A., Timpl, R., & Hohenester, E. (2001). Crystal structure and mutational analysis of a perlecan-binding fragment of nidogen-1. *Nature structural biology*, *8*(7), 634–640. https://doi.org/10.1038/89683

Hough, R., & Rechsteiner, M. (1984). Effects of temperature on the degradation of proteins in rabbit reticulocyte lysates and after injection into HeLa cells. *Proceedings of the National Academy of Sciences of the United States of America*, *81*(1), 90–94. https://doi.org/10.1073/pnas.81.1.90

Housden, B. E., Muhar, M., Gemberling, M., Gersbach, C. A., Stainier, D. Y. R., Seydoux, G., Mohr, S. E., Zuber, J., & Perrimon, N. (2017). Loss-of-function genetic tools for animal models: Cross-species and cross-platform differences. *Nature Reviews Genetics, 18*(1), 24–40. https://doi.org/10.1038/nrg.2016.118

Howe, K., Clark, M. D., Torroja, C. F., Torrance, J., Berthelot, C., Muffato, M., Collins, J. E., Humphray, S., McLaren, K., Matthews, L., McLaren, S., Sealy, I., Caccamo, M., Churcher, C., Scott, C., Barrett, J. C., Koch, R., Rauch, G.-J., White, S., … Stemple, D. L. (2013). The zebrafish reference genome sequence and its relationship to the human genome. *Nature, 496*(7446), 498–503. https://doi.org/10.1038/nature12111

Huang, C.-H., Shen, C. R., Li, H., Sung, L.-Y., Wu, M.-Y., & Hu, Y.-C. (2016). CRISPR interference (CRISPRi) for gene regulation and succinate production in cyanobacterium S. elongatus PCC 7942. *Microbial Cell Factories, 15*, 196. https://doi.org/10.1186/s12934-016-0595-3

Hwang, W. Y., Fu, Y., Reyon, D., Maeder, M. L., Tsai, S. Q., Sander, J. D., Peterson, R. T., Yeh, J.-R. J., & Joung, J. K. (2013). Efficient genome editing in zebrafish using a CRISPR-Cas system. *Nature Biotechnology, 31*(3), 227–229. https://doi.org/10.1038/nbt.2501

Jang, H., Jo, D. H., Cho, C. S., Shin, J. H., Seo, J. H., Yu, G., Gopalappa, R., Kim, D., Cho, S.-R., Kim, J. H., & Kim, H. H. (2021). Application of prime editing to the correction of mutations and phenotypes in adult mice with liver and eye diseases. *Nature Biomedical Engineering, 6*, 181–194. https://doi.org/10.1038/s41551-021-00788-9

Jao, L. E., Wente, S. R., & Chen, W. (2013). Efficient multiplex biallelic zebrafish genome editing using a CRISPR nuclease system. *Proceedings of the National Academy of Sciences of the United States of America*, *110*(34), 13904–13909. https://doi.org/10.1073/pnas.1308335110

Jiang, F., & Doudna, J. A. (2017). CRISPR-Cas9 Structures and Mechanisms. *Annual Review of Biophysics, 46*, 505–529. https://doi.org/10.1146/annurev-biophys-062215-010822

Jinek, M., Chylinski, K., Fonfara, I., Hauer, M., Doudna, J. A., & Charpentier, E. (2012). A programmable dual-RNA-guided DNA endonuclease in adaptive bacterial immunity. *Science (New York, N.Y.), 337*(6096), 816–821. https://doi.org/10.1126/science.1225829

Joly, E. (2007). Optimising Blue Fluorescent Protein (BFP) for use as a mammalian reporter gene in parallel with Green Fluorescent Protein (GFP). *Nature Precedings.* https://doi.org/10.1038/npre.2007.1259.1

Kelly, A., & Hurlstone A.F., (2011) The use of RNAi technologies for gene knockdown in zebrafish, *Briefings in Functional Genomics, 10*(4), 189-196, https://doi.org/10.1093/bfgp/elr014

Khalilgharibi, N., & Mao, Y. (2021). To form and function: On the role of basement membrane mechanics in tissue development, homeostasis and disease. *Open Biology, 11*(2), 200360. https://doi.org/10.1098/rsob.200360

Kher, G., Trehan, S., & Misra, A. (2011). Antisense Oligonucleotides and RNA Interference. In A. Misra (Ed) *Challenges in Delivery of Therapeutic Genomics and Proteomics*, (pp. 325–386). https://doi.org/10.1016/B978-0-12-384964-9.00007-4

Kimberland, M. L., Hou, W., Alfonso-Pecchio, A., Wilson, S., Rao, Y., Zhang, S., & Lu, Q. (2018). Strategies for controlling CRISPR/Cas9 off-target effects and biological variations in mammalian genome editing experiments. *Journal of Biotechnology, 284*, 91–101. https://doi.org/10.1016/j.jbiotec.2018.08.007

Kok, F. O., Shin, M., Ni, C.-W., Gupta, A., Grosse, A. S., van Impel, A., Kirchmaier, B. C., Peterson-Maduro, J., Kourkoulis, G., Male, I., DeSantis, D. F., Sheppard-Tindell, S., Ebarasi, L., Betsholtz, C., Schulte-Merker, S., Wolfe, S. A., & Lawson, N. D. (2015). Reverse Genetic Screening Reveals Poor Correlation between Morpholino-Induced and Mutant Phenotypes in Zebrafish. *Developmental Cell, 32*(1), 97–108. https://doi.org/10.1016/j.devcel.2014.11.018

Kontarakis, Z., & Stainier, D. Y. R. (2020). Genetics in Light of Transcriptional Adaptation. *Trends in Genetics 36*(12), 926–935. https://doi.org/10.1016/j.tig.2020.08.008

Kreiss, P., Cameron, B., Rangara, R., Mailhe, P., Aguerre-Charriol, O., Airiau, M., Scherman, D., Crouzet, J., & Pitard, B. (1999). Plasmid DNA size does not affect the physicochemical properties of lipoplexes but modulates gene transfer efficiency. *Nucleic Acids Research, 27*(19), 3792–3798. https://doi.org/10.1093/nar/27.19.3792

Krøvel, A. V., & Olsen, L. C. (2002). Expression of a vas::EGFP transgene in primordial germ cells of the zebrafish. *Mechanisms of Development, 116*(1–2), 141–150. https://doi.org/10.1016/s0925-4773(02)00154-5

Kurosaki, T., Popp, M. W., & Maquat, L. E. (2019). Quality and quantity control of gene expression by nonsense-mediated mRNA decay. *Nature Reviews Molecular Cell Biology, 20*(7), 406–420. https://doi.org/10.1038/s41580-019-0126-2

Leibowitz, M. L., Papathanasiou, S., Doerfler, P. A., Blaine, L. J., Sun, L., Yao, Y., Zhang, C.-Z., Weiss, M. J., & Pellman, D. (2021). Chromothripsis as an on-target consequence of CRISPR–Cas9 genome editing. *Nature Genetics, 53*(6), 895–905. https://doi.org/10.1038/s41588-021-00838-7

Lambert, T.J. (2019). FPbase: a community-editable fluorescent protein database. *Nature Methods, 16*(4), 277-278. https://doi.org/10.1038/s41592-019-0352-8

Li, H., Li, J., Chen, J., Yan, L., & Xia, L. (2020). Precise Modifications of Both Exogenous and Endogenous Genes in Rice by Prime Editing. *Molecular Plant, 13*(5), 671–674. https://doi.org/10.1016/j.molp.2020.03.011

Lieber, M. R. (2010). The Mechanism of Double-Strand DNA Break Repair by the Nonhomologous DNA End Joining Pathway. *Annual Review of Biochemistry, 79*, 181–211. https://doi.org/10.1146/annurev.biochem.052308.093131

Lien, S., Koop, B. F., Sandve, S. R., Miller, J. R., Kent, M. P., Nome, T., Hvidsten, T. R., Leong, J. S., Minkley, D. R., Zimin, A., Grammes, F., Grove, H., Gjuvsland, A., Walenz, B., Hermansen, R. A., von Schalburg, K., Rondeau, E. B., Di Genova, A., Samy, J. K. A., … Davidson, W. S. (2016). The Atlantic salmon genome provides insights into rediploidization. *Nature, 533*(7602), 200–205. https://doi.org/10.1038/nature17164

Lin, Q., Zong, Y., Xue, C., Wang, S., Jin, S., Zhu, Z., Wang, Y., Anzalone, A. V., Raguram, A., Doman, J. L., Liu, D. R., & Gao, C. (2020). Prime genome editing in rice and wheat. *Nature Biotechnology, 38*(5), 582–585. https://doi.org/10.1038/s41587-020-0455-x

Lino, C. A., Harper, J. C., Carney, J. P., & Timlin, J. A. (2018). Delivering CRISPR: A review of the challenges and approaches. *Drug Delivery, 25*(1), 1234–1257. https://doi.org/10.1080/10717544.2018.1474964

Liu, Y., Kao, H.-I., & Bambara, R. A. (2004). Flap endonuclease 1: A central component of DNA metabolism. *Annual Review of Biochemistry, 73*, 589–615. https://doi.org/10.1146/annurev.biochem.73.012803.092453

Liu, Y., Li, X., He, S., Huang, S., Li, C., Chen, Y., Liu, Z., Huang, X., & Wang, X. (2020). Efficient generation of mouse models with the prime editing system. *Cell Discovery, 6*, 27. https://doi.org/10.1038/s41421-020-0165-z

Loll-Krippleber, R., Feri, A., Nguyen, M., Maufrais, C., Yansouni, J., d'Enfert, C., & Legrand, M. (2015). A FACS-Optimized Screen Identifies Regulators of Genome Stability in Candida albicans. *Eukaryotic Cell, 14*(3), 311–322. https://doi.org/10.1128/EC.00286-14

Lu, J., Peatman, E., Tang, H., Lewis, J., & Liu, Z. (2012). Profiling of gene duplication patterns of sequenced teleost genomes: Evidence for rapid lineage-specific genome expansion mediated by recent tandem duplications. *BMC Genomics, 13*, 246. https://doi.org/10.1186/1471-2164-13-246

Ma, Z., & Chen, J. (2020). Premature Termination Codon-Bearing mRNA Mediates Genetic Compensation Response. *Zebrafish, 17*(3), 157–162. https://doi.org/10.1089/zeb.2019.1824

Ma, Z., Zhu, P., Shi, H., Guo, L., Zhang, Q., Chen, Y., Chen, S., Zhang, Z., Peng, J., & Chen, J. (2019). PTC-bearing mRNA elicits a genetic compensation response via Upf3a and COMPASS components. *Nature, 568*(7751), 259–263. https://doi.org/10.1038/s41586-019-1057-y

Mack, S., & Russell, I. A. (2021). CRISPR and Chromothripsis: Proceed with Caution. *The CRISPR Journal, 4*(3), 309–312. https://doi.org/10.1089/crispr.2021.29128.sma

Malicki, J. J., Pujic, Z., Thisse, C., Thisse, B., & Wei, X. (2002). Forward and reverse genetic approaches to the analysis of eye development in zebrafish. *Vision Research, 42*(4), 527–533. https://doi.org/10.1016/s0042-6989(01)00262-0

Marillonnet, S., & Grützner, R. (2020). Synthetic DNA Assembly Using Golden Gate Cloning and the Hierarchical Modular Cloning Pipeline. *Current protocols in molecular biology*, *130*, e115. https://doi.org/10.1002/cpmb.115

Marvel, M., Spicer, O. S., Wong, T.-T., Zmora, N., & Zohar, Y. (2018). Knockout of the Gnrh genes in zebrafish: Effects on reproduction and potential compensation by reproductive and feeding-related neuropeptides. *Biology of Reproduction, 99*(3), 565–577. https://doi.org/10.1093/biolre/ioy078

Matsumoto, D., Tamamura, H., & Nomura, W. (2020). A cell cycle-dependent CRISPR-Cas9 activation system based on an anti-CRISPR protein shows improved genome editing accuracy. *Communications Biology, 3*(1), 610. https://doi.org/10.1038/s42003-020-01340-2

McKinnon, K. M. (2018). Flow Cytometry: An Overview. *Current Protocols in Immunology, 120*, 5.1.1-5.1.11. https://doi.org/10.1002/cpim.40

Muñoz-Cueto, J. A., Zmora, N., Paullada-Salmerón, J. A., Marvel, M., Mañanos, E., & Zohar, Y. (2020). The gonadotropin-releasing hormones: Lessons from fish. General and Comparative *Endocrinology, 291*, 113422. https://doi.org/10.1016/j.ygcen.2020.113422

Nasevicius, A., & Ekker, S. C. (2000). Effective targeted gene 'knockdown' in zebrafish. *Nature Genetics, 26*(2), 216–220. https://doi.org/10.1038/79951

Neumann, E., Schaefer-Ridder, M., Wang, Y., & Hofschneider, P. H. (1982). Gene transfer into mouse lyoma cells by electroporation in high electric fields. *The EMBO Journal, 1*(7), 841–845.

Ohse, M., Takahashi, K., Kadowaki, Y., & Kusaoke, H. (1995). Effects of plasmid DNA sizes and several other factors on transformation of Bacillus subtilis ISW1214 with plasmid DNA by electroporation. *Bioscience, Biotechnology, and Biochemistry, 59*(8), 1433–1437. https://doi.org/10.1271/bbb.59.1433

Parichy, D. M., Elizondo, M. R., Mills, M. G., Gordon, T. N., & Engeszer, R. E. (2009). Normal table of postembryonic zebrafish development: staging by externally visible anatomy of the living fish. *Developmental dynamics : an official publication of the American Association of Anatomists*, *238*(12), 2975–3015. https://doi.org/10.1002/dvdy.2211

Park, S.-J., Jeong, T. Y., Shin, S. K., Yoon, D. E., Lim, S.-Y., Kim, S. P., Choi, J., Lee, H., Hong, J.-I., Ahn, J., Seong, J. K., & Kim, K. (2021). Targeted mutagenesis in mouse cells and embryos using an enhanced prime editor. *Genome Biology, 22*(1), 170. https://doi.org/10.1186/s13059-021-02389-w

Pauli A, Montague TG, Lennox KA, Behlke MA, Schier AF. (2015), Antisense Oligonucleotide-Mediated Transcript Knockdown in Zebrafish. *PLoS One, 10*(10), e0139504. https://doi:10.1371/journal.pone.0139504.

Petri, K., Zhang, W., Ma, J., Schmidts, A., Lee, H., Horng, J. E., Kim, D. Y., Kurt, I. C., Clement, K., Hsu, J. Y., Pinello, L., Maus, M. V., Joung, J. K., & Yeh, J.-R. J. (2021). CRISPR prime editing with ribonucleoprotein complexes in zebrafish and primary human cells. *Nature Biotechnology, 40*(2), 189-193. https://doi.org/10.1038/s41587-021-00901-y

Ribas, L., & Piferrer, F. (2014). The zebrafish (Danio rerio) as a model organism, with emphasis on applications for finfish aquaculture research. *Reviews in Aquaculture, 6*(4), 209–240. https://doi.org/10.1111/raq.12041

Roch, G. J., Busby, E. R., & Sherwood, N. M. (2014). GnRH receptors and peptides: skating backward. *General and comparative endocrinology*, *209*, 118–134. https://doi.org/10.1016/j.ygcen.2014.07.025

Rosen, J. N., Sweeney, M. F., & Mably, J. D. (2009). Microinjection of Zebrafish Embryos to Analyze Gene Function. *Journal of Visualized Experiments : JoVE,* (25), Article e1115. https://doi.org/10.3791/1115

Rossi, A., Kontarakis, Z., Gerri, C., Nolte, H., Hölper, S., Krüger, M., & Stainier, D. Y. R. (2015). Genetic compensation induced by deleterious mutations but not gene knockdowns. *Nature, 524*(7564), 230–233. https://doi.org/10.1038/nature14580

Salanga, C. M., & Salanga, M. C. (2021). Genotype to Phenotype: CRISPR Gene Editing Reveals Genetic Compensation as a Mechanism for Phenotypic Disjunction of Morphants and Mutants. *International journal of molecular sciences*, *22*(7), 3472. https://doi.org/10.3390/ijms22073472

Schene, I. F., Joore, I. P., Oka, R., Mokry, M., van Vugt, A. H. M., van Boxtel, R., van der Doef, H. P. J., van der Laan, L. J. W., Verstegen, M. M. A., van Hasselt, P. M., Nieuwenhuis, E. E. S., & Fuchs, S. A. (2020). Prime editing for functional repair in patient-derived disease models. *Nature Communications, 11*(1), 5352. https://doi.org/10.1038/s41467-020-19136-7

Schubert, S., Keddig, N., Hanel, R., & Kammann, U. (2014). Microinjection into zebrafish embryos (Danio rerio)—A useful tool in aquatic toxicity testing? *Environmental Sciences Europe, 26*, 32. https://doi.org/10.1186/s12302-014-0032-3

Serobyan, V., Kontarakis, Z., El-Brolosy, M. A., Welker, J. M., Tolstenkov, O., Saadeldein, A. M., Retzer, N., Gottschalk, A., Wehman, A. M., & Stainier, D. Y. (2020). Transcriptional adaptation in Caenorhabditis elegans. *ELife, 9*, Article e50014. https://doi.org/10.7554/eLife.50014

Shanmugam, M. M., & Santra, T. S. (2016). Microinjection for Single-Cell Analysis. In F.-G. Tseng & T. S. Santra (Eds.), *Essentials of Single-Cell Analysis: Concepts, Applications and Future Prospects* (pp. 85–129). Springer. https://doi.org/10.1007/978-3-662-49118-8

Singleman, C., & Holtzman, N. G. (2014). Growth and maturation in the zebrafish, Danio rerio: a staging tool for teaching and research. *Zebrafish*, *11*(4), 396–406. https://doi.org/10.1089/zeb.2014.0976

Spicer, O. S., Wong, T.-T., Zmora, N., & Zohar, Y. (2016). Targeted Mutagenesis of the Hypophysiotropic Gnrh3 in Zebrafish (Danio rerio) Reveals No Effects on Reproductive Performance. *PLOS ONE, 11*(6), Article e0158141. https://doi.org/10.1371/journal.pone.0158141

Stainier, D. Y. R., Kontarakis, Z., & Rossi, A. (2015). Making Sense of Anti-Sense Data. *Developmental Cell, 32*(1), 7–8. https://doi.org/10.1016/j.devcel.2014.12.012

Steven, C., Lehnen, N., Kight, K., Ijiri, S., Klenke, U., Harris, W. A., & Zohar, Y. (2003). Molecular characterization of the GnRH system in zebrafish (Danio rerio): Cloning of chicken GnRH-II, adult brain expression patterns and pituitary content of salmon GnRH and chicken GnRH-II. *General and Comparative Endocrinology, 133*(1), 27–37. https://doi.org/10.1016/S0016-6480(03)00144-8

Straume, A. H., Kjærner-Semb, E., Skaftnesmo, K. O., Güralp, H., Kleppe, L., Wargelius, A., & Edvardsen, R. B. (2020). Indel locations are determined by template polarity in highly efficient in vivo CRISPR/Cas9-mediated HDR in Atlantic salmon. *Scientific reports*, *10*(1), 409. https://doi.org/10.1038/s41598-019-57295-w

Straume, A. H., Kjærner-Semb, E., Skaftnesmo, K. O., Güralp, H., Lillico, S., Wargelius, A., & Edvardsen, R. B. (2021). Single nucleotide replacement in the Atlantic salmon genome using CRISPR/Cas9 and asymmetrical oligonucleotide donors. *BMC genomics*, *22*(1), 563. https://doi.org/10.1186/s12864-021-07823-8

Summerton, J., & Weller, D. (1997). Morpholino antisense oligomers: design, preparation, and properties. *Antisense & nucleic acid drug development*, *7*(3), 187–195. https://doi.org/10.1089/oli.1.1997.7.187

Sztal, T. E., McKaige, E. A., Williams, C., Ruparelia, A. A., & Bryson-Richardson, R. J. (2018). Genetic compensation triggered by actin mutation prevents the muscle damage caused by loss of actin protein. *PLOS Genetics, 14(*2), Article e1007212. https://doi.org/10.1371/journal.pgen.1007212

Sztal, T. E., & Stainier, D. (2020). Transcriptional adaptation: a mechanism underlying genetic robustness. *Development (Cambridge, England)*, *147*(15), dev186452. https://doi.org/10.1242/dev.186452

Tiebe, M., Lutz, M., Levy, D., & Teleman, A. A. (2018). Phenotypic characterization of SETD3 knockout Drosophila. *PLOS ONE, 13*(8), Article e0201609. https://doi.org/10.1371/journal.pone.0201609

Torgersen, J., Nourizadeh-Lillabadi, R., Husebye, H., & Aleström, P. (2002). In silico and in situ characterization of the zebrafish (Danio rerio) gnrh3 (sGnRH) gene. *BMC genomics*, *3*(1), 25. https://doi.org/10.1186/1471-2164-3-25

Uddin, F., Rudin, C., & Sen, T. (2020). CRISPR Gene Therapy: Applications, Limitations, and Implications for the Future. *Frontiers in Oncology, 10,* 1387. https://doi.org/10.3389/fonc.2020.01387

Wagnerberger, J.H. (2020) *CRISPR based functional characterization of the abcg2b gene contribution to muscle pigmentation in Atlantic salmon* [Master's thesis, Norwegian University of Life Sciences]. Brage. https://nmbu.brage.unit.no/nmbu-xmlui/handle/11250/2726396?locale-attribute=en

Xin, Y., & Duan, C. (2018). Microinjection of Antisense Morpholinos, CRISPR/Cas9 RNP, and RNA/DNA into Zebrafish Embryos. In L. Eric Huang (Ed.), *Methods in Molecular Biology, Hypoxia,* (pp. 205–211). Humana New York, NY. https://doi.org/10.1007/978-1-4939-7665-2_18

Yan, J., Cirincione, A., & Adamson, B. (2020). Prime Editing: Precision Genome Editing by Reverse Transcription. *Molecular cell*, *77*(2), 210–212. https://doi.org/10.1016/j.molcel.2019.12.016

Yang, Y., Xu, J., Ge, S., & Lai, L. (2021). CRISPR/Cas: Advances, Limitations, and Applications for Precision Cancer Research. *Frontiers in Medicine, 8*, 649896. https://doi.org/10.3389/fmed.2021.649896

Yin, W., Xiang, P., & Li, Q. (2005). Investigations of the effect of DNA size in transient transfection assay using dual luciferase system. *Analytical Biochemistry, 346*(2), 289–294. https://doi.org/10.1016/j.ab.2005.08.029

Yuan, S., & Sun, Z. (2009). Microinjection of mRNA and morpholino antisense oligonucleotides in zebrafish embryos. *Journal of visualized experiments : JoVE*, (27), Article e1113. https://doi.org/10.3791/1113

Zhang, Q., Kopp, M., Babiak, I., & Fernandes, J. M. O. (2018). Low incubation temperature during early development negatively affects survival and related innate immune processes in zebrafish larvae exposed to lipopolysaccharide. *Scientific Reports, 8*(1), 4142. https://doi.org/10.1038/s41598-018-22288-8

Zhao, D., Jones, J. L., Gasperini, R. J., Charlesworth, J. C., Liu, G.-S., & Burdon, K. P. (2021). Rapid and efficient cataract gene evaluation in F0 zebrafish using CRISPR-Cas9 ribonucleoprotein complexes. *Methods, 194*, 37–47. https://doi.org/10.1016/j.ymeth.2020.12.004

Zhu, P., Ma, Z., Guo, L., Zhang, W., Zhang, Q., Zhao, T., Jiang, K., Peng, J., & Chen, J. (2017). Short body length phenotype is compensated by the upregulation of nidogen family members in a deleterious nid1a mutation of zebrafish. *Journal of Genetics and Genomics*, 44(11), 553–556. https://doi.org/10.1016/j.jgg.2017.09.011

Zimmer, A. M., Pan, Y. K., Chandrapalan, T., Kwong, R. W. M., & Perry, S. F. (2019). Loss-of-function approaches in comparative physiology: Is there a future for knockdown experiments in the era of genome editing? *Journal of Experimental Biology*, 222(7):jeb.175737 https://doi.org/10.1242/jeb.175737

Zohar, Y., Muñoz-Cueto, J. A., Elizur, A., & Kah, O. (2010). Neuroendocrinology of reproduction in teleost fish. *General and Comparative Endocrinology, 165*(3), 438–455. https://doi.org/10.1016/j.ygcen.2009.04.017

6. APPENDIX

1) Reference sequence for ZFU6 and G->B pegRNA encoding sequence. Backbone sequence marked in grey

5’ - ...
CGACTGGATCCACCTCAACAAAAGCTCCTCGATGTCACACAGGAAGTTCAGGAACTTATCCAATCACTCTAAA
GAAACGGCCTGTTTCCTTCGCATACGCTTACAGCTCCAAAACTCTACGGTAAACCTACATAAACTGCTGGTTTT
CAAATTTTAAAGAATTTAAGGGTTTACAGGTTTACTACTACACAGTGATTTACTGACACATGTAGGTGTAAATG
AGTTGAATAAGTAAGTAAGCTATATACCACACATGAAACACATACCCAGAAGTCACTGGTATATATAGCCGTC
CTCCAGACTCCCAGAAACACCCGAGACCGTAGTCAAAAGCCTCCGGTCGGAGGCTTTTGACTTGGCTGAGGA
GTGCCACACCGCTCGTGACCACCCTGACCTACGGGTTTTAGAGCTAGAAATAGCAAGTTAAAATAAGGCTAGT
CCGTTATCAACTTGAAAAAGTGGCACCGAGTCGGTGCTGCACGCCGTGGGTCAGGGTGGTCAGATCC ... -3’

2) Reference sequence for ZFU6 and EGFP KO pegRNA encoding sequence. Backbone sequence marked in grey

5’ - ...
CGACTGGATCCACCTCAACAAAAGCTCCTCGATGTCACACAGGAAGTTCAGGAACTTATCCAATCACTCTAAA
GAAACGGCCTGTTTCCTTCGCATACGCTTACAGCTCCAAAACTCTACGGTAAACCTACATAAACTGCTGGTTTT
CAAATTTTAAAGAATTTAAGGGTTTACAGGTTTACTACTACACAGTGATTTACTGACACATGTAGGTGTAAATG
AGTTGAATAAGTAAGTAAGCTATATACCACACATGAAACACATACCCAGAAGTCACTGGTATATATAGCCGTC
CTCCAGACTCCCAGAAACACCCGAGACCGTAGTCAAAAGCCTCCGGTCGGAGGCTTTTGACTTGGCTGAGGA
GTGCCACACCGCTCGTGACCACCCTGACCTACGGGTTTTAGAGCTAGAAATAGCAAGTTAAAATAAGGCTAGT
CCGTTATCAACTTGAAAAAGTGGCACCGAGTCGGTGCAGCACTGCACGCCGGTCAGGGTGGTCAGATCC ... -3’

Norges miljø- og biovitenskapelige universitet
Noregs miljø- og biovitskapelege universitet
Norwegian University of Life Sciences

Postboks 5003
NO-1432 Ås
Norway